TEMPERATURE AND TIME DEPENDENT BEHAVIORS OF A WOOD-POLYPROPYLENE COMPOSITE

By

Andrew Joseph Schildmeyer

A thesis submitted in partial fulfillment of
the requirements for the degree of

MASTER OF SCIENCE IN CIVIL ENGINEERING

WASHINGTON STATE UNIVERSITY
Department of Civil and Environmental Engineering

AUGUST 2006

To the Faculty of Washington State University:

The members of the Committee appointed to examine the thesis of ANDREW JOSEPH SCHILDMEYER find it satisfactory and recommend that it be accepted.

Michael P. Wolcott
Chair

TEMPERATURE AND TIME DEPENDENT BEHAVIORS

OF A WOOD-POLYPROPYLENE COMPOSITE

Abstract

by: Andrew Joseph Schildmeyer, M.S.
Washington State University
August 2006

Chair: Michael P. Wolcott

Wood-plastic composites (WPCs) are poised to become a viable alternative to traditional civil engineering building materials in select structurally-demanding capacities. The main impediment to utilizing these materials as structural members is the lack of performance data in adverse conditions. The two conditions investigated in this study are: the static performance in tension and compression at elevated temperatures and the long-term creep behavior in tension and compression of a polypropylene-pine WPC at a full allowable design stress via accelerated testing. The first interest for this study was the static tensile and compressive strength, stiffness, and straining behaviors at elevated temperatures. Inverse relationships for ultimate strength and stiffness were found, while a direct relationship for maximum strain was observed. An analysis to determine the nonlinear constitutive relations was conducted; showing appropriate stress-strain behavior for tension and compression can be interpolated for any likely temperature service condition. Furthermore, a method to assess and implement design

reduction factors consistent with timber design methodologies is recommended based upon the performance of the specimens at different temperature levels.

The second focus of this work was to evaluate the creep performance of this formulation and to assess the validity of using temperature as the accelerant for an accelerated testing procedure (TTSP). The short-term creep behavior is modeled using Findley's power law. Appropriate short-term creep parameters were determined from the model parameter trends. The short-term tests are then combined to generate master curves in tension and compression for a maximum allowable design load case of 40% of ultimate load at 21.1°C. The predictive capability of these master curves was 5.7-years in tension and 2.7-years in compression. Temperature was proven to be a more efficient variable for generation of accelerated test data than previous studies which used stress.

TABLE OF CONTENTS

LIST OF TABLES

LIST OF FIGURES

CHAPTER ONE

INTRODUCTION

1.1 Background

Wood-plastic composites (WPCs) are a class of engineered materials comprised mainly of a lignocellulosic (wood) component and a plastic component (Clemons, 2002; Wolcott, 2001). The majority of WPCs employ the use of thermoset plastics such as polyvinyl chloride (PVC), polypropylene (PP), high-density polyethylene (HDPE) or low-density polyethylene (LDPE). Various species of wood have been tested, with the most common being pine, maple, and oak (Clemons, 2002). In addition to wood species variations, the wood component can be integrated into the composite in one of three main ways: as wood flour, short wood fibers or long wood fibers, with wood flour being the most common form (Clemons, 2002; Wolcott 2001). With all the possible combinations of thermoplastics, wood species, and wood form, there is a vast spectrum of mechanical properties for the permutations of the three variables. Past work by Slaughter (2004) has determined a WPC formulation with an optimum blend of moisture resistance, dimensional stability and other physical properties with strength, stiffness and other mechanical properties. The developed formulation will be the material used in this work.

From their beginning, WPC products have been utilized primarily in light or non-structural applications. For example, the first recorded use of a wood-thermoset composite was as a gearshift for Rolls Royce in 1916 (Clemons, 2002). Currently, they are most commonly found as the superstructure on residential decks, sills for windows and doors, or interior paneling for automobiles. Selection of WPC materials in these

markets is based less upon mechanical performance, and more upon water-resistance, durability and/or low-maintenance qualities inherent in this class of product (Wolcott , 2001). WPCs have not been widely used in structural applications because their long-term performance is not documented well enough to make suitable engineering assumptions and judgments. However, advantages of WPC products (i.e. moisture resistance, durability and low-maintenance, the ability to easily construct complex cross-sections, the efficient nature of extrusion processing, and the ability to use recycled materials) are becoming increasingly appealing for select structural applications.

The remaining obstacles for WPC use in structural applications are in finding ways to ensure adequate strength, stiffness and long-term performance of a member throughout its design life. To this end, strength with regard to optimum component percentages has been addressed specifically in previous work by Slaughter (2004). Kobbe (2005) further characterized the mechanical strength of one particular pine-polypropylene WPC formulation in tension, compression and flexural behavior. Flexural rigidity for a given material composition can be addressed through extrusion processes (such as a stranding die and extrusion processes (Laver, 1996)) and complex cross-section design. The remaining major impediment to full utilization is long-term performance with regard to strength deterioration and deflection over time. Kobbe employed the Time-Stress Superposition Principle to begin to address time-dependent performance, but was very limited in the predictive scope of that work (less than 270 days of predictive data). Longer time scales will produce better data from which to make engineering assumptions but requires longer timeframes for civil engineering applications. With a more firm understanding of the mechanical behavior of WPCs,

structural utilization of WPCs can be achieved by providing designers with necessary behavioral information to appropriately design for performance and safety.

1.2 Incentive

The WPC market has been primarily restricted to low-stress structural applications, such as interior automobile paneling, residential decking and railing components, industrial flooring, and window/door sills (Clemons, 2002; Wolcott and Smith, 2004). By 2004, the WPC industry in North America was worth $750 million, with the decking and railing industry being the largest contributor and controlling approximately 15% of the market (Wolcott and Smith, 2004; LeGault, 2005). Double-digit annual WPC market growth should continue, although this will be at a somewhat slower growth rate (Anonymous, 2005).

To move these products into more sophisticated structural applications, the long-term performance and weight-to-strength ratio of these products must be addressed (Wolcott and Smith, 2004). One area that WPCs could be applied in a structural sense would be as deck substructures. Even in decks utilizing WPC rails and deck superstructure, virtually all deck substructures are constructed with treated lumber; a market worth approximately $2.0 billion annually (Wolcott and Smith, 2004). Assuming WPC components could achieve a 15% market share of the deck substructure market (similar to the deck superstructure market), the total market value of *all* WPCs would see a 40% increase over present levels. Other structural applications beside decking substructure will add to the potential WPC market when the roadblocks to structural performance are addressed.

Another motivation to pursue WPC performance characterization is the environmental consideration of replacing treated lumber with WPC materials. The Environmental Protection Agency (EPA) has become increasingly critical of many traditional wood-treatment chemicals (e.g. the EPA banned the use of chromated copper arsenate (CCA)). Products that are intrinsically moisture-resistant, such as WPC materials, are a viable solution to using more expensive and still environmentally reactive treatment chemicals (Clemons, 2002; Wolcott and Smith, 2004).

Applications for the Navy are another venue that would capitalize upon the inherent water-resistant and durable nature of WPC materials while also providing load-bearing performance. Treated lumber replacement costs for Navy pier maintenance are estimated at approximately $250 million dollars annually (LeGault, 2005). Additionally, the concept of "Energy Efficient Housing Design" along with a cry for increased durability of low-rise buildings has cost the navy around $600 million dollars a year (Wolcott and Smith, 2004). Both costs are driven by a lack of durability for traditional materials when exposed to moisture. Because WPC products are intrinsically durable and moisture-resistant they are well suited for these applications. The first applications of WPC materials in naval facilities were as pier chocking in California and pier decking designed to support forklift loads in Rhode Island (LeGault, 2005). On a long-term basis, the use of WPCs should lower the annual cost of maintaining these structures due to their improved durability in adverse environment conditions over traditional materials. Naval applications provide a unique market for WPCs to utilize their intrinsic moisture-resistant properties and mechanical performance.

The current WPC market continues to grow in the light-structural markets where in-roads have been made. However, a slowing growth rate in these markets combined with the potential growth opportunities of structural applications pose a need to address the long-term performance and weight-to-strength ratio. Once these issues are addressed, WPCs can be designed using consistent design procedures, to fully utilize both mechanical performance and their intrinsic advantages.

1.3 Research and Development

In many structural applications involving polymers, an understanding of the effect of temperature on mechanical properties is essential (Bathgate, Wang, and Pang, 1997). Previous work by Pooler (2001) and Kobbe (2005) illustrated vastly different behavior over a practical in-service range of temperatures for HDPE and polypropylene formulations, respectively. Due to the temperature dependent performance of the HDPE material, further investigation on the polypropylene material previously studied by Kobbe (2005) should be conducted investigating mechanical properties due to changes in temperature.

Creep is the phenomena of a material experiencing time-dependent strains when the stress applied to that material remains constant (Findley, 1960; Altenbach, 2002). Concrete and wood are good examples of traditional civil engineering materials that exhibit creep behavior (Begtsson, 2000). Materials that undergo creep, therefore, have two components to strain: an elastic (instantaneous) component and a creep (time-dependent) component. Because of this second component, there exists the possibility of appreciable amounts of deformation to accrue over the life span of the structure and long-

term performance must be taken into account in design (Lou and Schapery, 1971; Altenbach, 2002). Many researchers have shown that WPC materials, including the WPC of interest in this work, exhibit appreciable creep behavior (Wolcott and Smith, 2004; Pooler, 2001; Kobbe, 2005).

The creep behavior of WPCs classifies these materials as non-linear viscoelastic materials. These materials are so labeled because they exhibit time-dependent (viscoelastic) behavior where the behavioral path depends upon the stress applied to the composite. This results in compliance behavior vastly different between identical specimens loaded to different stresses. Research has pursued modeling of viscoelastic materials, with some investigations founded upon the microstructure of the solid and others looking for purely empirical methods to accurately describe the behavior of this class of materials (Lou and Schapery, 1971; Findley, 1960; Brinson et al., 1984; Rand, 1995). Kobbe (2005) previously conducted testing on the time-dependent behavior of the WPC considered in the current investigation, where via the Time-Stress Superposition Principle (TSSP), master curves were been developed. Master curves are generated using data at accelerated creep conditions by adjusting them to create a single, comprehensive curve in "reduced time". These creep master curves generated from the TSSP employed by Kobbe did not produce creep data to time scales on the order of typical civil engineering scope. Therefore, other avenues, such as using temperature as an accelerant to creep behavior may allow data to be obtained for a suitable design lifetime based solely upon short-term creep testing. To model master curves, a mathematical expression of exponentials with different retardation times has been shown to fit acceptably. This mathematical expression is called a Prony series.

1.4 Objectives

Engineered applications for WPC materials depend upon more fully understanding their short and long-term performance. One major performance attribute not fully understood is the temperature-dependent stress-strain behavior of the composite. Long term creep deformations must be addressed in order to incorporate these materials into structural applications. The applicability of WPCs in structural markets that capitalize upon their intrinsic advantages is clearly evident (i.e. markets involving the replacement of expensive lumber treatments). Therefore, the specific objectives of this research are to:

1) Examine the effect of increased temperature upon static tension and compression behavior for a well-established wood-polypropylene formulation.
2) Examine the effect of temperature upon the short-term creep behavior, with regard to modeling parameters of elastic modulus and maximum strain for a given testing time when loaded to an allowable design-level stress.
3) Utilize Time-Temperature Superposition Principle (TTSP) to generate master curves for creep performance in pure loading modes at moderate stress levels, thus extending short-term creep data to design-life time scales.

1.5 References

Altenbach, H., "Creep Analysis of Thin-Walled Structures." Z. Agnew. Math. Mech., Vol. 82, No. 8, pp. 507-533, 2002.

Anonymous. "Wood Composites Keep Growing." Plastics in Canada, Vol. 12, Iss. 4, pp.12-13, July/August 2005

Bathgate, R.G., Wang, C.H. and Pang, F., "Effects of Temperature on the Creep Behaviour of Woven and Stitched Composites." Composite Structures, Vol. 38, No. 1-4, pp 435-445, 1997

Bengtsson, C., "Creep of Timber in Different Loading Modes – Material Property Aspects." World Conference on Timber Engineering, Whistler Resort, British Colombia, Canada, July 31 – August 3, 2000.

Brinson, H.F., Hiel, C.C., Cardon, A.H. and De Wilde, W.P., "Nonlinear Viscoelastic Characterisation of Polymeric Materials." Polymer Processing and Properties, pp311-317, Plenum Press, New York, NY, 1984.

Clemons, C., "Wood-Plastic Composites in the United States, The Interfacing of Two Industries." Forest Product Journal, Vol. 52, No. 6., pp. 10-18, 2002.

Findley, W.N., "Mechanisms and Mechanics of Creep in Plastics." SPEJ, Vol. 16, pp. 57-65, January 1960.

Kobbe, R.G., "Creep Behavior of a Wood-Polypropylene Composite." Master Thesis, Washington State University, August 2005.

Laver, T.C., "Extruded Synthetic Wood Composition and Methods for Making Same." U.S. Patent Number 5,516,472, 1996.

LeGault, M., "More Than Just Decking." Canadian Plastics, Vol 63, Iss. 7, pp. 13-16, July/August 2005.

Lou, Y.C. and Schapery, R.A., "Viscoelastic Characterization of a Nonlinear Fiber-Reinforced Plastic." Journal of Composite Materials, Vol. 5, pp. 208-234, 1971.

Pooler, D.J., "The Temperature Dependent Non-Linear Viscoelastic Response of a Wood Plastic Composite." Master Thesis, Washington State University, August 2001.

Rand, J.L., "A Nonlinear Viscoelastic Creep Model." Tappi Journal, Vol. 78, No. 7, pp. 178-182, July 1995.

Slaughter, A.E., "Design and Fatigue of a Structural Wood-Plastic Composite." Master Thesis, Washington State University, August 2004.

Wolcott, M.P., "Wood-Plastic Composites." In: Encyclopedia of Materials: Science and Technology, pp. 9759-9763, Ed. Buschow et al., Elsewier Press, NY, 2001.

Wolcott, M.P. and Smith, P.M., "Opportunities and Challenges for Wood-Plastic Composites in Structural Applications." Proceedings of Progress in Woodfibre-Plastic Composites-2004 Toronto, ON, 2004.

CHAPTER TWO

EXPERIMENTAL INVESTIGATION OF THE TEMPERATURE-DEPENDENT MECHANICAL BEHAVIOR OF A POLYPROPYLENE-PINE COMPOSITE

2.1 Abstract

Wood-plastic composites (WPCs) have been recognized as versatile and practical materials for use in many light-structural applications during the past two decades. Recently, more structurally demanding applications have surfaced. These applications require improved mechanical performance while also capitalizing upon the inherent non-structural advantages of WPCs (e.g. durability, moisture resistance and low maintenance). Research investigating environmental influences (e.g. service temperature) on mechanical performance with the goal of assigning structural design values is lacking. This work examines the effect of operating temperature on the mechanical performance of a polypropylene-pine composite formulation. The composite used in this research was dry-blended and extruded on-site from commercially available components. Static tests were performed at temperatures between 21.1ºC (70ºF) and 80.0ºC (176ºF) to determine the material constitutive relations and ultimate properties in tension and compression. A statistical approach for climate was proposed to assess design thermal loads according to geographical location. Both the modulus of elasticity and ultimate stress were found to degrade with temperature, while maximum strain increased linearly with temperature. Simple temperature adjustment factors for both strength and material stiffness are proposed to adjust for different in-service temperatures. Strength values for temperatures below 37.8ºC (100ºF) call for a factor of

0.8 in both compression and tension. For temperatures between 37.8ºC (100ºF) and 51.7ºC (125ºF), factors of 0.70 and 0.80 for compression and tension respectively were determined. A third temperature level, between 51.7º and 65.6ºC (125º and 150ºF), requires a tension factor of 0.70 and a compression value of 0.60. And for temperatures greater than 65.6ºC (150ºF), factors of 0.50 and 0.60 for compression and tensile failure modes, respectively, are recommended. To reduce material stiffness at high temperatures, this work recommends factors of 0.70 and 0.80 for tension and compression, respectively for temperatures between ambient and 37.8ºC (100ºF). Between 37.8 and 51.7ºC (100 and 125ºF) factors of 0.60 for tension and 0.70 for compression should be applied. Higher temperatures, between 51.7ºC and 65.6ºC (125 to 150ºF), would require greater reductions of 0.50 in tension and 0.60 in compression. Lastly, for temperatures above 65.6ºC (150ºF), factors of 0.40 and 0.50 were determined for tension and compression, respectively.

2.2 Introduction

Wood-plastic composites (WPC) are a class of materials made primarily from a synthetic thermoplastic and natural fibers. Currently, WPC materials are primarily used in applications with low structural demands; such as automobile substrates, residential decking, deck rails, and windows (Clemons, 2002). Water-resistance, durability, and low maintenance are intrinsic features emphasized and have driven WPCs to applications where less emphasis is given to structural performance. Inherent beneficial qualities combined with the prospect of improved structural function in strength, material stiffness and long-term performance, give WPCs significant advantages over traditional materials in select applications where structural performance is the primary focus.

To address the market expansion into more-demanding structural applications, a testing and evaluation process to ascertain allowable design values must be established. However, because of the variability among WPC formulations, it has been difficult to fully characterize the behavior of the entire material class. Specific formulations of WPCs vary in thermoplastic and wood type, as well as various polymeric and inorganic additives. The most commonly used thermoplastics are polyethylene (PE), polyvinyl chloride (PVC), and polypropylene (PP), whereas frequently used wood species include pine, maple, and oak (Wolcott, 2001; Clemons, 2002). Previous research has addressed the mechanical performance of different formulations due to the components included (i.e. polymer type, wood species, wood form, coupling agents, etc.), as well as a comparison of performance in different loading modes (i.e. tension, compression, flexure and dowel bearing) (Haiar, 2000; Adcock et al., 2001; Slaughter, 2004; Kobbe, 2005). However, little data has been published to characterize the influence temperature has on

the performance of WPCs. Testing to develop temperature-dependent performance characterization for this one formulation will outline a testing procedure by which other formulations can be tested and compared, perhaps allowing for a more general WPC characterization in the future.

This research is focused on the influence service temperature has on the constitutive relations and ultimate performance of a polypropylene-based WPC formulation. Elevated temperature performance is especially important for WPCs because the thermoplastic component exhibits strong temperature dependence for both static and time-dependent behaviors. The use of thermally stable fillers (e.g. wood) within the plastic phase decreases the effect that temperature exerts upon a thermoplastic. Central to this work is establishing the degree to which elevated in-service temperatures influence strength and MOE performance.

In support of developing a methodology to assess the temperature dependence of mechanical properties for WPCs, the specific objectives of this work are to:

1. Quantify the changes in ultimate stress, maximum strain and elastic modulus over a valid service temperature range.
2. Use analytical models to describe constitutive relations for this material over a range of service temperatures.
3. Develop temperature-dependent adjustment factors for design of WPC materials by evaluating the changes in mechanical performance with temperature.

2.3 Materials and Methods

The WPC was manufactured using a formulation composed of 58.8% pine (*Pinus spp.*) flour, 33.8% Polypropylene (PP), 4.0% talc, 2.3% maleated polypropylene (MAPP) and 1.0% lubricant by mass (Slaughter, 2004). Manufacturer details for each specific product included can be found in Table 2.1. Commercial 60-mesh pine (*Pinus spp.*) flour was dried in a steam tube dryer to a moisture content of less than 2%. The formulation components were dry-blended in powder form using a 1.2-m (4-ft) drum mixer in a series of 25-kg (55-lb) batches. An 86-mm conical counter-rotating twin-screw extruder (Cincinnati-Milacron TC 86), operating between 5 to 12 rpm, was used to produce the sections from which specimens were obtained. Barrel and screw temperature profiles were pre-arranged according to previous research (Kobbe, 2005) and are included in Table 2.2.

The formulated WPC material was extruded into a three-box cross-section using a stranding die (Laver, 1996). The section (Figure 2.1) had overall nominal dimensions of 45.7 by 165.1-mm (1.8 by 6.5-in) with nominal wall and flange thicknesses of 10.2-mm (0.4-in). Test specimens were machined from 1.22-m (4-ft) lengths of this extruded profile. The dimensions of individual tension and compression specimens were measured using digital calipers, recorded and used in all property calculations (i.e. cross-sectional area).

2.3.1 Mechanical Testing

Mechanical testing was conducted to determine material properties at various temperatures. To achieve this, a 222-kN (50-kip) servo-hydraulic test frame (MTS 810 with MTS 407 controller) was used for load application. Data was collected during

testing by computer at a sampling rate of 2-Hz. Displacement over a 25.4-mm (1-in) gauge length was measured using an extensometer (MTS Model 634.12E-24). Applied loads were determined by a 22.2 and 244.7-kN (5-kip Interface 1210AJ-5k-B and 55-kip MTS 661.22C-01) in-line load cell for tension and compression tests, respectively. A constant strain rate of 0.01-mm/mm was applied by a controlled crosshead displacement rate of 2.03-mm/min (0.08-in/min) for both tension and compression.

An environmental chamber was mounted within the test frame to control test conditions at a variety of potential service temperatures. Specifically, tests were conducted at 21.1°, 30°, 40°, 50°, 65.6° and 80°C (70°, 86°, 104°, 122°, 150° and 176°F) within a tolerance of ±2°C (9°F) throughout any given test. It was considered that the mechanical behavior of the material could potentially be affected by molecular rearrangement at higher temperature tests, thereby relaxing potential processing stresses in some, higher-temperature, test temperatures but not all conditions. This concern was addressed by conditioning all specimens at 65.6°C (150°F) for 48-hours prior to testing at any of the prescribed service conditions. This temperature was judged as an appropriate upper bound to the realistic service conditions At each temperature level, 28 specimens were tested to ensure a representative average value and to allow for a valid 5% exclusion limit at 75% confidence level if needed.

The modulus of elasticity (MOE) of this material was determined using a secant modulus technique, applied between 5% and 10% of ultimate load (Kobbe, 2005). This procedure was adopted to maintain consistency in analyzing the nonlinear stress-strain behavior of this material.

2.3.1.1 Tension

Mechanical properties in tension were established by following procedures outlined in ASTM D683 with the exceptions of the test temperature and conditioning procedures. Type III dog-bone specimens were sampled from the top and bottom flanges of the three-box boards. During preparation, the flanges were cut and planed to ensure uniform thickness and eliminate surface defects. These planed flanges were then cut to the required dimensions and shaped to their final configuration using a guide and router.

2.3.1.2 Compression

Mechanical properties in compression were established by following procedures outlined in ASTM D695, except for test temperatures, conditioning procedures, and specimen geometry. Previous experiments testing small-scale compressive specimens according to the ASTM standard have yielded unrepresentative values for full-scale specimen performance. For this reason, a single-box compression specimen 203-mm (8-in) long was cut from the outer boxes of the three-box section (Hermanson, et al., 2001). This specimen was produced by detaching the outer boxes at the two flanges and machining the cut edges until smooth. All specimen dimensions were measured using digital calipers and recorded. These dimensions were used in relevant calculations for section area. The nominal specimen dimensions were 45.7 by 61.0-mm (1.8 by 2.4-in) with four 10.2-mm (0.4-in) thick walls.

2.4 Results and Discussion

2.4.1 Static Mechanical Properties

The temperature dependence of tension and compression properties (σ_{ult}, ε_{max}, and E) are presented in Figures 2.2-2.4; respectively. In general, increases in service temperature resulted in decreased values for σ_{ult} and E, while ε_{max} showed an increase, indicating a more ductile response. Representative mean curves were computed by averaging the load values at common strain levels from the 28 specimens in each loading condition. These curves, along with the fit constitutive relation curves, are found in Figures 2.7 and 2.8 for tension and compression, respectively.

For both tension and compression, σ_{ult} decreased linearly with increasing temperature. At 21.1ºC (70ºF), the ultimate tensile strength of this material was found to be 18.14-MPa (2.631-ksi) and decreased to 12.03-MPa (1.745-ksi) at 80ºC (176ºF). A similar trend is found in compression, however the σ_{ult} at ambient temperature was approximately 4x greater at 48.91-MPa (7.094-ksi). Again, as temperature increased to 80ºC (176ºF), σ_{ult} decreased linearly to 24.90-MPa (3.611-ksi).

When examining ε_{max} values, the tension and compression gain differed in magnitude, with compression displaying a much more ductile response. For tension the ε_{max} linearly doubled from a value of 0.00901-mm/mm at 21.1°C (70°F) to 0.01925-mm/mm at 80°C (176°F). The compression strains were nearly 3.5x larger than tension strains at ambient temperatures. The temperature dependence for ε_{max} in compression was more modest than the tensile trend, however, and remained nearly constant at 0.035-mm/mm regardless of temperature tested.

A decreasing trend for E is expected due to decreasing strength and increasing ductility with respect to temperature. At ambient temperature E values for both tension and compression were nearly identical with values of 3489-MPa (506-ksi) and 3447-MPa (500-ksi) for tension and compression, respectively. In both modes of loading the values of E decreased. In tension, E decreased according to a second-order function to a value of 1593-MPa (231-ksi) at 80ºC (176ºF). In compression, a linear decrease was found and at 80ºC a value of 1751-MPa (254-ksi).

Summary statistics for σ_{ult}, ε_{max}, and E at each temperature level can be found in Table 2.3. For ε_{max}, coefficient of variation (COV) values were between 10% to 16% for tension and 10% to 22% for compression. There was slightly less scatter for the E data where COVs ranged between 9% and 18.5% in tension and 7.5% to 13% in compression. The least scatter among the groups of data is found in ultimate strength. COV values for this were all below 10% with only one exception at 21.1ºC in tension where the value is 11.2%.

Detection of the α-phase transition prompted an investigation into the behavior of polypropylene over the temperature range of interest. Previous research has conducted DMA testing on specimens of neat polypropylene and polypropylene-binder composites that show glass transition at -8ºC (17.6ºF) and an α-phase transition between 70 and 100ºC (158 to 212ºF). These phase transitions of the composite materials at 70ºC exhibit less pronounced changes in the DMA results than neat PP. This decrease in prominence is thought to be a "masking" effect due to including the thermally stable wood phase.

It is proposed that at the α-phase transition a lamellar slip mechanism and rotation of the crystalline phase begins (Amash and Zugenmaier, 1996). Detection of the α-phase

transition is important because it indicates a change in microstructure response to stress and could manifest itself in significant changes in mechanical properties at 75ºC

2.4.2 Constitutive Relations

The non-linear nature of this material requires a more complex relation than materials where linear proportionality exists. Separate works by Conway (1967), Lockyear (1999), Murphy (2003) and Kobbe (2005), have investigated expressions using hyperbolic functions to describe constitutive relations for non-linear materials. Two possible constitutive relations could be appropriate for modeling this material, one utilizing the arc-hyperbolic sine and the other using the hyperbolic tangent functions. Previous research on this specific formulation by Kobbe (2005) has indicated that the arc-hyperbolic sine function with two curve fitting parameters (*a* and *b*) most accurately represents the initial stress-strain behavior:

$$\sigma = a \cdot \mathrm{a}\sinh(b \cdot \varepsilon) \qquad \text{(eq. 1)}$$

Values for the constants *a* and *b* were determined for mean stress-strain curves at all temperatures and are presented in Table 2.4. Values for these constants were determined by minimizing the residual sum of the squares between the predicted and experimental data. The quality of fit can be judged in Figure 2.7 and Figure 2.8, where the constitutive relations are plotted against experimental data.

Clear trends for these empirical parameters can be seen in Figure 2.5 and Figure 2.6 showing a decreasing trend for *a* and an increasing trend for *b* with increasing temperatures. Because of the wide range of temperatures tested, the likely in-service high temperature condition of any user-end application should fall within this range.

Therefore, appropriate constitutive equations can be interpolated from this data to arrive at reasonable predictions.

2.4.3 Development of Design Factors

The mechanical testing results indicate that performance of WPCs is strongly dependent upon temperature. This dependence should therefore lead to adjustments in the allowable design process when elevated in-service temperatures are expected.

Temperature effects for civil engineering materials other than timber do not provide much guidance for expected service temperatures. For steel, concrete, and masonry design, no reductions are proposed for the temperature range studied in this work (Salmon and Johnson, 1996; MacGregor, 1997). Decreases for steel and concrete are only assessed at much higher temperatures for fire-resistance and welding considerations. Because timber construction is the only material widely used within the civil engineering community with temperature-dependent strength, and WPC products are likely to be used as replacements for timber components, an approach similar to timber design is logical to develop. For this reason, the same ranges for temperature factor limits are considered for WPCs as in the timber code; $T < 37.8°C$, $37.8°C < T < 51.7°C$, and $51.7°C < T < 65.6°C$ ($T < 100°F$, $100°F < T < 125°F$, and $125°F < T < 150°F$).

Interpretation of the results presented here suggests that the decrease in E with temperature should also be addressed to appropriately deal with some load-bearing phenomena (i.e. buckling of columns, serviceability limits, etc.). Both strength and material stiffness degradation can be addressed using a factor-based design methodology with timber design as a model to develop these procedures.

2.4.3.1 Proposed Design Factors

To arrive at an appropriate allowable design value for a given loading property (F_x), the mean value of the property must be first adjusted for variability to arrive at a characteristic value (B), that is then further modified by a series of adjustment factors (C_i) which account for service conditions that differ from testing conditions. The following equation has previously been proposed for WPC materials and is similar in form to the NDS method for timber design:

$$F_{allowable} = B * C_a * C_t * C_m * C_v * C_d \quad \text{(eq. 3)}$$

Where:

B represents the characteristic allowable property modified for variability
C indicates various property adjustment factors
Subscripts a, t, m, v, d represent adjustments for safety, temperature, moisture, volume, and load duration; respectively

From strength and MOE trends found in this investigation, an equation to calculate specific C_t factors for specific thermal loads has been found. This equation takes a quadratic polynomial form to encompass second-order effects that are found in material stiffness degradation:

$$C_t = 1 - \beta_1(\Delta T) - \beta_2(\Delta T)^2 \quad \text{(eq. 4)}$$

Where:

C_t is the temperature adjustment for a specific thermal load
$\beta_{1,2}$ are empirical coefficients (Table 2.5)
ΔT is the difference in thermal load temperature from ambient (21.1°C or 70°F)

Equation 4 can be applied to calculate reduction factors for both strength and E. Furthermore, investigating the reduction of these properties indicated unique decreases in properties between tension and compression. Therefore, different empirical factors

should be applied to calculate the thermal reduction parameter depending on the mode of loading that a member will experience. Table 2.5 contains the empirical β-coefficients that apply to Equation 4 above.

A more simplified approach can also be employed to determine the C_t factor for these materials. This approach considers temperature ranges over which a single reduction factor is calculated. Values of C_t have been calculated for the same temperature intervals as the NDS approach for timber design and are presented in Table 2.6. It is important to mention that this approach is always conservative by converting the prevailing temperatures to the low end of the interval.

Comparing the approach developed here with previous attempts to determine temperature adjustment factors offers four obvious differences. First, this study has determined a strong dependence between loading mode and degradation path. This is most clearly illustrated in Figures 2.9 and 2.10 by the difference between tension and compression values for C_t. Secondly, is the ability to calculate a case-specific thermal adjustment by presenting an equation-based method to determine the temperature reduction factor. This will allow for full utilization of these materials rather than only providing an approach that may unduly penalize the performance of the material at the low end of a temperature range. Next, a method to determine thermal loads follows in this work to determine thermal loads where no approach had previously been suggested to the knowledge of the author. Lastly, the magnitudes of the reduction factors found here are different than those previously proposed for the same temperature intervals proposed by the NDS and similar to the ranges previously approximated for WPCs (Haiar, 2000; NDS, 2001).

2.4.3.2 Considerations for Thermal Loads

Reductions to WPC strength and material stiffness with increased temperature are more severe than for timber because a stronger temperature dependence exists. Furthermore, because the loss in strength and MOE for timber at high temperatures is often offset by gains from lower moisture contents, most residential construction assesses no adjustment (Breyer, et al., 1999, NDS 2005). Application of temperature factors in timber design focuses upon sustained temperatures upon a member due to the slow strength degradation wood undergoes at high temperatures. Degradation in timber is due to hydrolysis of the hemicellulose components and is non-recoverable due to the chemical breakdown of components.

A different approach is appropriate for WPCs because strength and material stiffness degradation occur quickly. Mechanical performance decreases with temperature in WPCs because of a softening of the thermoplastic matrix, rather than chemical degradation as in the case of timber. Strength and MOE of WPCs is recoverable then as the temperature decreases and the polymer matrix hardens. It is still unclear the degree to which these properties recover after heating. Transient periods of high temperature must therefore be evaluated in the design process to coincide with the worst-case performance of the material, rather than a sustained load approach where appreciable short-term decreases in strength and MOE may be overlooked. It is important then to address what temperature should be considered a design level temperature.

Many design loads are considered on a 50-year recurrence timeframe (i.e. snow loads in the International Building Code (IBC)). This will provide a temperature that should be exceeded only once every 50-years, and probabilistically should only have a 2-

percent annual likelihood of being exceeded. This approach is recommended to find a thermal load for WPCs based on air temperature with regard to geographical location. One credible source for data to calculate the 50-year temperature is the ASHRAE Fundamentals Handbook (ASHRAE, 2001). This source includes extreme air temperature annual daily maximums, the standard deviation of those maximums with respect to all historical data present for a given location, and the equation used to calculate the 50-year maximum temperature. This extreme annual mean and standard deviation data is presented in tabular form for hundreds of cities in the United States and Canada, as well as for select other cities worldwide.

Following are example calculations for two locations in the United States with very different climate considerations:

Parameter	Phoenix, Arizona	Seattle, Washington
The Mean Extreme Annual Temperature	45.5°C (114°F)	33.3°C (92°F)
Standard Deviation of the Mean Extreme Temperature	1.2°C (2.2°F)	2.0°C (3.6°F)
Extreme Hourly Temperature with a 50-yr Recurrence	48.9°C (120°F)	38.3°C (101°F)

The mean extreme annual temperatures are found in Table 1A of the ASHRAE Fundamentals Handbook (ASHRAE, 2001) and the process outlined in Chapter 27 of that resource. The temperature load to consider for design is calculated using the following equation found in ASHRAE and is based upon an assumed Gumbel distribution fitted with the method of moments:

$$T_n = M + (F \cdot s) \qquad \text{(eq. 2)}$$

Where:

T_n is the n-year return period value for ambient air temperature

M is the mean extreme annual temperature (column 6a of Table 1A (ASHRAE, 2001))

s is the standard deviation of the extreme annual temperature (column 6c of Table 1A(ASHRAE, 2001))

$$F = \frac{-\sqrt{6}}{\pi}\left\{0.5772 + \ln\left[\ln\left(\frac{n}{n-1}\right)\right]\right\} = 2.59228 \text{ if n=50-years}$$

Not all locations in the United States are included in ASHRAE tables. In this case, it is recommended to contact a local source for information on extreme temperatures with as much historical data as possible. This is similar to the IBC approach for undocumented snow loads.

Furthermore, appropriate engineering judgment must be employed when considering temperatures at which loads will be applied. At high temperatures when solar incident heating would occur, oftentimes the application will not see full design loads. The difficulty in addressing issues such as solar incident heating and assessing non-uniform thermal gradients within a cross-section is a lack of a standardized method to address these issues. Until a standardized process is established to account for these influences, the judgment of competent design engineers must be trusted. A designer must consider the probability of experiencing both solar incident heating and full design load, keeping in mind that reductions for strength and material stiffness are temporary while high-temperature conditions exist. Furthermore, in applications such as decking superstructures, to achieve a full design load on the deck would effectively block the sunlight from the members themselves and negate any incident effects. Heating effects beyond ambient air temperature must be considered on an individual application basis,

with reasonable assessment for the application of loads and applicability of additional heating.

2.4.3.3 Considerations for Implementation

Final implementation of temperature factors should include some consideration for the mode of failure for the designed member. When members are constructed for only compressive loadings, factors based on the compressive testing here would recommend values of 0.80, 0.70, 0.60, and 0.50 for the respective temperature ranges of the previous section (Section 2.4.3). This would apply to situations like deck foundation columns where only compressive axial forces are of interest. Similarly, calculations for buckling stress and other performance issues relating to stiffness should be checked using a reduced E in order to ensure adequate stiffness during high temperature conditions.

If the mode of loading is a flexural or pure tensile application, the σ_{ult} temperature factors should more closely resemble the tensile factors of 0.80, 0.80, 0.70, and 0.60. At a "design level" stress, a flexural member would be designed such that maximum tensile and compressive stresses are less than or equal to approximately 40% of their respective ultimate strengths. At this loading level, compressive and tensile behavior should be roughly equal in magnitude (Kobbe, 2005). However, the disparity between compressive and tensile capacities is such that a load level equal to the ultimate design level stress in tension (40% of 2630 psi or 1052 psi) would only be 15% of the compressive capacity on the opposite extreme fibers in the member. Thus, failures will initiate in the tensile face of flexural members (Kobbe, 2005). The factors developed for the tensile failure mode would then be the appropriate mode to combat flexural failure. Applying the more

conservative (smaller in magnitude) compressive factors would create an overly conservative case because of the disparity in strength between tension and compression.

2.5 Conclusions

Experimental results have provided the opportunity to track the performance of a pine-polypropylene composite material over a temperature range of 21.1ºC (70ºF) to 80ºC (176ºF). Different magnitudes of σ_{ult} were measured for tension and compression, but the trend for both loading modes with respect to increasing temperature both decrease linearly. Tension loadings for ε_{max} increased appreciably with temperature, whereas a nearly constant maximum strain was determined for compression regardless of temperature. E in both tension and compression both measured near 3447-MPa (500-ksi) at ambient temperatures and decreased by nearly half of that at 80ºC (176ºF), with a linear inverse relationship in compression and a quadratic relationship for tension.

The nonlinear behavior of this material class dictated that an arc-hyperbolic sine function with two empirically fit parameters be used to adequately describe the constitutive behavior of this material. An inverse relationship between the first empirical parameter, *a*, while a direct relationship for the second parameter, *b*, was determined to occur with increasing temperatures. Correct determination of constitutive relations with respect to temperature will allow for more accurate analytical results from finite element, moment curvature or other analytical tools.

One possible method for determining thermal loads upon a structure based upon geographical location was explored, and sample calculations were presented. This method is based on historical climactic data in the ASHRAE Handbook and has solid

engineering principles supporting it. A 50-year extreme maximum temperature is recommended for design. However, proper engineering judgment and consideration of competing factors (i.e. reduced live loads at high temperatures and issues regarding solar incident heating) should be taken into account by the individual designer for appropriate use of these materials.

Based upon the test results and trends over this temperature range, adjustment factors were proposed at temperature levels similar to timber design for both ultimate stress and material stiffness in tension and compression. Considering ultimate stresses, for ambient temperature to 37.5ºC (100ºF) a reduction of 0.80 is appropriate for both tension and compression members. The next temperature range is between 37.8ºC (100ºF) and 51.7ºC (125ºF) and factors of 0.80 and 0.70 for tension and compression, respectively were determined. The next range found factors of 0.70 for tension and 0.60 for compression and applies between 51.7ºC and 65.6ºC (125ºF to 150ºF). Above 65.6ºC (150ºF) a factor of 0.60 for tension and 0.50 for compression will appropriately reduce the allowable stress allowed on a member to account for the reduction of strength at the elevated temperature condition.

MOE reductions similar to those for σ_{ult} are also proposed for the same temperature levels to address decreases in E. From ambient to 37.8ºC (100ºF) factors of 0.70 and 0.80 were determined for tension and compression, respectively. Above that, for temperatures between 37.8ºC (100ºF) and 51.7ºC (125ºF) reduction values of 0.50 and 0.60 apply for tension and compression. Lastly, at temperatures greater than 65.6ºC (150ºF), factors of 0.40 and 0.50 are recommended to adequately reduce E.

2.6 References

Adcock, T., Hermanson, J.C., and Wolcott, M.P., "Engineered Wood Composites for Naval Waterfront Facilities." Washington State University, Project End Report. June, 2001

Amash, A., and Zugenmaier, P., "Thermal and Dynamic Mechanical Investigations on Fiber-Reinforced Polypropylene Composites." Journal of Applied Polymer Science, Vol. 63, Iss. 9, pp.1143-1154, 1997.

ASHRAE Handbook, Fundamentals. "Climactic Design Information." Chapter 27, American Society of Heating, Refrigerating and Air-Conditioning Engineers, Inc., 2001.

ASTM D683-99, "Standard Test Methods for Tensile Properties of Plastics." American Society for Testing and Materials, 1999.

ASTM D695-96, "Standard Test Methods for Compressive Properties of Rigid Plastics." American Society for Testing and Materials, 1996.

Breyer, D.E., Fridley, K.J., and Cobeen, K.E., "Design of Wood Structures ASD." Fourth Edition, pp. 4.45. McGraw-Hill, New York, NY, 1999.

Clemons, C., "Wood-Plastic Composites in the United States, The Interfacing of Two Industries." Forest Product Journal, Vol. 52, No. 6., pp. 10-18, 2002.

Conway, J.B., "Numerical Methods for Creep and Rupture Analyses." Gorgon and Breach, Science Publishers, Inc., New York, NY, 1967.

Haiar, K.J., "Performance and Design of Prototype Wood-Plastic Composite Sections." Master Thesis, Washington State University, May 2000.

Hermanson, J.C., Adcock, T., and Wolcott, M.P., Evaluation of Extruded Materials Group, "Project End Report." Washington State University, 2001.

Kobbe, R.G., "Creep Behavior of Wood-Polypropylene Composites." Master Thesis, Washington State University, June 2005.

Laver, T.C., "Extruded Synthetic Wood Composition and Method for Making Same." Patent Number 5,516,472. 1996.

Lockyear, S.A., "Mechanical Analysis of Transversely Loaded Wood/Plastic Sections." Master Thesis, Washington State Universtiy, December 1999.

MacGregor, J.G., "Reinforced Concrete: Mechanics and Design." Third Edition, pp. 74-75. Prentice-Hall, Inc., Upper Saddle River, NJ, 1997.

Murphy, J.F., "Characterization of Nonlinear Materials." USDA Forest Products Laboratory Technical Note, Madison, WI. December 31, 2003.

National Design Specification for Wood Construction (NDS). Section 2.3.3 and Apendix C. American Forest and Paper Assosciation, 2005.

Salmon, C.G., and Johnson, J.E. "Steel Structures: Design and Behavior." Fourth Edition, pp. 55-56. Prentice-Hall, Inc., Upper Saddle River, NJ, 1996.

Slaughter, A.E., "Design and Fatigue of a structural Wood-Plastic Composite." Master Thesis, Washington State University, August 2004.

Wolcott, M.P., "Wood-Plastic Composites." In: Encyclopedia of Materials: Science and Technology, pp. 9759-9763, Ed. Buschow et al., Elsewier Press, NY, 2001.

2.7 Tables

Table 2.1. Product details for extruded materials.

Material	Manufacturer	Product
Polypropylene	Solvay	HB9200
Pine Flour	American Wood Fibers	#6020
Talc	Luzenac	Nicron 403
Coupling Agent	Honeywell	950P
Lubricant	Honeywell	OP100

Table 2.2. Extruder temperature profile for all material produced.

		Temperature, ºC (ºF)
Barrel Zone	1	188 (370)
	2	188 (370)
	3	185 (365)
	4	182 (360)
Screw		182 (360)
Die Zone	1	182 (360)
	2	185 (365)
	3	188 (370)

Table 2.3. Mean values for testing parameters with respect to loading mode and temperature of test. (COV values shown in second line of each cell)

	Tension			Compression		
Temperature (ºC)	σ_{ult}, MPa (ksi)	ε_{max}	E, MPa (ksi)	σ_{ult}, MPa (ksi)	ε_{max}	E, MPa (ksi)
21.1	18.14 (2.630) 11.19%	0.0090 15.06%	3487.3 (505.8) 18.29%	48.91 (7.094) 5.25%	0.0315 21.26%	3434.9 (498.2) 12.72%
30.0	17.49 (2.537) 9.41%	0.0115 15.74%	3047.1 (442.0) 17.69%	43.54 (6.315) 6.19%	0.0343 11.31%	3074.4 (445.9) 10.65%
40.0	15.30 (2.219) 6.20%	0.0128 16.74%	2367.1 (343.3) 16.00%	40.08 (5.813) 6.99%	0.0367 17.43%	2787.5 (404.3) 7.76%
50.0	14.36 (2.082) 7.63%	0.0148 11.08%	1990.9 (288.8) 16.16%	35.85 (5.200) 4.13%	0.0366 10.39%	2474.4 (358.9) 8.08%
65.6	12.77 (1.852) 8.51%	0.0173 13.19%	1794.0 (260.2) 9.56%	29.47 (4.274) 3.81%	0.0358 14.48%	2059.2 (298.7) 9.64%
80	12.03 (1.745) 8.04%	0.0193 10.76%	1593.9 (231.2) 10.17%	24.90 (3.611) 2.63%	0.0357 11.89%	1755.7 (254.6) 9.04%

Table 2.4. Values for the parameters, *a* and *b*, for the constitutive relation modeling at each temperature for each mode of loading.

Temperature (ºC)	Tension		Compression	
	a (MPa)	b	*a* (MPa)	b
21.1	9.35	387.91	19.12	213.93
30.0	8.20	402.63	16.02	236.87
40.0	6.79	400.54	14.59	242.91
50.0	6.20	383.82	12.06	292.53
65.6	4.90	468.80	9.38	351.25
80.0	4.62	441.21	7.66	385.85

Table 2.5. Summary of β-coefficients for the equation form to calculate C_t.

	σ_{ult}		E	
	Tension	Compression	Tension	Compression
β1	6.329E-3	8.755E-3	1.918E-2	8.807E-3
β2	0	0	-1.719E-4	0
R^2	0.961	0.986	0.989	0.983

Table 2.6. Summary of recommended temperature adjustment factors for σ_{ult} and E.

Temperature, ºC (ºF)	σ_{ult}		E	
	Tension	Compression	Tension	Compression
T < 37.8 (T < 100)	0.80	0.80	0.70	0.80
37.8 < T < 51.7 (100 < T < 125)	0.80	0.70	0.60	0.70
51.7 < T < 65.6 (125 < T < 150)	0.70	0.60	0.50	0.60
T > 65.6 (T > 150)	0.65	0.50	0.40	0.50

2.8 Figures

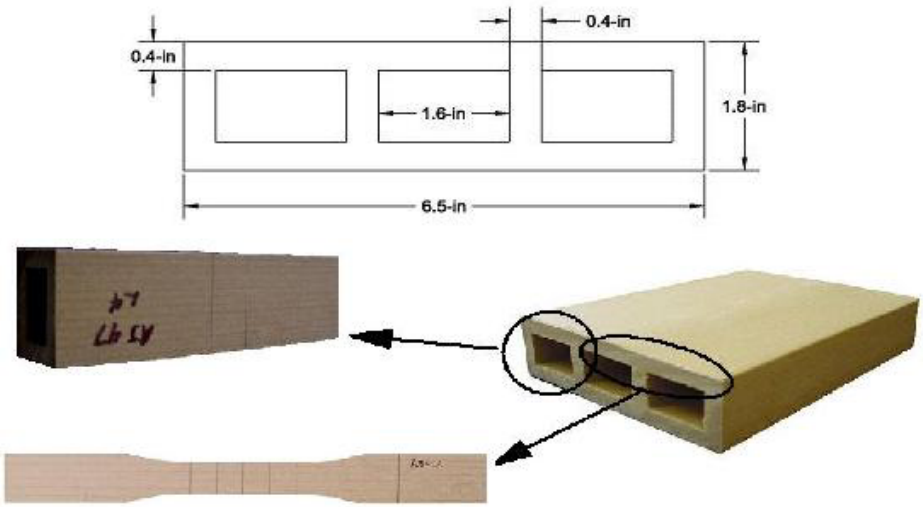

Figure 2.1. Triple box extrusion profile including nominal member dimensions, along with specimen location in cross-section.
(Kobbe, 2005)

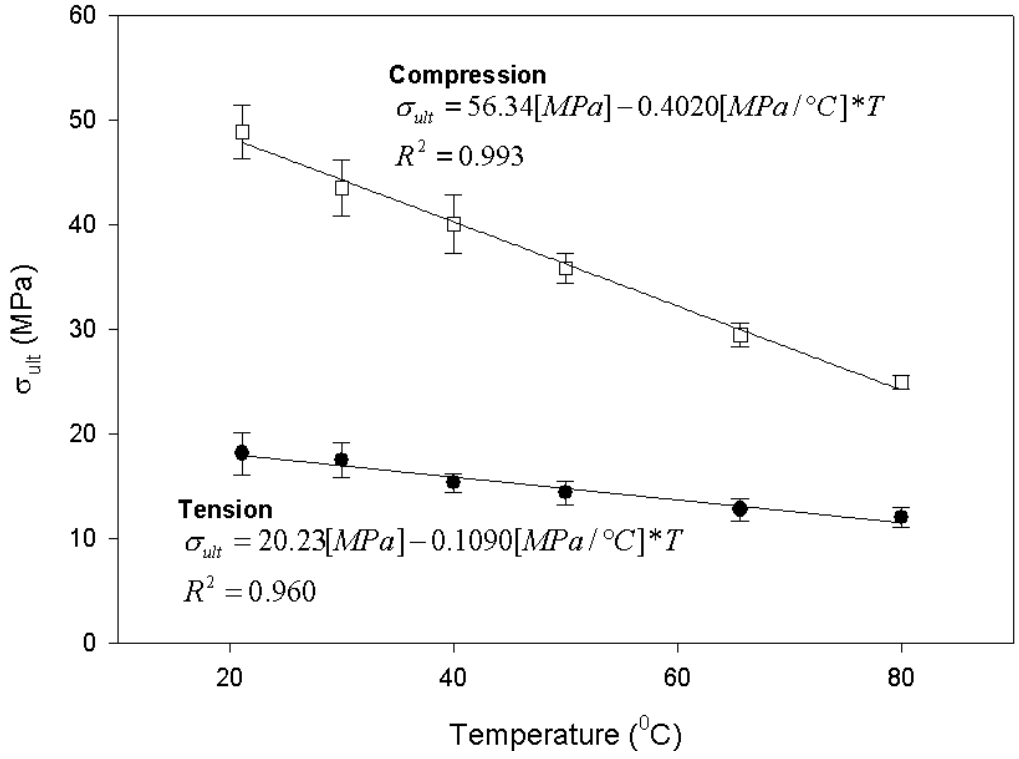

Figure 2.2. Relationship between maximum specimen stress and increasing temperature.

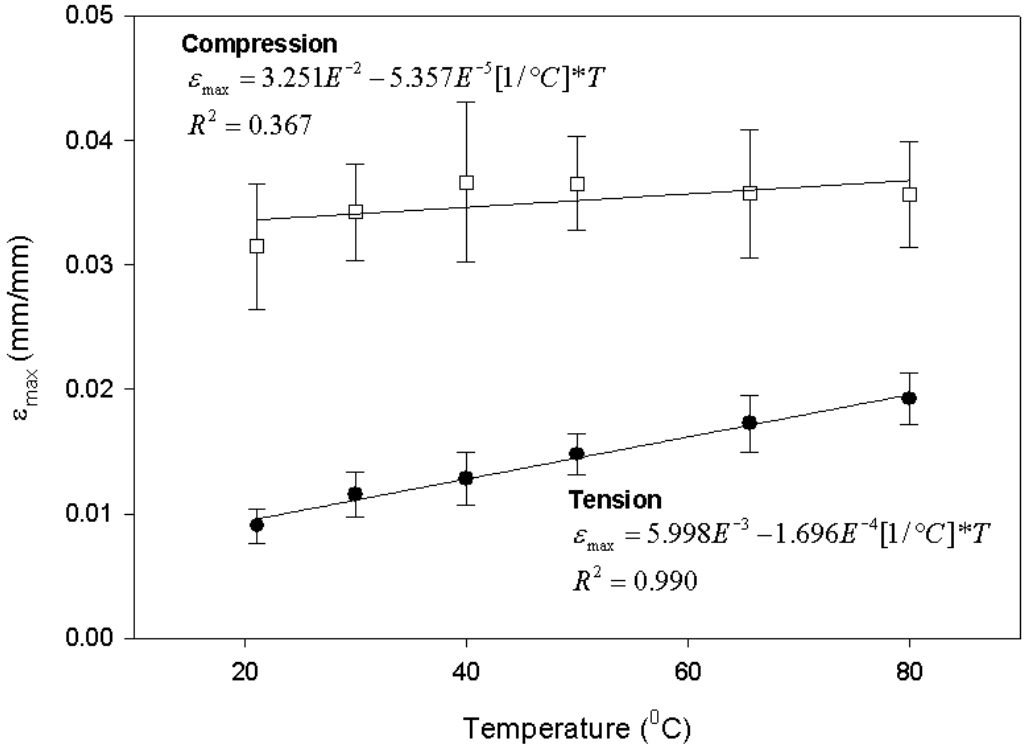

Figure 2.3. Relationship between maximum specimen strain and increasing temperature.

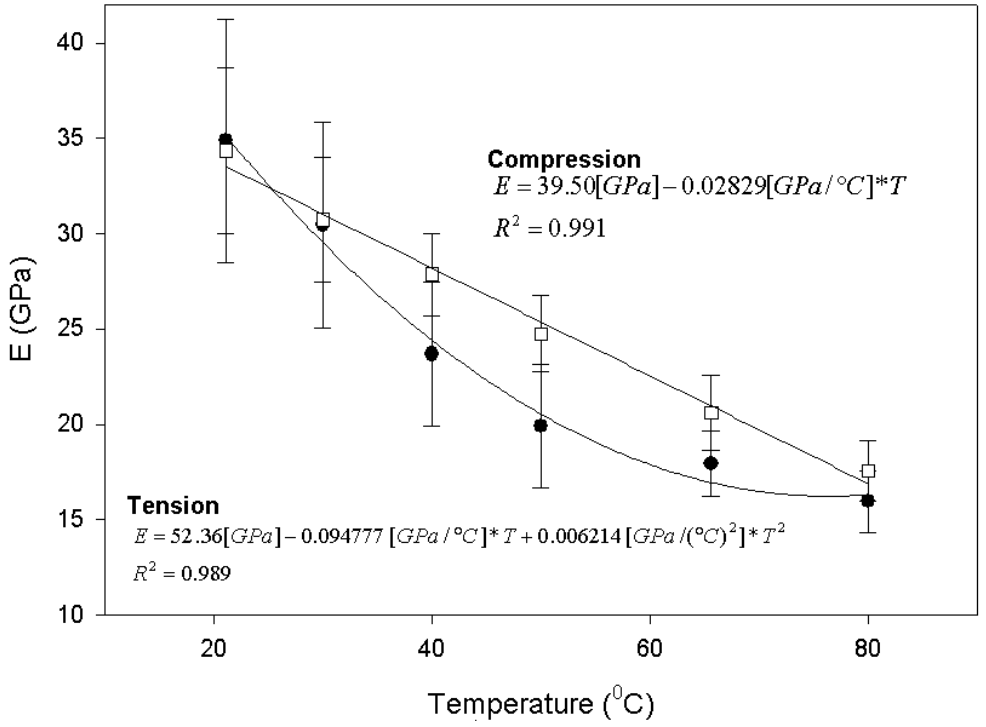

Figure 2.4. Relationship between secant elastic modulus with respect to temperature.

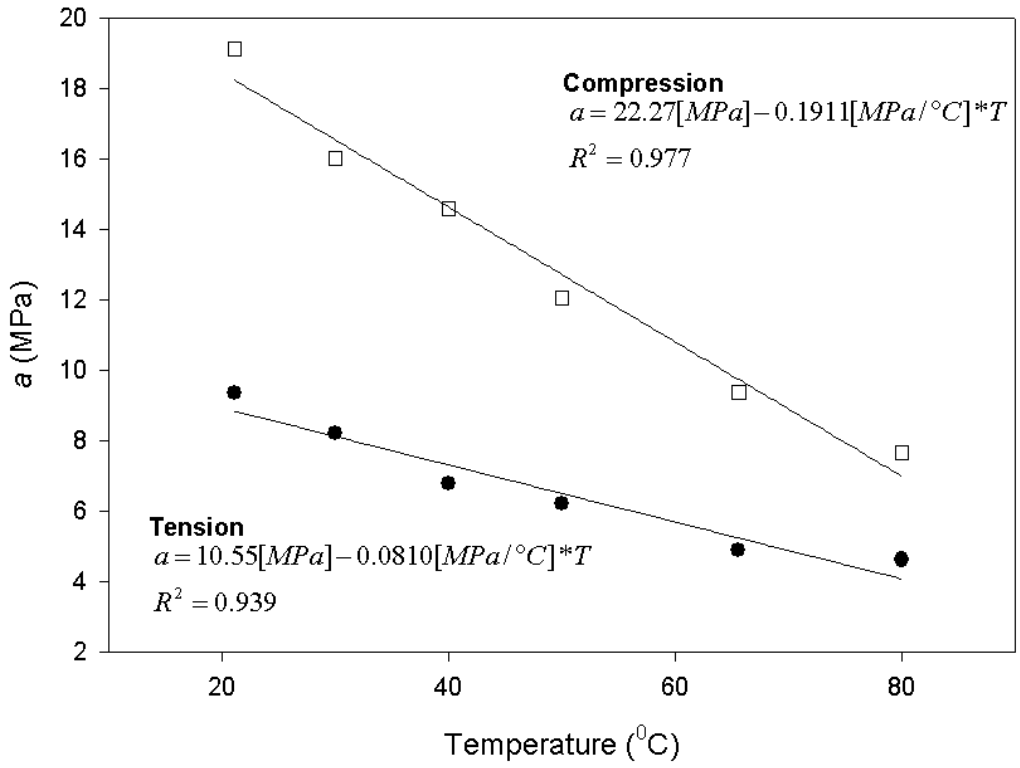

Figure 2.5. Curve fitting constitutive relation parameter "a" with respect to temperature.

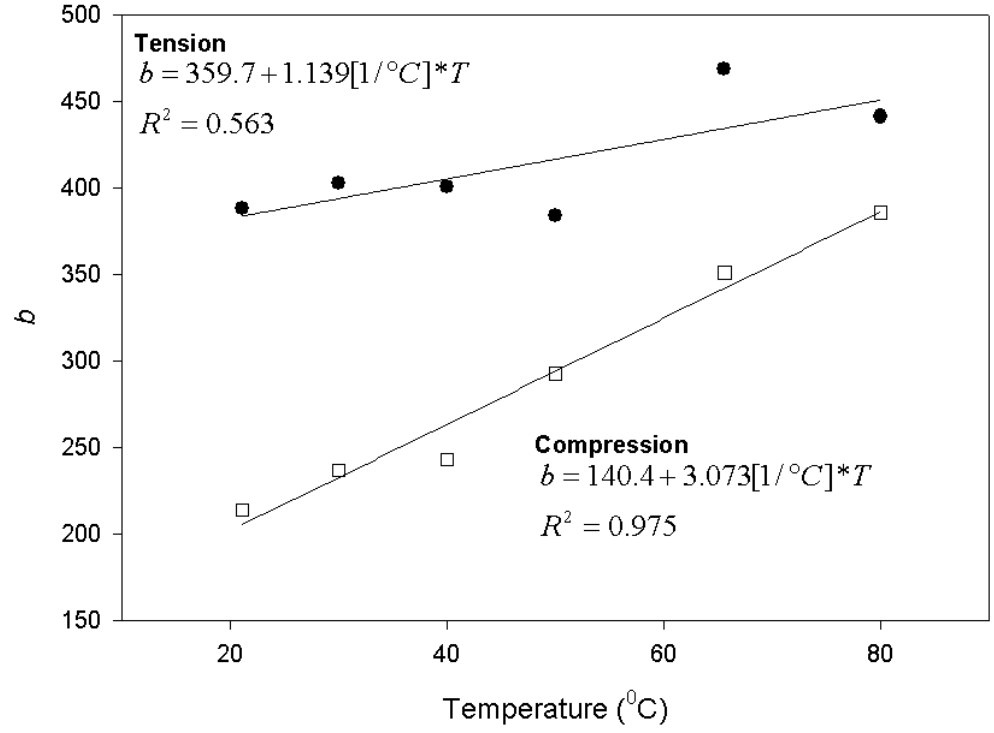

Figure 2.6. Curve fitting constitutive relation parameter "b" with respect to temperature.

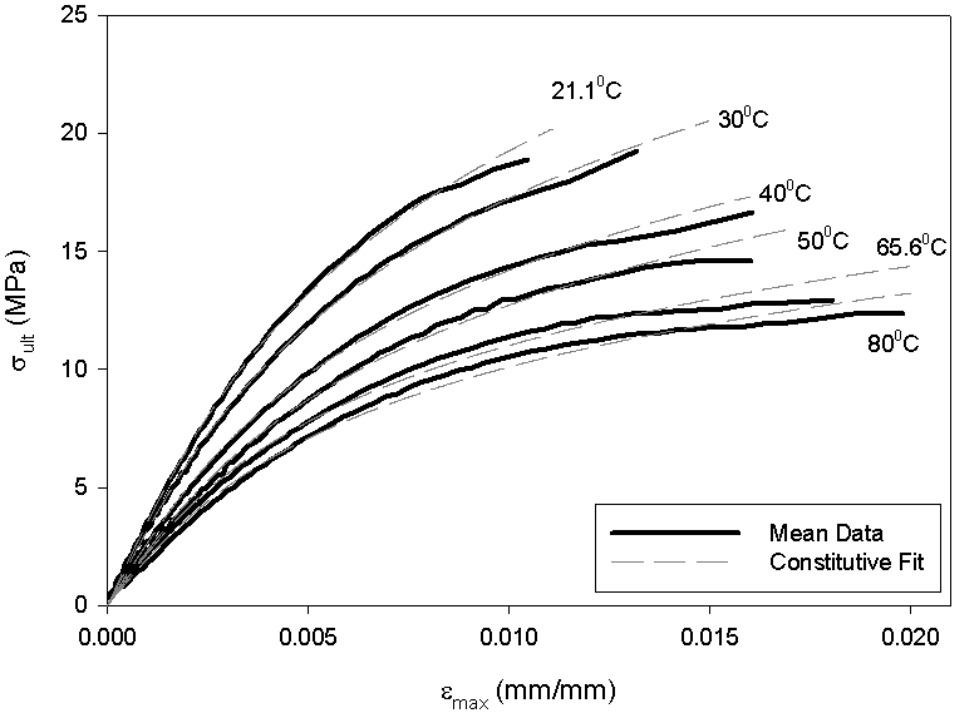

Figure 2.7. Mean tensile testing curves (solid lines) for each temperature level along with the fit curves using the arc-hyperbolic sine model (dashed, gray lines).

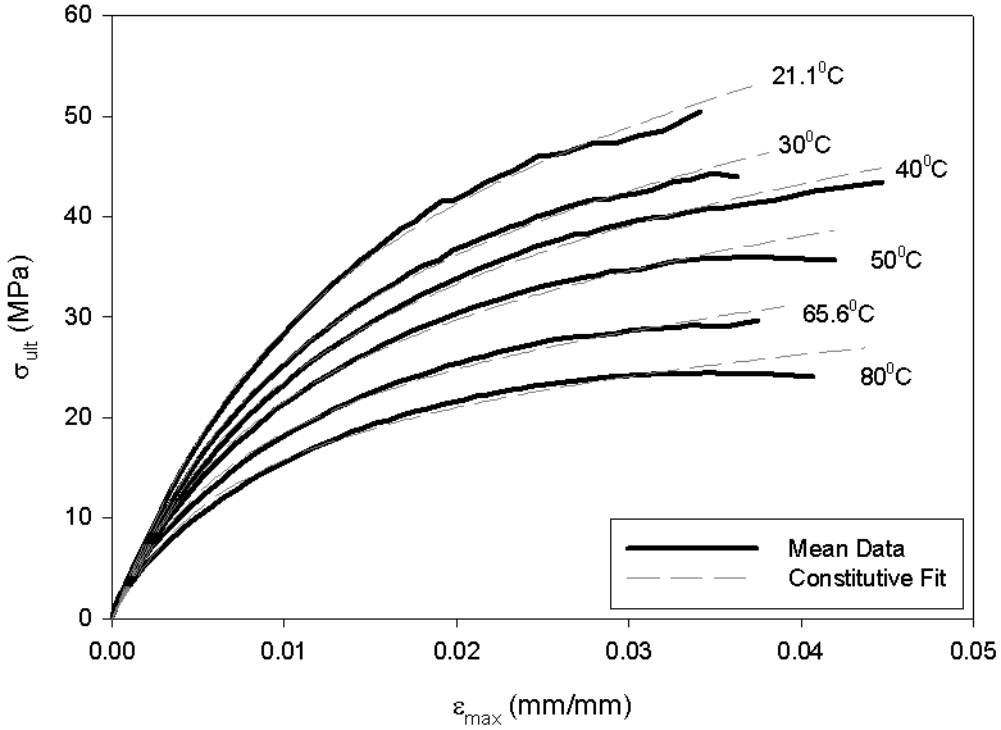

Figure 2.8. Mean compressive testing curves (solid lines) for each temperature level along with the fit curves using the arc-hyperbolic sine model (dashed, gray lines).

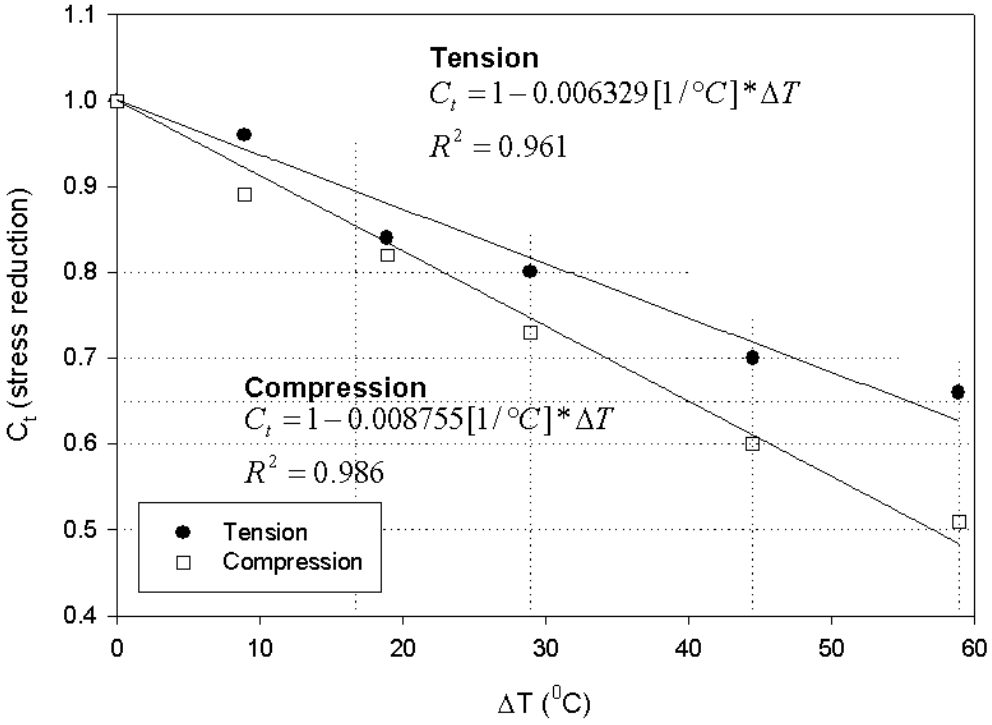

Figure 2.9. Temperature adjustment factor with change from ambient temperature (stress adjustments).

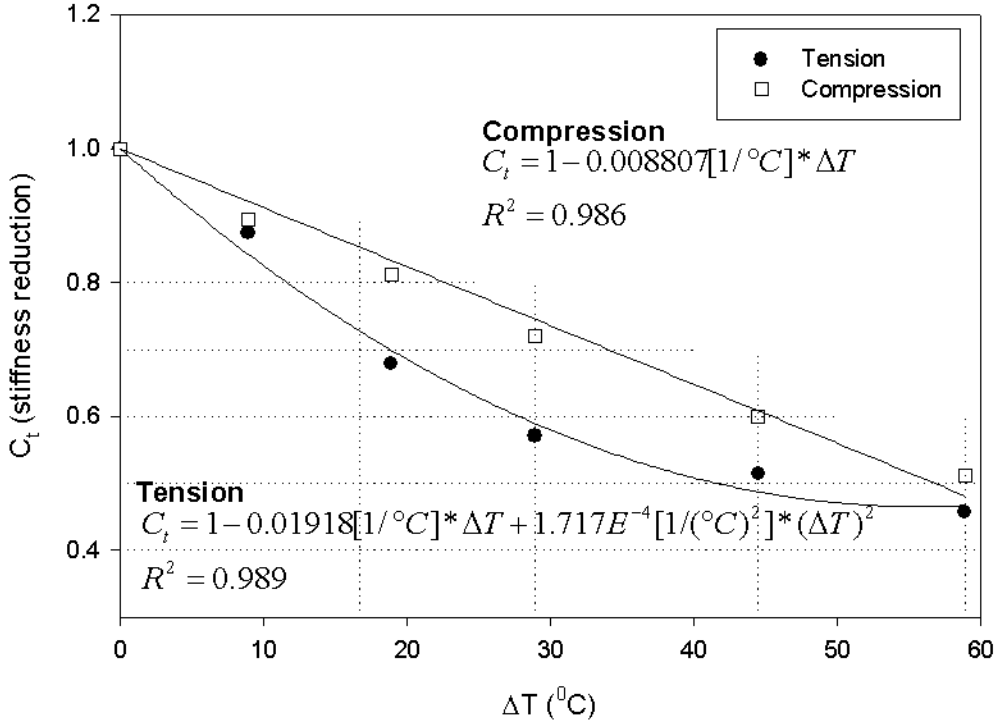

Figure 2.10. Temperature adjustment factor with change from ambient temperature (material stiffness adjustment).

CHAPTER THREE

TIME-DEPENDENT BEHAVIOR OF A STRUCTURAL POLYPROPYLENE-PINE COMPOSITE

3.1 Abstract

New, more structurally demanding, applications for wood plastic composites (WPCs) require improvements in mechanical performance while also maintaining inherent non-structural advantages (e.g. durability, moisture resistance and low maintenance). Published research investigating long-term deformation behavior (creep) of WPCs is insufficient to adequately develop engineering assumptions for performance of these materials in demanding structural applications. The research presented here examines the creep behavior of a polypropylene-pine formulation in tension and compression. The polypropylene/wood composite material was dry-blended and extruded using a conical twin screw extruder. A battery of 100-minute creep experiments were conducted at five temperature levels between 21.1°C and 65.6°C. These short-term creep tests were used to develop temperature-dependent modeling parameters of a Findley power law fit to this data. Secondly, the time-temperature superposition principle (TTSP) is applied to the short-term test data to generate master curves for this material with the goal of potentially predicting long-term behavior at full structural load to an approximate 10-year structural design condition. This study was unable to achieve the targeted time scale, but was able to achieve 5.7 and 2.7-year master curves in tension and compression, respectively. This is a considerable improvement in predictive value from a previous study on the same material using stress as a time accelerant. Upper and

lower 95th percentile curves for tension and compression creep are included to facilitate the application of creep data to structural design considerations. TTSP shows potential as an accelerated test method to predict long-term performance, and may be more useful than techniques previously explored.

3.2 Introduction

Wood-plastic composites (WPCs) are a class of material made primarily from a synthetic thermoplastic matrix and natural fiber reinforcement. Development of WPCs has traditionally focused on intrinsic properties such as moisture resistance, durability and low maintenance costs rather than structural performance (strength and material stiffness). Therefore, WPC markets have been limited (i.e. automobile substrates, residential decking, deck rails, and windows). Recent research of WPCs has increased focus on structural performance, but additional research is needed to facilitate full structural implementation. Early studies on structural performance have investigated short-term strength and material stiffness and provide insight into one facet of code implementation (Haiar, 2000; Slaughter, 2004; Wolcott and Smith, 2004). Brandt and Fridley (2003) have evaluated various formulations of WPCs to assess load-duration performance and suggest a method to account for this behavior in structural design. Little consideration has been paid to developing performance adjustments for design value assignment, rather than failure criteria such as found by Brandt and Fridley (2003). Furthermore, evaluation methods to develop these adjustments should be as economical and efficient as possible to reduce impediments for new product assessment. To further facilitate structural implementation, the long-term strength and MOE must be better understood and evaluative tools developed.

Creep is the accumulation of strain in a member over time when subjected to a constant stress and is important to applications where long-term loads must be supported. Much previous work has been conducted on creep of plastics and synthetic fiber-reinforced plastics (Findley, 1960; Lou and Schapery, 1971; Brinson et. al., 1978;

Brinson and Dillard, 1982; Findley, 1987) but fewer studies address WPCs (Sain et. al., 2000; Pooler and Smith, 2004; Kobbe, 2005). WPCs exhibit a nonlinear viscoelastic behavior with significant creep deflections that are dependent on the stress level (Kobbe, 2005). However, this stress dependency appears to be thermo-rheologically simple and therefore TTSP may be applicable (Pooler and Smith, 2004). An extensive examination of thermo-rheological simplicity is presented by Wortmann and Schulz (1995) with the central tenet being the need for *only* horizontal (reduced time) shifting. A more robust discussion of the viscoelastic nature of this WPC formulation can also be found elsewhere (Kobbe, 2005).

This research addresses the creep behavior of a single WPC formulation at a load that approximates full design conditions. The long-term behavior was considered using an accelerated testing technique called time-temperature superposition principle (TTSP). The approach taken here addresses the possibility of using TTSP as an efficient and economical means for product assessment.

To promote understanding of long-term creep performance for WPCs, the specific aims of this research are:

1. Investigate short-term creep performance of a single WPC formulation at different temperatures.
2. Determine model parameters for a Findley power law model of short-term creep performance.
3. Evaluate the use of TTSP as a technique to assess long-term creep behavior.

4. Qualitatively evaluate the efficiency of using temperature as an accelerant to generate data for TTSP.

3.3 Analytical Methods

Modeling of experimental data is necessary to bridge the gap between material behavior and useful engineering design. Therefore, static tension and compression constitutive relations have been developed from testing (Kobbe, 2005; Schildmeyer, 2006). Complex constitutive relations for WPCs are dictated by non-linear stress-strain behavior. Non-linear material modeling has been, and continues to be, the subject of research by investigators with a wide variety of proposed models (Findley, 1960; Lou and Schapery, 1971; Rand, 1995). A Findley power law was chosen to model the short-term creep performance of this material (Kobbe, 2005) because of its past success as an effective modeling tool (Cessna, 1971; Dillard, et al., 1987; Findley, 1987; Yen and Williamson, 1990; Ma et al., 1997).

Assessing the applicability of using TTSP as an accelerated testing technique for WPC design considerations requires the conversion of short-term creep curves at various temperatures to a master curve depicting creep compliance against reduced time (*t'*). To accomplish this step, creep compliance, *D(T,t)*, is shifted along the log-time scale to develop temperature dependent shift factors (a_T).

$$t' = \frac{t}{a_T} \qquad \text{(eq. 1)}$$

Where:

t' is the shifted, or reduced, time
t is the elapsed time of a test
a_T is the shift factor specific to a test

The mathematical models employed to represent the temperature dependence of shift factors is the Williams-Landel-Ferry (WLF) Equation:

$$\log(a_T) = \frac{-C_1(T - T_o)}{C_2 + (T - T_o)} \qquad \text{(eq. 2)}$$

Where:

a_T is the horizontal shift factor
C_1 and C_2 are empirical constants
T_o is the reference temperature (21.1°C or 70°F, here)
T is the temperature at the accelerated state of interest

This is a widely accepted function that TTSP shift factors have been shown to follow (Cessna, 1971; Luo, 2001). Furthermore, once the parameters to the WLF Equation are found, and the data is shifted accordingly, mathematical modeling of that master curve will be conducted using a Prony Series. This model was chosen because of the complementary t' shifting axis and the judicial selection of retardation times to match.

3.3.1 Findley's Power Law

The power law developed by Findley (1960) was used to model the short-term creep at various temperatures. This model is proven to adequately model creep of polyvinyl chloride for up to 26 years (Findley 1987). Whereas this model has the advantage of being mathematically simple and robust in description, limitations also exist (i.e. upper bounds on stress levels, inability to accommodate creep mechanism changes).

The general form of Findley's power law is:

$$\varepsilon_t = \varepsilon_o + m\left(\frac{t}{t_o}\right)^n \quad \text{(eq. 3)}$$

Where:

ε_t is the time-dependent strain
ε_o is the instantaneous (elastic) strain at load application
m is the coefficient of time-dependent strain
t is the time after load application
t_o is a time increment (usually taken as unity)
n is a material constant parameter

Values for m and n are determined by calculating the slope and intercept of the log-log plot between time and the change in strain with time. Initial strain, ε_o, is recorded during experimentation as the strain immediately following load application. It is important to note that ε_0, m, and n are all temperature dependent parameters.

3.3.2 Time-Temperature Superposition Principle (TTSP)

TTSP is used to develop the long-term response of polymeric materials from short-term testing. This tool allows compliance curves developed at different accelerated states (i.e. higher temperatures) to be horizontally shifted on a log-time scale. Reduced time is found by addressing Equation 1 above.

This technique is only valid for thermo-rheologically simple materials through assessment of TTSP curves for characteristic behaviors. For instance, tests conducted at elevated temperatures have the same general shape, allowing for smooth horizontal shifting along the *t'* axis thereby forming a single contiguous curve; called a master curve. In turn, the degree to which each accelerated state must be shifted is determined by the shift factor (a_T) that also follows a known relationship (i.e. the WLF Equation, Equation 2).

Free volume theory provides one explanation behind the accelerated accumulation of creep deformations and the variation of shift factors. This theory proposes that creep deformations are the macroscopic manifestation of molecular relaxations. Free volume theory dictates that the mechanism behind time-dependent deformation is controlled by molecules seeking to attain a state of thermodynamic equilibrium with the applied stress. Accelerated states, such as higher stresses or temperatures, increase the free volume between molecules and facilitate space for, and thereby the rate of, molecular relaxation. Past research (Luo et al., 2001) has examined a more general accelerated testing procedure, time-temperature-stress superposition principle (TTSSP), as it applies to nonlinear viscoelastic materials and its foundation in free volume theory. One outcome of the link between free volume theory and TTSP is the Williams-Landel-Ferry (WLF) Equation, reported earlier as Equation 2 (Williams et al., 1955). Values of C_1 and C_2 in the equation are found by minimizing the sum squares of error between the model curve and the mean experimental curve. These constants can, however, also be determined through fundamentally derived relations to free volume states (Luo et al., 2001).

Shift factors, a_T, pertain to a specific non-reference temperature condition where a_T must be less than one to produce the accelerated response. The temperature-dependent creep compliance, $D(T,t)$, is shifted along the t' axis by the relationship:

$$D(T,t) = \frac{\varepsilon(T,t)}{\sigma_o} = D\left(T_o, \frac{t}{a_T}\right) \qquad \text{(eq. 4)}$$

Where:

$D(T,t)$ is the time dependent compliance at a specific temperature level
$D(T_o,t/a_T)$ is the compliance curve shifted on the *t'* axis to correspond to the reference temperature condition
T_o is the reference temperature (21.1°C or 70°F, here)
T is the temperature at the accelerated state of interest
a_T is the shift factor for that temperature

Higher test temperatures correspond to more accelerated time states and will shift further right along the *t'* axis. Studies involving TTSP have shown it to be a valid tool to assess the long-term performance of various materials through short-term testing (Cessna, 1971; Wortmann and Schulz, 1995; Luo et al., 2001).

TTSP shift factors have a broader significance than just shifting of compliance tests for master curve generation. These shift factors correspond to many viscoelastic parameters of a given material including shifting of dynamic properties on a log frequency axis.

3.3.3 Prony Series Modeling

A Prony series was used to mathematically represent the master curve for subsequent modeling and comprises a series of decaying exponentials with as many terms as necessary to adequately capture the trend of the master curve. This model exhibits computational efficiency by correlating the logarithmic t' axis to retardation times spaced at decades of time. A Prony series can be represented as:

$$D(t) = D(0) + \sum_{i=1}^{N} D_i \left[1 - e^{-t/\tau_i}\right] \qquad \text{(eq. 4)}$$

Where:

D(t) is the time dependent compliance
D(0) is the instantaneous, elastic compliance
i is the summation index
D_i is a compliance constant at retardation time, i
τ_i is the retardation time, in minutes
t is the elapsed time, in minutes

3.4 Materials and Methods

The WPC formulation investigated was composed of 58.8% pine (*Pinus spp.*) flour, 33.8% polypropylene, 4.0% talc, 2.3% maleated polypropylene (MAPP) and 1.0% lubricant by mass (Slaughter, 2004). Manufacturer details for the included ingredients can be found in Table 3.1. Commercial 60-mesh pine (*Pinus spp.*) flour was dried in a steam tube dryer to a moisture content of less than 2%. A 1.2-m (4-ft) drum mixer was used to dry-blend the ingredients in a series of 25-kg (55-lb) batches. An 86-mm conical counter-rotating twin-screw extruder (Cincinnati-Milacron TC 86), operating between 5 and 12 rpm, was used to produce the sections from which specimens were obtained. Barrel and screw temperature profiles were established according to previous research (Kobbe, 2005) and are included in Table 3.2.

This formulation was then extruded through a stranding die (Laver, 1996) into a hollow three-box cross-section (Figure 3.1) and cut into 1.22-m (4-ft) lengths from which individual test specimens were machined. The dimensions of each specimen was measured with digital calipers and used to calculate properties for each individual specimen (i.e. cross-sectional area).

3.4.1 Mechanical Testing

Mechanical testing was conducted to assess the short-term creep performance of this material at six temperature levels. To achieve this, a 222-kN (50-kip) servo-hydraulic test frame (MTS 810 with MTS 407 controller) was used in load control. A pre-determined load was applied in less than 5-seconds and maintained for 100-minutes after application. Data was collected during testing by computer at a sampling rate of 2-Hz. Displacement over a 25.4-mm (1-in) gauge length was measured using an extensometer (MTS Model 634.12E-24). Applied loads were regulated and monitored using a 22.2 and 244.7-kN (5-kip Interface 1210AJ-5k-B and 55-kip MTS Model 661.22C-01) in-line load cells for tension and compression testing, respectively.

An environmental chamber was mounted within the test frame to control the test environment at a variety of temperatures. Specifically, tests were conducted at 21.1°, 30°, 40°, 50°, 65.6°, and 80°C (70°, 86°, 104°, 122°, 150° and 176°F) within a tolerance of ±2°C (9°F) throughout any given test. It was considered that the mechanical behavior of the material could potentially be affected by molecular rearrangement at higher temperature tests, thereby relaxing any potential processing stresses in high-temperature test conditions but not affecting the processing stresses of lower-temperature tests. This concern was addressed by conditioning all specimens at 65.6°C (150°F) for 48-hours prior to testing; a temperature deemed to be an appropriate limit for realistic service conditions. At each temperature level, 8 specimens were tested to ensure a representative average while minimizing testing time. Loads applied for both tensile and compressive testing correspond to 40% of the ultimate strength from static tests at ambient temperature (Schildmeyer 2006). Justification for choosing this stress level was based

upon two general design calculation procedures previously proposed (Haiar, 2000; Davidow and Fridley, 2003). A full description of the justification and calculations can be found in Schildmeyer (2), (2006).

3.4.1.1 Tension

Type III dog-bone specimens were sampled from the top and bottom flanges of the three-box section. During preparation, the flanges were cut and planed to ensure uniform thickness and eliminate surface defects. These planed flanges were then cut to the required dimensions and shaped to their final configuration using a guide and router. A constant tensile load was applied such that an engineering stress of 7.26-MPa (1053-psi) was applied throughout the 100-minute test.

3.4.1.2 Compression

Previous work (Hermanson, et al., 2001) determined that testing of small-scale compressive specimens called for in ASTM D695 yielded unrepresentative values for full-scale specimen performance. For this reason, a single-box compression specimen 203-mm (8-in) long was cut from the outer box of the three-box section. This specimen was produced by detaching the two outer boxes of a section and planning the cut edges until smooth. All specimen dimensions were measured using digital calipers, recorded, and used for relevant calculations (i.e. specimen cross-sectional area). The specimens were nominally 45.7 by 61.0-mm (1.8 by 2.4-in) with 10.2-mm (0.4-in) thick walls. A constant compressive stress of 19.57-MPa (2838-psi) was applied throughout the 100-minute test.

3.4.2 Dynamic Mechanical Analysis (DMA)

Dynamic mechanical analysis (DMA) was performed using a Rheometrics Solid Analyzer (RSA II) on small flexure specimens sampled from the same flange material as the tension testing. A frequency/temperature sweep test to assess shift factors developed for tension and compression was performed. Prior to testing, specimens were conditioned at elevated temperature (65.6°C or 150°F) for 48-hours to provide similar thermal history for this material and the tension and compression specimens tested. A three-point bending geometry was used. Specimens were shaped using a milling machine (Sherline Model 2000) to the nominal dimensions of 45 by 8 by 3-mm (1.78 by 0.31 by 0.12-in); precise dimensions were measured using digital calipers. A strain of $1.0x10^{-4}$-mm/mm was verified to be in the linear viscoelastic range for the material and used for both temperature scan and frequency/temperature sweep tests.

For the frequency/temperature sweep test, the temperature was varied between 20 and 80°C (68 to 176°F) at 10°C (18°F) increments. At each test temperature, the sample was tested over a frequency range of 0.1 to 10-Hz. Temperature soak times associated with each temperature step was set for 3-minutes to ensure uniformity throughout the specimen during the frequency sweep.

3.5 Results and Discussion

3.5.1 Short-Term Creep and Findley's Power Law

Short-term creep was evaluated at 21.1°, 30°, 40°, 50° and 65.6°C (70°, 86°, 104°, 122° and 150ºF) for 100-minute tests. Preliminary tests to extend the temperature range to 80°C were not successful. The creep deformation ranged from primary to tertiary

creep stages, with a wide variety of behavior among the 8 specimens. Some specimens exhibited creep-rupture within the 100-minute test period. Therefore, 65.6°C (150°F) is the highest valid temperature for the creep data to be included in the TTSP for the material investigated here.

Plots of the mean creep curves for tension and compression at these temperature levels are included in Figures 3.2 and 3.3, respectively. Dashed lines represent the Findley power law fit to the mean data. Specific values for ε_o, m and n are presented in Table 3.3. Findley power law modeling provides a good fit to the data, although at times near 100-minutes for some temperature levels the model does begin to deviate from mean data. This can be seen for the 65.6°C (150°F) tests shown in Figure 3.3.

Initial strain at 65.6ºC (150ºF) was more than double that at ambient temperatures for both tension and compression (Figure 3.4). Tension values of ε_0 followed a linearly increasing path over this temperature range, while the compressive values took on a second-order shape with increasing slope. The quadratic shape to the compressive curve may result from higher stresses applied to the compressive specimens.

The creep coefficient, m, is fundamentally related to the speed to which creep accumulates at a given temperature and exhibited an increasing magnitude with temperature (Figure 3.5). Again, the tension values increased linearly while the compression values increased quadratically. Values for m double in tension over the temperature range tested, while a 5x increase is found in compression from ambient temperatures to 65.6ºC (150ºF).

Trends for the material constant, n, were different than those for the other Findley parameters. This parameter did exhibit second-order, increasing slope values for

compression testing, and increased by about half of the ambient value (Figure 3.6). In tension the n-values also followed a second-order function and increased approximately 60% over the range of temperatures tested in this work.

3.5.2 Application of TTSP for Master Curves

Both the original and shifted creep data are presented in Figures 3.7 and 3.8. The creep data at all test temperatures agree in their general form, but differ in the magnitude of the creep compliance values. A single, contiguous master curve was easily produced for both tension and compression by a simple horizontal shift of each curve along the reduced time (*t'*) axis. A side-by-side comparison of the tension and compression behavior can be found as Figure 3.11.

The constants involved in applying the WLF Equation are presented in Table 3.4. The resulting values for a_T and the fit WLF relations (Equation 2) are presented for tension and compression in Figure 3.10. In general, the data was in good agreement with the WLF relations, thereby supporting applicability of TTSP to this data set.

Lastly, a further validation of the TTSP method was undertaken using DMA testing. Here, temperature dependent storage modulus (E'(T)) was shifted along the log-frequency axis (Figure 3.9). To produce independent verification, the resulting values for a_T were plotted against the tension and compression values (Figure 3.10). Because the flexure mode used in the DMA is a mechanical combination of tension and compression behaviors, it is expected that the tension and compression shift factor values will provide upper and lower bounds for the resulting ones from the DMA *E'* shifting. This holds true for temperatures below 40ºC (104ºF), but does not continue at higher temperatures. Because the DMA shift factors are not bounded by the tension and compression shift

factors at higher-temperature levels (50° and 65.6ºC or 122° and 150ºF), a more exclusive temperature range than employed here may be more appropriate for predictive uses of TTSP on WPC materials. Long-term validation testing will be necessary to conclude the absolute temperature limits, therefore, caution should be employed until such validation has been conducted.

3.5.3 Discussion of Master Curves and Applications

Master curves for tension and compression are included in Figures 3.11 to 3.13. These master curves predict creep performance at a realistic design stress level and ambient temperatures out to 5.7-years for tension and 2.7-years for compression. The predictive capabilities of temperature as an accelerant were limited by the upper bound imposed by the α-transition of the polypropylene matrix at high temperatures (approximately 70°C). Furthermore, these predictive time scales include data sets recorded at 50° and 65.6ºC (122° and 150ºF), where less confidence is given due to the DMA validation previously performed. Free volume theory is able to explain the discrepancy between predictive capability in tension and compression modes as due to the cooperation between tension and increased free volume between molecules within a specimen.

Additionally, for these master curves to be incorporated into design considerations, it is appropriate to assess upper and lower bounds on the creep behavior via establishing a percentile level. This is done in order to have a higher degree of confidence in predicted behavior. A statistical approach was applied to the master curves where upper and lower 95^{th} percentile values were calculated from testing. Figures 3.12

and 3.13 illustrate the range of performance for these confidence levels in tension and compression, respectively.

The adjusted master curves were then modeled using a Prony series with retardation times and compliance coefficients found in Table 3.5. This was done to provide a mathematical expression by which the behavior can be modeled rather than simply producing an experimental curve. Comparisons between the Prony series fit to previous work at similar load levels on this material (Kobbe, 2005) and the Prony series developed from this work are in Figures 3.14 and 3.15 for tension and compression, respectively. They show general agreement between the past work and this study. The differences in initial compliance for these figures may be due to any combination of differences in conditioning procedures, aging of the WPC material, or the applied stresses (this work applied higher stresses for master curves by 505-psi in compression and 125-psi in tension).

3.6 Conclusions

Short-term creep performance exhibited significant changes with increased temperatures. This indicates that not only the initial, elastic strain at loading increases dramatically (it doubled over the likely service temperature range of these materials) with temperature, but the accumulation of strain increases as well. This may prove to make high-temperature applications of these materials difficult to meet serviceability and creep-rupture considerations at high operating temperatures.

Application of Findley's power law has allowed short-term creep behavior of this formulation to be well documented over the range of temperatures tested. A good

approximation for the behavior can be found through interpolation of the power law parameters for which trends were found over the temperature range tested. Appropriate use with regard to short-term creep for this specific formulation can therefore be modeled very accurately up to 100-minutes for any temperature these materials are likely to be exposed to by interpolating the model parameters for a given condition. Furthermore, this modeling technique allows for WPC behavior to be predicted by lending itself well to finite element and other computer-driven analysis techniques.

Characteristics of the short-term creep test data indicated that TTSP may be a valid technique to employ to generate the long-term performance of this WPC formulation. Master curves were developed using shift factors that fit the known shift behavior of the WLF Equation. Master curves in tension extended to 5.7-years and strains at the end of this time were approximately 6x larger than the initial strains at load application. In compression, the master curve extended to only 2.7-years, with strains increasing approximately 7-fold. These master curves include data sets at high temperatures where DMA verification of the shift factors showed less support. True verification of the full master curve inclusion of these data sets can come from non-accelerated long-term testing.

Furthermore, TTSP appears to be an efficient technique to predict long-term performance. Past work examining the viability of time-stress superposition (TSSP), was only able to achieve predictive time scales of 270-days in compression and 734-minutes in tension. Both TTSP and TSSP fall under a broader umbrella of time-temperature-stress superposition (TTSSP). Of the two avenues, the temperature investigation conducted here was able to achieve longer predictive times while running fewer

accelerated states. Qualitatively, therefore, temperature is a more efficient and cost-effective avenue to pursue the accelerated testing route for new product assessment.

Possible future extensions from this work could include computationally extending the tension and compression behaviors found here into time-dependent pure flexural performance by a moment-curvature or reverse finite-element approach. Investigation into the shear mechanics of this material would also provide a more robust general understanding of the load-response and could further expand moment-curvature analyses to include a more general flexural case where shear contributions are accounted for. Assessing long-term flexural performance will open avenues for improving cross-section design and allow for other use-specific optimizations.

Another opportunity that this research has addressed, but cannot fully pursue, is the generation of code provisions for creep of WPCs. 95^{th} upper and lower percentile curves were presented, from which some appropriate confidence can be drawn for performance of these materials in creep. However, a full code for WPCs based solely upon this work would be premature because of the single formulation tested. Also, this study did not include a flexural testing mode (the mode most common among current applications for WPCs). Lastly, the use of WPCs in civil engineering applications would benefit from a predicited behavioral curve out to 10-years of full allowable design stress behavior. This would address long-term performance similarly to timber design in that any given member is not expected to see a full design load for a total duration of 10 years over the much longer lifetime of the structure. This study has not achieved predictive curves thus far in the future, but the increase over the previous TSSP is at least 3-fold. Furthermore, it may be possible to achieve time scales of this magnitude by using either

(1) a combination of temperature and stress accelerated testing or (2) by simply extending the time scale of the high-temperature tests. Examination of the master curves indicates that a 10-year time scale could be achieved by simply using 1000-minute tests at 65.6°C.

3.7 References

ASTM D695-96, "Standard Test Methods for Compressive Properties of Rigid Plastics." American Society for Testing Materials, 1996.

Brandt, C.W., and Fridley, K.J., "Load-Duration Behavior of Wood-Plastic Composites." Journal of Materials in Civil Engineering, ASCE, November/December, 2003.

Brinson, H.F., and Dillard, D.A., "The Prediction of Long Term Viscoelastic Properties of Fiber Reinforced Plastics." Proceedings of "Progress in Science and Engineering of Composites, Tokyo, Japan, 1982.

Brinson, H.F., Morris, D.H. and Yeow, Y.T., "A New Experimental Method for the Accelerated Characterization of Composite Materials." 6th International Conference on Experimental Stress Analysis, Munich, Germany, September 18-22, 1978.

Cessna, L.C., "Stress-Time Superposition of Creep Data for Polypropylene and Coupled Glass-Reinforced Polypropylene." Polymer Engineering and Science, Vol. 11, No. 3, pp. 211-219, May 1971.

Davidow, S.A. and Fridley, K.J., "Development of Design Values for Wood-Plastic Composite Materials." Journal of Materials in Civil Engineering, Vol. 15, Iss. 5, pp. 415-418, 2003.

Dillard, D.A, Straight, M.R. and Brinson, H.F., "The Nonlinear Viscoelastic Characterization of Graphite/Epoxy Composites." Polymer Engineering and Science, Vol 27, No. 2, pp. 116-123, 1987.

Findley, W.N., "26-year Creep and Recovery of Polyvinylchloride and Polyethelene." Polymer Engineering and Science, Vol. 27, No.8, pp. 582-585, 1987.

Findley, W.N., "Mechanisms and Mechanics of Creep in Plastics." SPEJ, Vol. 16, pp.57-65, January 1960.

Haiar, K.J., "Performance and Design of Prototype Wood-Plastic Composite Sections." Master Thesis, Washington State University, May 2000.

Hermanson, J.C., Adcock, T. and Wolcott, M.P., Evaluation of Extruded Materials Group, "Project End Report." Washington State University, 2001.

Kobbe, R.G., "Creep Behavior of a Wood-Polypropylene Composite." Master Thesis, Washington State University, August 2005.

Laver, T.C., "Extruded Synthetic Wood Composition and Method for Making Same." Patent Number 5,516,472; 1996.

Lou, Y.C. and Schapery, R.A., "Viscoelastic Characterization of a Nonlinear Fiber-Reinforced Plastic." Journal of Composite Materials, Vol 5, pp. 208-234, 1971.

Luo, W.B, Yang, T.Q. and An, Q.L., "Time-Temperature-Stress Equivalence and its Application to Nonlinear Viscoelastic Materials." Acta Mechanica Solida Sinica, Vol. 14, No. 3, pp. 195-199, 2001.

Ma, C.C.M., Tai, N.H., Wu, S.H., Lin, S.H., Wu, J.F. and Lin, J.M., "Creep Behavior of Carbon-fiber-reinforced Polyetheretherketone (PEEK) $[\pm 45]_{4s}$ Laminated Composites." Composites Part B, 28B, pp. 407-417, 1997.

Pooler, D.J. and Smith, L.V., "Nonlinear Viscoelastic Response of a Wood-Plastic Composite Including Temperature Effects." Journal of Thermoplastic Composite Materials, Vol. 17, No. 5, pp. 427-445, 2004.

Rand, J.L., "A Nonlinear Viscoelastic Creep Model." Tappi Journal, Vol. 78, No. 7, pp. 178-182, July 1995.

Sain, M.M., Balatinecz, J. and Law, S., "Creep Fatigue in Engineered Wood Fiber and Plastic Compositions." Journal of Applied Polymer Science, Vol. 77, pp. 260-268, 2000.

Schildmeyer, A.J., "Temperature and Time Dependent Behaviors of a Wood-Polypropylene Composite." Chapter 2, Master Thesis, Washington State University, July 2006.

Schildmeyer, A.J. (2), "Temperature and Time Dependent Behaviors of a Wood-Polypropylene Composite." Appendix A, Master Thesis, Washington State University, July 2006.

Slaughter, A.E., "Design and Fatigue of a Structural Wood-Plastic Composite." Master Thesis, Washington State University, August 2004.

Williams, M.L., Landel, R.F. and Ferry, J.D., "The Temperature Dependence of Relaxation Mechanisms in Amorphous Polymers and Other Glass-forming Liquids." Journal of American Chemical Society, Vol. 77, pp. 3701-3707, July 20, 1955.

Wolcott, M.P., and Smith, P.M., "Opportunities and Challenges for Wood-Plastic Composites in Structural Applications." Proceedings of Progress in Woodfibre-Plastic Composites-2004 Toronto, ON, 2004.

Wortmann, F.J. and Schulz, K.V., "Investigations on the Thermorheological Simplicity of Polypropylene Fibres in the α-transition Range." Polymer, Vol. 36, No. 8, pp. 1611-1615, 1995.

Yen, S.C. and Williamson, F.L., "Accelerated Characterization of Creep Response of an Off-Axis Composite Material." Composite Science and Technology, Vol. 38, pp. 103-118, 1990.

3.8 Tables

Table 3.1. Product details for extruded material.

Material	Manufacturer	Product
Polypropylene	Solvay	HB9200
Pine Flour	American Wood Fibers	#6020
Talc	Luzenac	Nicron 403
Coupling Agent	Honeywell	950P
Lubricant	Honeywell	OP100

Table 3.2. Extruder temperature profile for all material produced.

		Temperature, ºC (ºF)
Barrel Zone	1	188 (370)
	2	188 (370)
	3	185 (365)
	4	182 (360)
Screw		182 (360)
Die Zone	1	182 (360)
	2	185 (365)
	3	188 (370)

Table 3.3. Findley power law parameters for 100-minute tests in tension and compression.

	Tension			Compression		
Temperature, °C	ε_0	m	n	ε_0	m	n
21.1	1.881e-3	6.260e-4	0.2577	3.813e-3	8.810e-4	0.2853
30	2.586e-3	5.680e-4	0.2865	3.876e-3	1.211e-3	0.2892
40	3.240e-3	9.140e-4	0.2992	4.611e-3	1.809e-3	0.2954
50	3.398e-3	1.074e-3	0.3165	6.401e-3	2.540e-3	0.3162
65.6	4.355e-3	1.532e-3	0.3948	8.963e-3	4.688e-3	0.3489

Table 3.4. Constants for the WLF Equation for the shifting of compression, tension, and DMA testing conducted, including the R^2 fit value.

Loading Mode	C_1	C_2 [^{0}C]	R^2
Tension	8.819	44.32	0.997
Compression	2.628e5	2.906e6	0.987
DMA	1.394e5	9.612e5	0.965

Table 3.5. Compliance constants and retardation times for the Prony series model used to represent the tension and compression master curves.

	Tension		Compression	
i	τ_i	D_i	τ_i	D_i
0	∞	2.467e-6	∞	1.701e-6
1	10^1	2.960e-7	10^1	2.821e-7
2	10^2	6.167e-7	10^2	5.574e-7
3	10^3	5.269e-7	10^3	9.694e-7
4	10^4	1.351e-6	10^4	1.165e-6
5	10^5	9.792e-7	10^5	2.177e-6
6	10^6	3.995e-6	10^6	4.575e-6
7	10^7	1.080e-5	10^7	4.136e-6

3.9 Figures

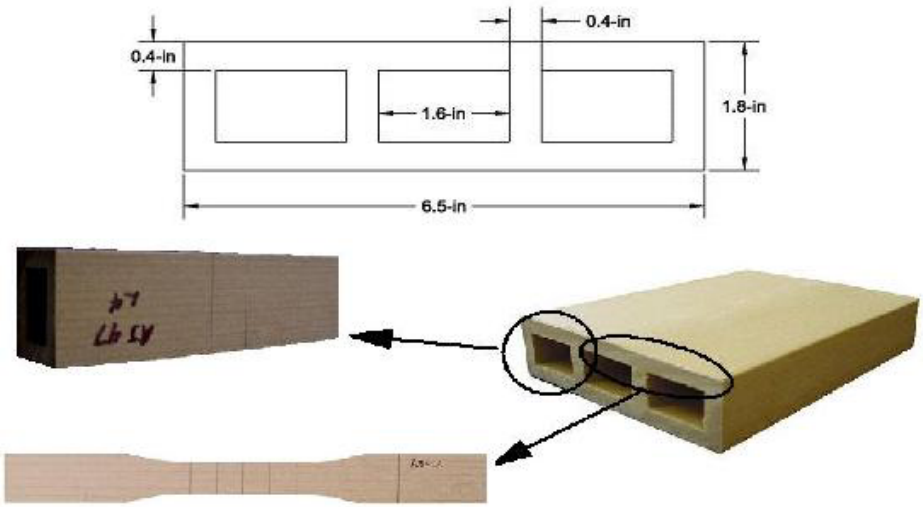

Figure 3.1. Triple box extrusion profile including nominal member dimensions, along with specimen location in cross-section.
(Kobbe, 2005)

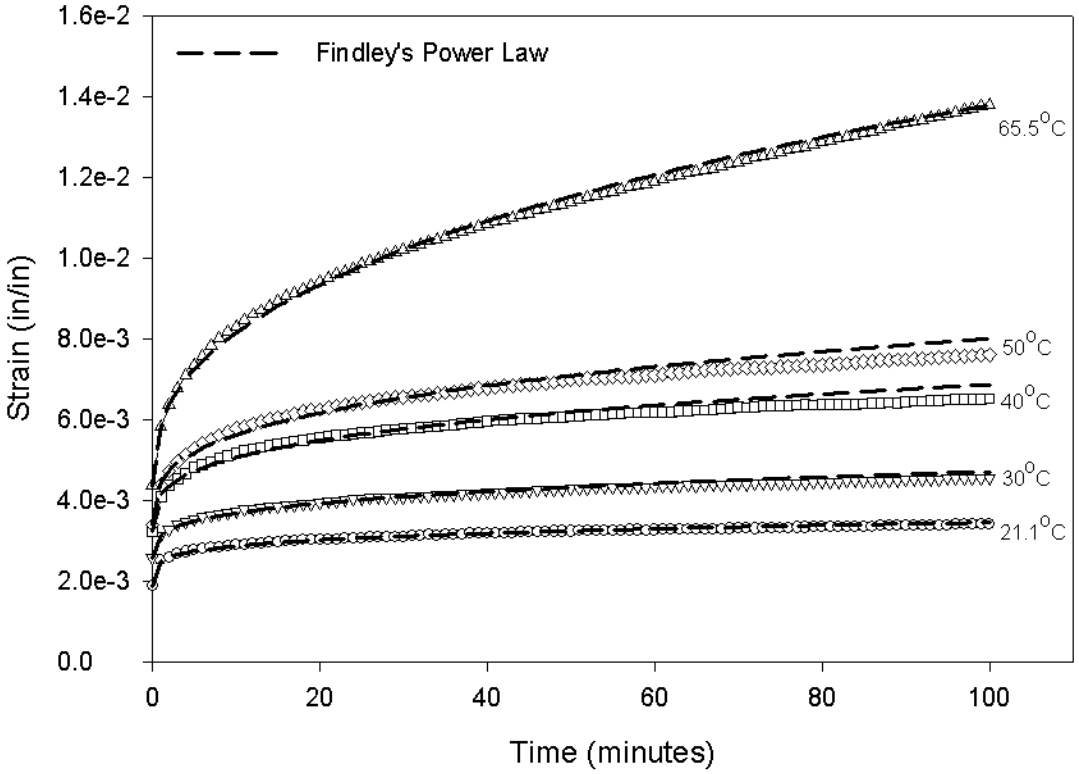

Figure 3.2. Mean short-term tensile creep results at different temperatures, including the Findley power law fit at each temperature.

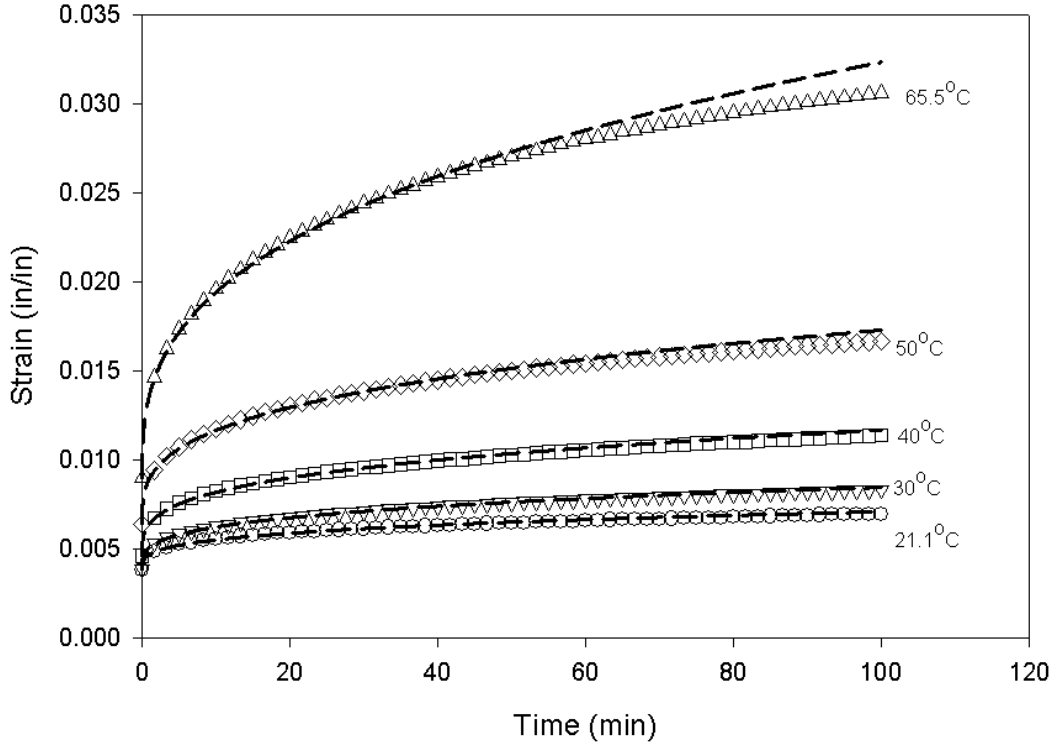

Figure 3.3. Mean short-term compressive creep results at different temperatures, including the Findley power law fit at each temperature.

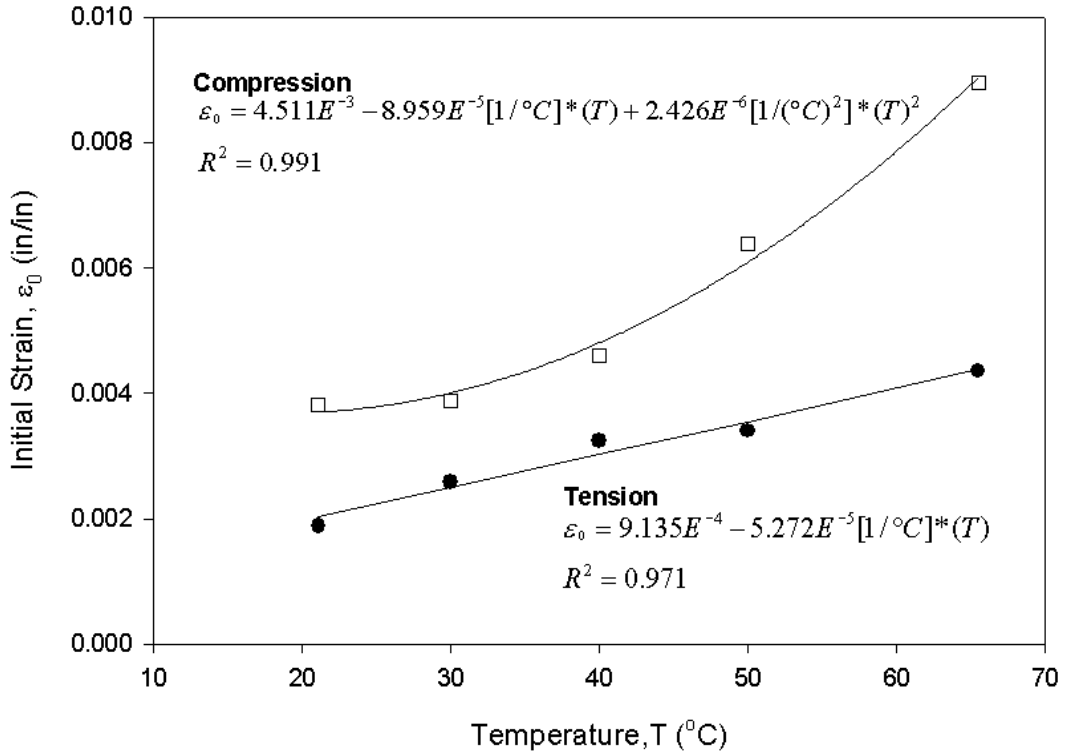

Figure 3.4. Trend for the initial strain, ε_0, Findley power law parameter with respect to temperature.

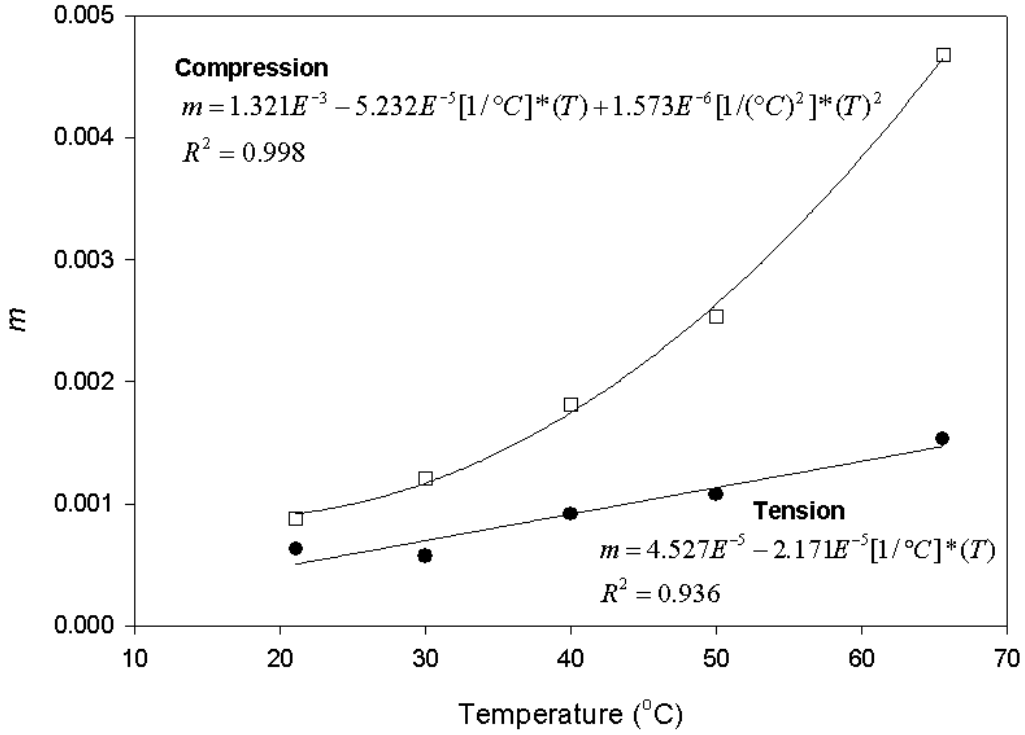

Figure 3.5. Trend for the Findley power laws parameter *m* with respect to temperature.

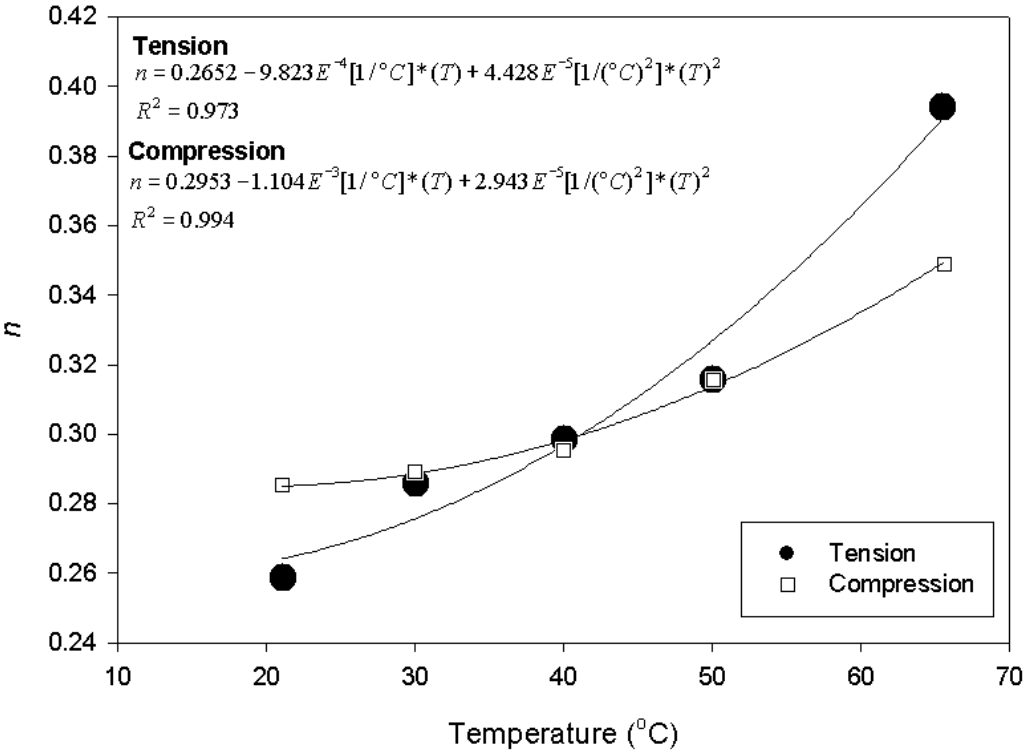

Figure 3.6. Trend for the Findley power law material parameter *n* with respect to temperature.

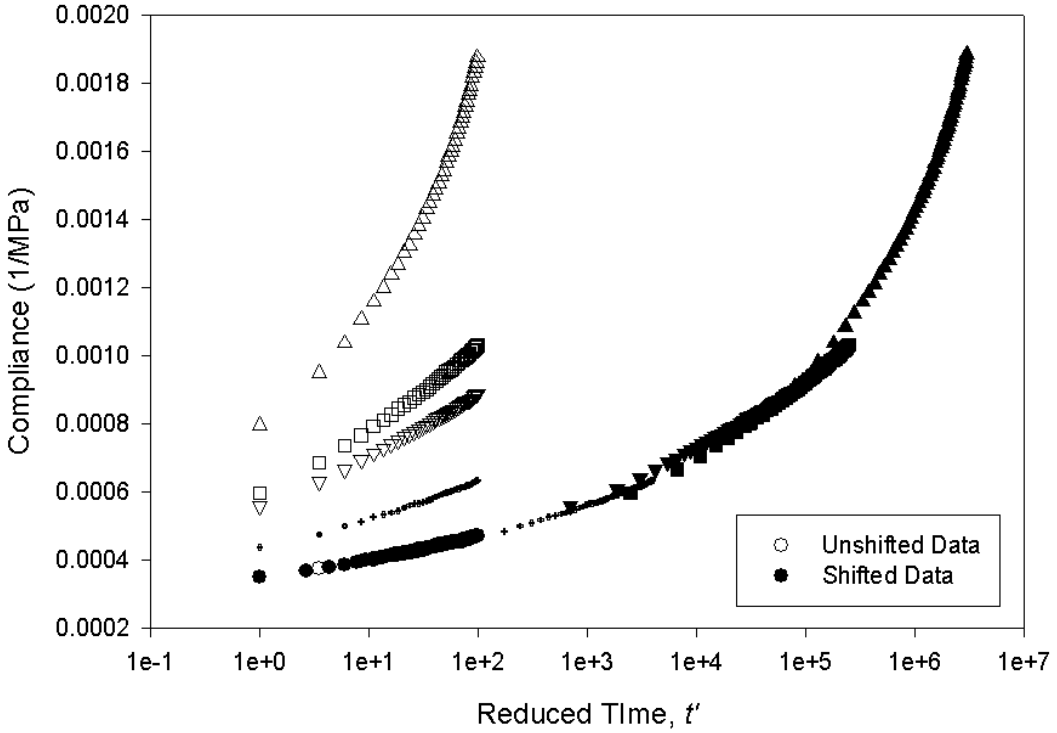

Figure 3.7. Shifted curves for short term creep tests in tension to master curve.

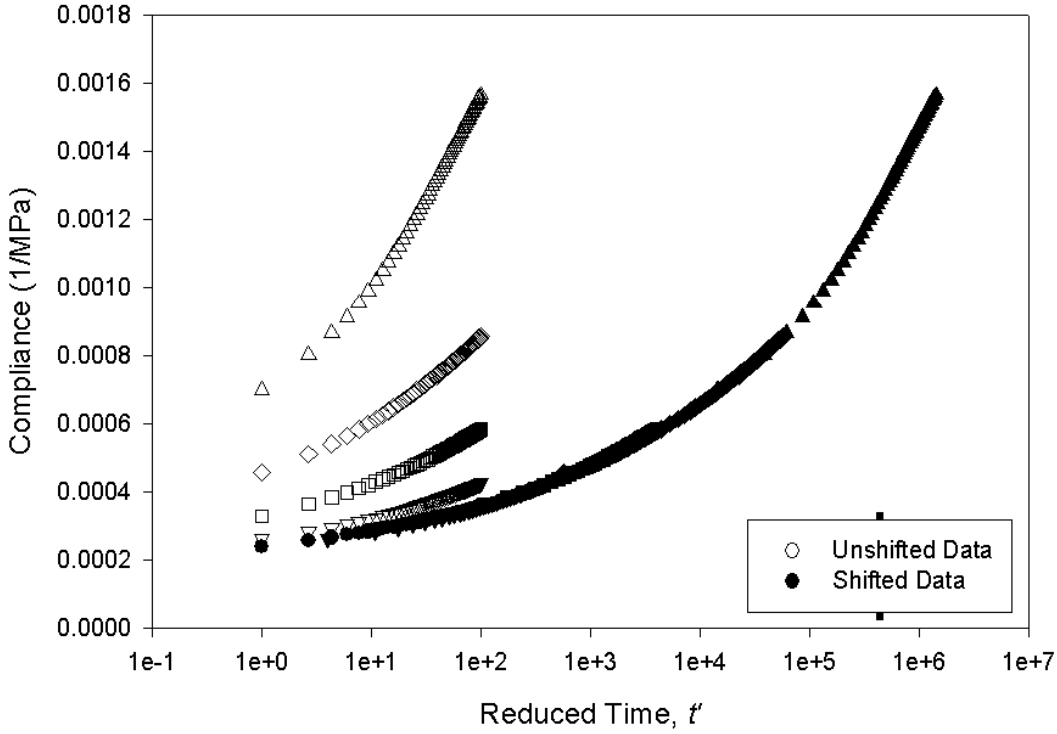

Figure 3.8. Shifted curves for short term creep tests in compression to master curve.

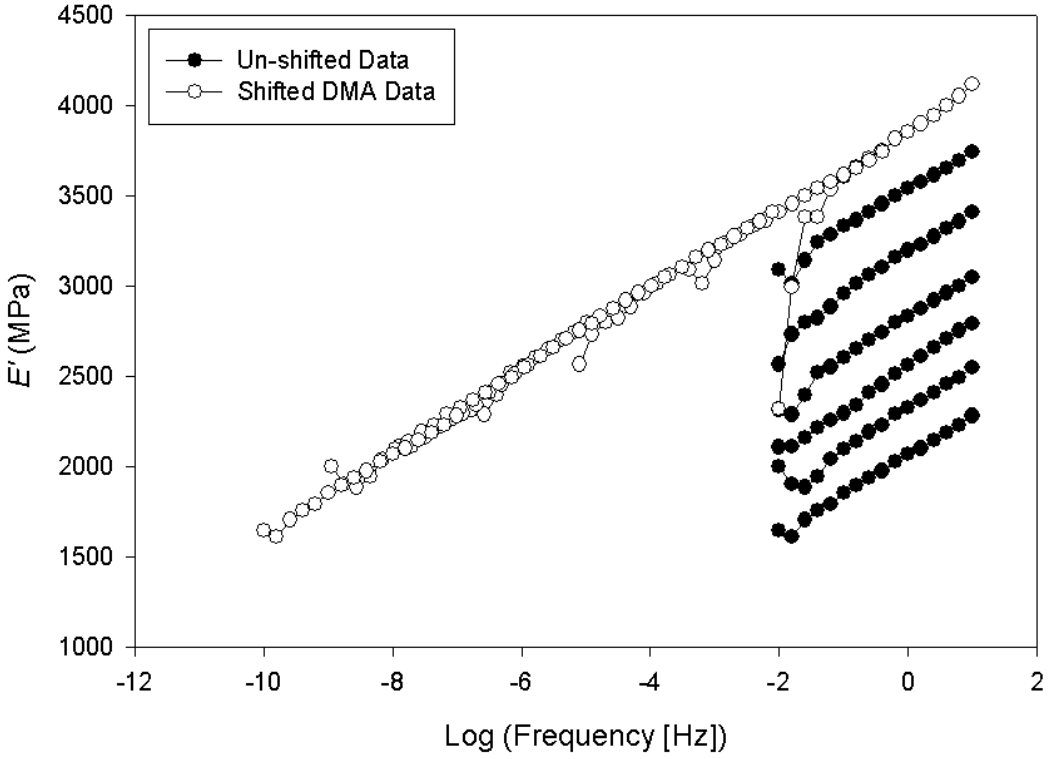

Figure 3.9. Shift of DMA data to generate a single smooth, contiguous curve in support of the thermorheological simplicity of this formulation.

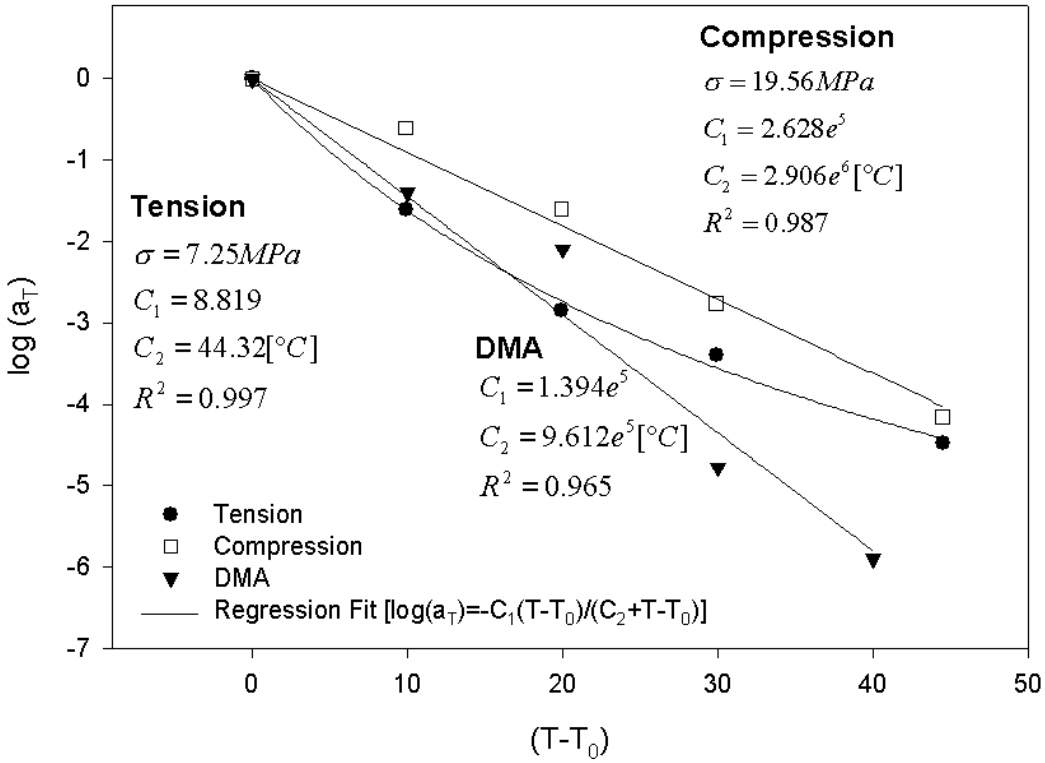

Figure 3.10. Master curve shift factors, and the values for C_1 and C_2 in the WLF Equation for tension, compression and DMA testing.

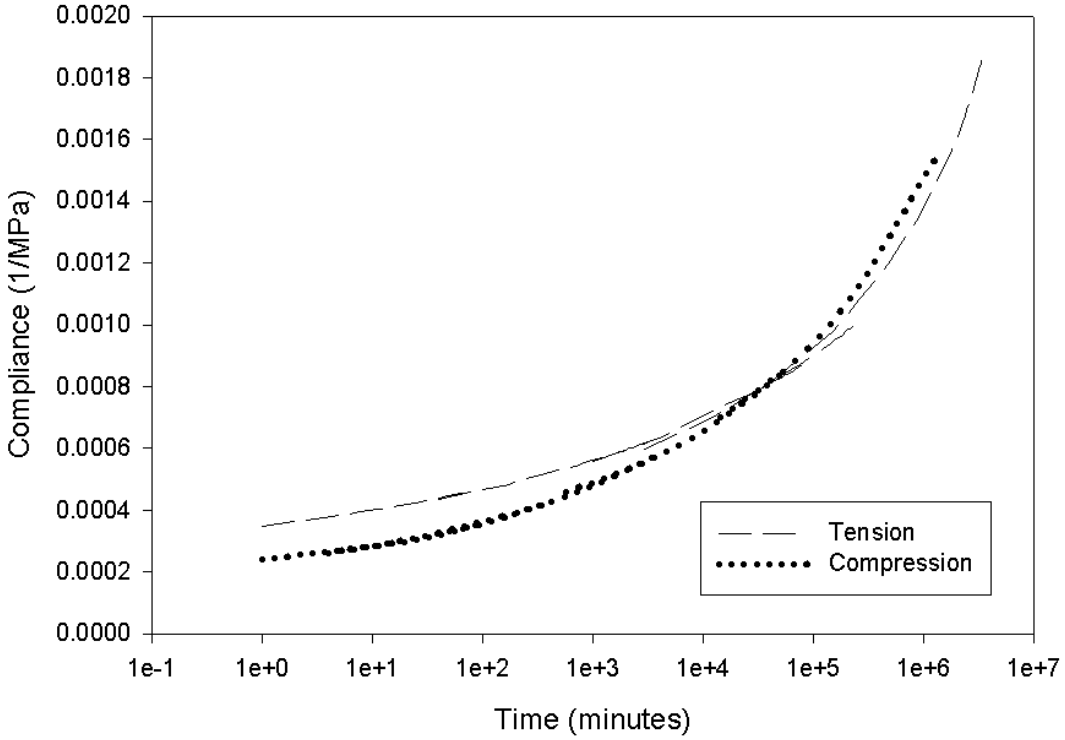

Figure 3.11. Creep master curves for tension and compression.

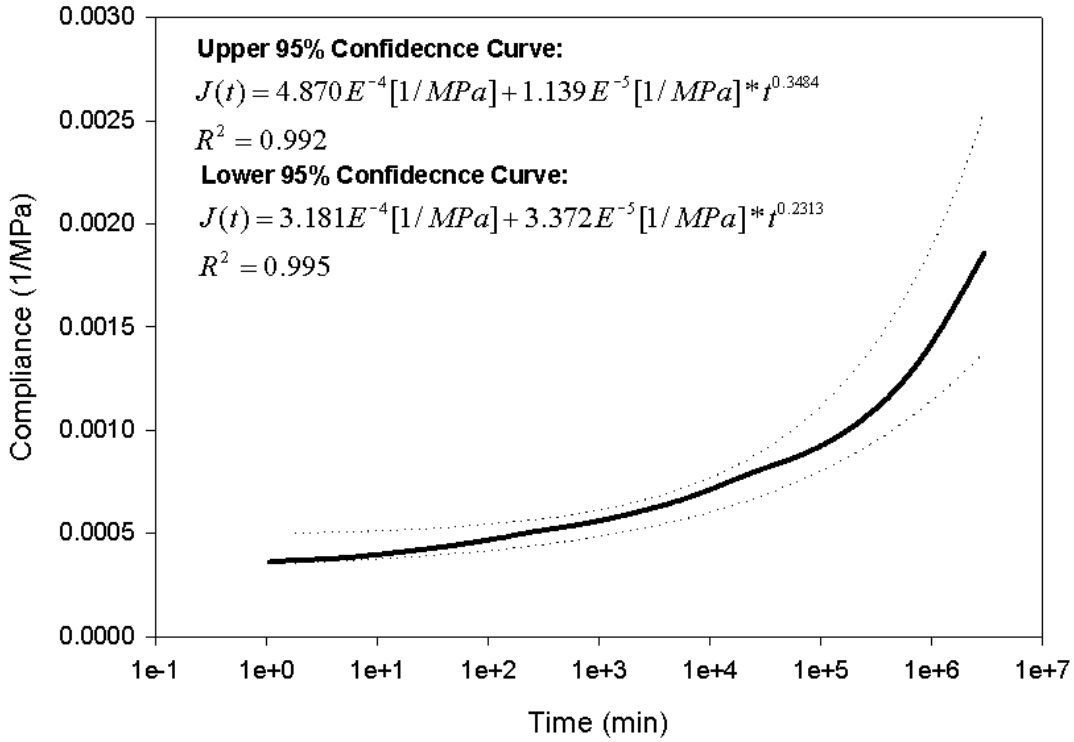

Figure 3.12. Tension master curve with 95th percentile upper and lower bounds from test data.

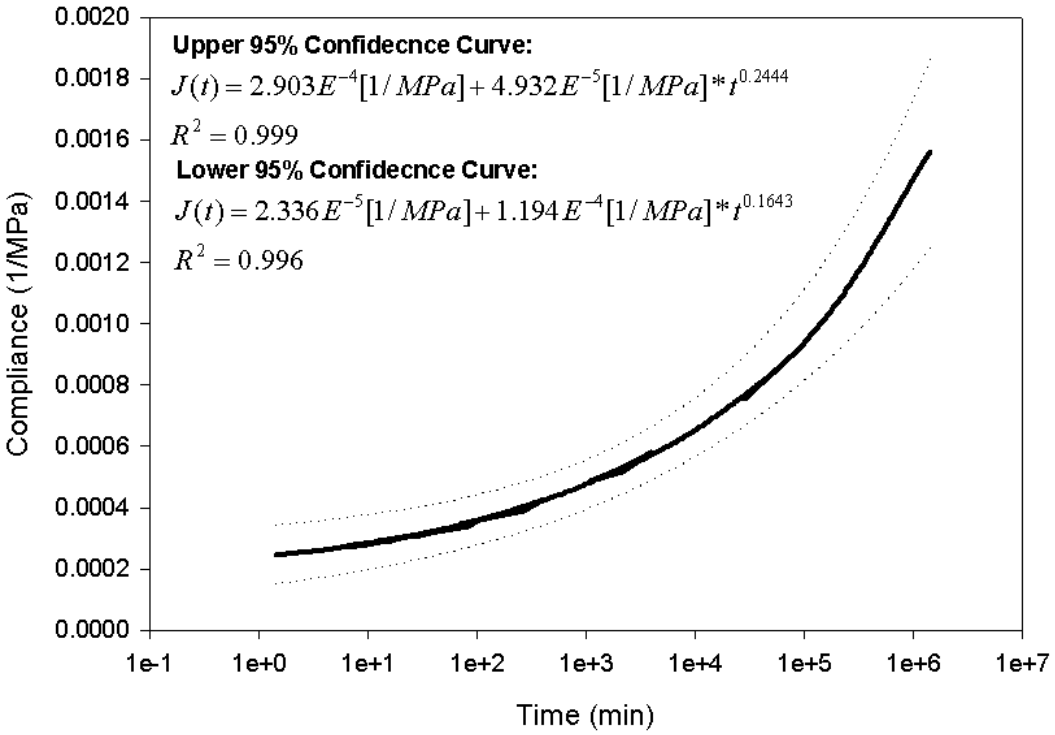

Figure 3.13. Compression master curve with 95th percentile upper and lower bounds from test data.

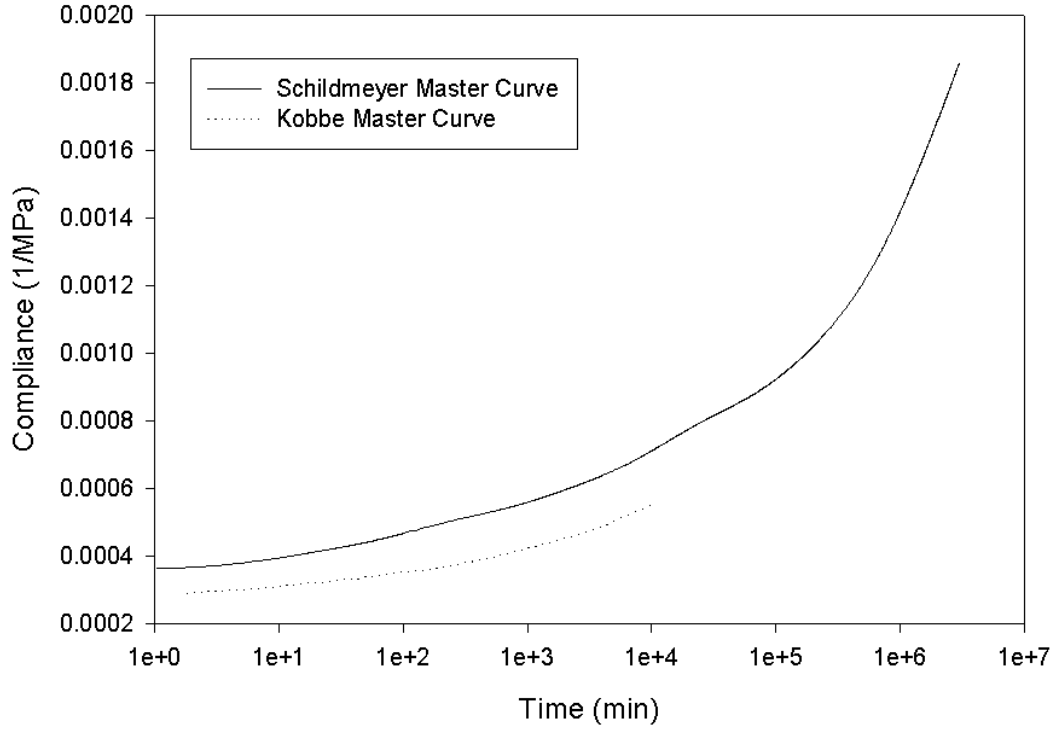

Figure 3.14. Tension master curve developed compared to the master curve developed by Kobbe (applied stress as the creep accelerant).

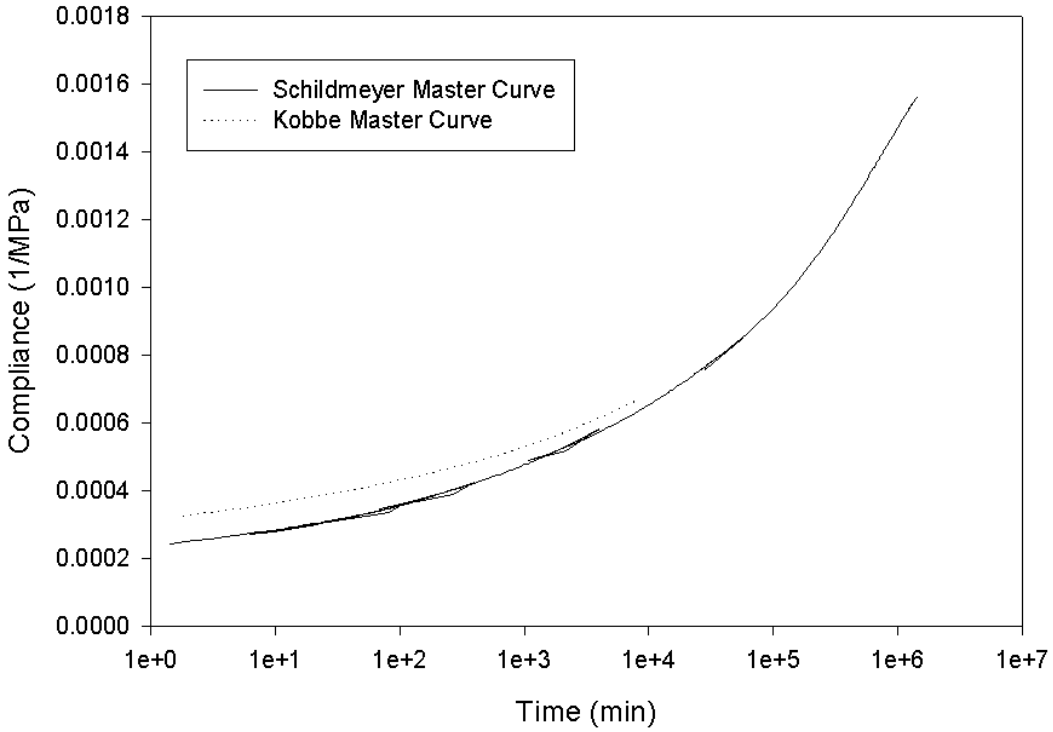

Figure 3.15. Compression master curve developed compared to the master curve developed by Kobbe (applied stress as the creep accelerant).

APPENDIX A

DISCUSSION/JUSTIFICATION OF CREEP STRESS LEVEL

A.1. Discussion of Creep Stress Level

For this work only one stress level was tested to avoid introducing both temperature and stress as confounding accelerating influences. Applied stresses of 40% of the ultimate stress determined from static testing at 21.1ºC were applied at all temperature levels (Schildmeyer, 2006). This percentage should serve as an upper-bound for long-term loads that would contribute to creep in these materials.

Two methods have been used to assess the validity of choosing 40% of ultimate as an upper bound (Haiar, 2000; Davidow and Fridley, 2003). The first method follows an allowable stress design (ASD) method to arrive at typical civil engineering load levels. This method addresses the design stresses for a WPC member by calculating a 5% exclusion limit at 75% confidence and applies reduction factors for changes in size (from small scale testing to full-scale members), environmental conditions, safety, and mode of loading (i.e. tension, compression, shear, flexure). In a conservative case where reductions for temperature, volume and moisture are taken as highest allowable stress scenario conditions, the percent of stress after the design process relative to ultimate capacities at ambient conditions are 37.9% and 30.1% for compression and tension, respectively. Applying 40% of ultimate capacity is a close percentage but errs on the side of caution for conducting these experiments.

A second method to assess appropriate design stresses is proposed by Davidow and Fridley (2003). This method is based upon energy considerations to find an

equivalent yield point on the nonlinear stress-strain diagram for a WPC material. A rough estimate procedure is outlined in Davidow and Fridley's work (2003) in which design stress values are approximately 40% of ultimate capacity. Following the outlined procedure, design stress values of 39.3% in tension and 20.7% in compression of ultimate capacity were determined for design stresses. The estimated ratio calculated for compression is much lower than expected and can be explained by an overly conservative estimate due to a higher degree of non-linearity in this loading mode. This tendency for nonlinear materials to produce an unrealistically low value is considered in the paper and is one concern researchers must keep in mind when applying this approach to materials such as these. Again, this approach indicates a 40% threshold to be realistic yet conservative.

Consideration must also be given to the duration for which these design-level stresses will be applied. In most cases, loads consist of long-duration components, such as dead loads associated with material or permanent machinery and more transient loads such as live, snow, rain or wind contributions. Transient loads are not typically considered for creep considerations (other than member capacities at 10-years must still accommodate all loads to the structure). Adopting a conservative stress level of 40% of ultimate capacity provides more than sufficient leeway to accommodate the total contributions from both long-term and transient load contributions to creep. Summaries of each method supporting the decision to apply 40% of ultimate follow:

A.2. Calculations proposed by Haiar (2000)

Haiar (2000) proposes a design method based on allowable stress methodologies. The governing equation for this method is:

$$\sigma_{allow} = B * C_a * C_t * C_v * C_m \quad \text{(eq. 1)}$$

where B is a characteristic design value based upon static testing, C_a is a property adjustment factor, C_t is a temperature adjustment factor, C_v is a volume adjustment factor and C_m is a moisture adjustment factor. The characteristic value and the temperature adjustment factor were determined for this work by static testing (Schildmeyer, 2006). Values for the property adjustment factor, volume factor and moisture factor were developed elsewhere (Haiar, 2000). The calculations presented in this section seek to find a maximum design stress from the material static testing, so each factor is taken as a "worst case scenario" to find the least amount of reduction to the characteristic value.

First, a characteristic value for the material is determined via the equation:

$$B = X_{mean} - X_{mean}(k * COV) \quad \text{(eq. 2)}$$

where B is the characteristic value, X_{mean} is the average strength of a sample of static tests, k is a statistical confidence factor, and COV is the coefficient of variation defined as the standard deviation of a sample over the mean. For compression and tension, different characteristic values and property adjustment factors are found. The magnitudes of design level stresses are then very different for tensile and compressive modes of loading, with the calculations for both following:

Tension

X_{mean} = 2630.52 psi
k = 1.8794
(or a 5% exclusion limit at 75% Confidence)
COV = 0.1119

$$B = X_{mean} - X_{mean}(k * COV)$$
$$B = 2630.52 - 2630.52 \cdot (1.8794 * 0.1119)$$
$$B = 2077.31 psi$$

$C_a = 0.476$ (according to Haiar (2000))
$C_t = 0.80$ (according to Schildmeyer 2006)

Compression

X_{mean} = 7094.10 psi
k = 1.8794
(or a 5% exclusion limit at 75% Confidence)
COV = 0.0525

$$B = X_{mean} - X_{mean}(k * COV)$$
$$B = 7094.10 - 7094.10 \cdot (1.8794 * 0.0525)$$
$$B = 6394.14 psi$$

$C_a = 0.526$ (according to Haiar (2000))
$C_t = 0.80$ (according to Schildmeyer 2006)

$C_v = 1.0$ (according to Haiar (2000))
$C_m = 1.0$ (according to Haiar (2000))

$\sigma_{design} = B * C_a * C_t * C_v * C_m$
$\sigma_{design} = 2077.31 * 0.476 * 0.80 * 1.0 * 1.0$
$\sigma_{design,tension} = 971.04\,psi$
(30.1% of Capacity)

$C_v = 1.0$ (according to Haiar (2000))
$C_m = 1.0$ (according to Haiar (2000))

$\sigma_{design} = B * C_a * C_t * C_v * C_m$
$\sigma_{design} = 6394.14 * 0.526 * 0.80 * 1.0 * 1.0$
$\sigma_{design,compression} = 2690.65\,psi$
(37.9% of Capacity)

Therefore, from the proportion of allowable design stress to ultimate capacity for each loading mode, an estimate of 40% of ultimate is a reasonable upper bound to investigate for creep performance.

A.3. Calculations proposed by Davidow and Fridley (2003)

Davidow and Fridley (2003) propose a design method based upon energy. In this method, an equivalent yield point is determined by considering the strain energy under the stress-strain curve. A consideration of energy is justified according to Davidow and Fridley (2003) because of the difference between the linear elastic wood and nonlinear WPC behaviors. Once an equivalent yield point is determined by energy considerations, the yield point can be used in design rather than values based upon ultimate stress and strain.

To determine the equivalent yield point a series of static tests must be performed to generate a curve for the stress-strain behavior of the material. The exact integrated area is then calculated at every point along the curve, starting at the origin and progressing toward specimen failure. Simultaneously, the linear elastic approximation to each point is calculated. Because of the nonlinear behavior of the WPC, as these calculated points move further along the diagram, a greater discrepancy between the

exact strain energy and the approximated linear strain energy will develop. Once this difference between the two quantities reaches a threshold level (a difference >5% is recommended in the paper), that point is determined as the equivalent yield point. This approach is illustrated for the tensile stress strain behavior in Figure A.1.

This approach to determine an equivalent yield point was followed for both tension and compression. In the tensile mode of loading, a value of 1018 psi was determined as the equivalent yield point. This value corresponds to 39.3% of the ultimate capacity in this mode. For compression, a value of 1550 psi was found for the equivalent yield point, and corresponds to 20.7% of the ultimate capacity in compression.

The percentages of ultimate capacity found using the energy considerations compare reasonably with the assumption of 40% of capacity for this work. The greatest concern when comparing this approach to the load applied in the tests here is that the compressive equivalent yield point is calculated to be a much lower percentage than the load that was applied in those tests. This discrepancy is due to the high level of nonlinearity in this mode causing an overly conservative yield point to be calculated. Again, this tendency to underestimate a yield point for "highly nonlinear materials" (materials that exhibit an unreasonably low equivalent yield point) is directly addressed by Fridley and Davidow (2003) and is just one consideration that must be kept in mind when applying this approach.

A.4. References

Davidow, S.A. and Fridley, K.J., "Development of Design Values for Wood-Plastic Composite Materials." Journal of Materials in Civil Engineering, Vol. 15, Iss. 5, pp. 415-418, 2003.

Haiar, K.J., "Performance and Design of Prototype Wood-Plastic Composite Sections." Master Thesis, Washington State University, May 2000.

Schildmeyer, A.J., "Temperature and Time Dependent Behaviors of a Wood-Polypropylene Composite." Chapter 2, Master Thesis, Washington State University, July 2006.

A.5. Figures

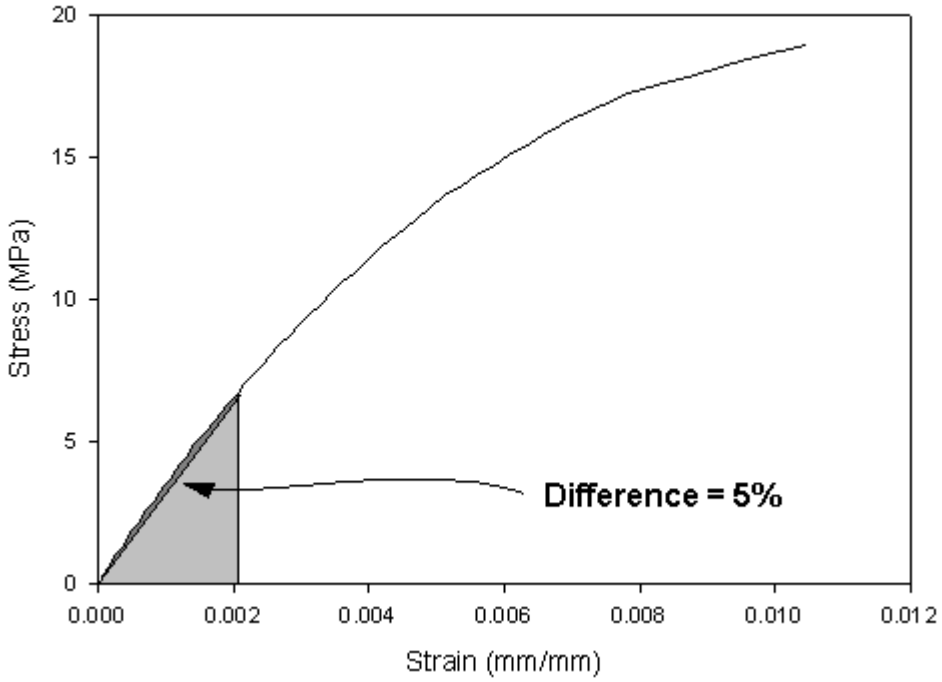

Figure A.1. The approach of comparing an exact strain energy calculation to a linear approximated strain energy to determine an equivalent yield point (here, in tension).

APPENDIX B

COMPARISON OF FLEXURAL CREEP BETWEEN A KNOWN AND AN UNKNOWN FORMULATION FOR WPCs

B.1 Introduction

The widespread use of wood plastic composites in engineering applications requires sufficient material property knowledge and predictive capability. Most polymer-based composites exhibit time dependent mechanical behavior, typically referred to as viscoelasticity (Jazouli, 2005). Theories available to predict linear viscoelasticity are well advanced and capable of predicting creep behavior of linear materials with remarkable accuracy (Findley et al., 1976; Findley, 1960; Fung, 1965; Flugge, 1967). Non-linear viscoelastic theories continue to be the subject of considerable research and are hampered by a lack of experimental results (Findley, 1960; Lou and Schapery, 1971; Rand, J.L., 1995; Schapery, 1969). The goal of this research is to identify the range of linear viscoelastic response for two materials and propose appropriate models from which generalizations on time-dependent responses can be based. Further, comparisons of performance between the two materials will illustrate the differences and similarities between their typical design behaviors.

B.2 Analytical Approach

A reliable and widely recognized creep model was used to evaluate the time-dependent deformation of WPCs tested in this study. The creep model used here is the power law proposed by Findley (Findley et al., 1976; Findley, 1960). This model is

reasonably simple and has been proven to apply to a variety of viscoelastic materials loaded at moderate levels, including fiber reinforced plastics. In addition, this model has been validated by creep tests with a total duration of up to 26 years (Findley, 1987). A full description of the stress dependent and stress independent power law proposed by Findley can be found in Kobbe (2005).

B.3 Materials and Methods

B.3.1 Control Material

The control material investigated was a polypropylene wood-plastic composite. These have a solid cross-section and are designed for use as deck boards. These have dimensions of 1-in (2.54-cm) by 5.5-in (13.97-cm) and were produced using a conical counter-rotating twin-screw extruder. All control specimens were composed of a polypropylene (PP) based formulation consisting of 58.8-percent pine (*Pinus* spp.) flour (60-mesh, American Wood Fibers 6020), 33.8-percent polypropylene (PP) matrix resin (Solvay HB9200), 4-percent talc (Luzenac Nicron 403), 2.3-percent MAPP coupling agent (Honeywell 950P), and 1.0-percent lubricant (Honeywell OP100) by weight. From previous static bending tests (Slaughter, 2004) the mean flexural mechanical properties were found to be:

- Ultimate strain ($\varepsilon_{failure}$) = 0.012-in/in
- Modulus of elasticity (MOE) = 794,081-psi (5475.0-Mpa)
- Modulus of rupture (MOR) = 6,494-psi (44.8-Mpa).

B.3.2 Experimental (unknown formulation) Material

The other, experimental material, from the University of Maine tested is an unknown composition wood-plastic composite. These boards have a complex, four-box cross-section and are assumed to also be deck boards. These specimens have nominal dimensions of 5.365-in (13.63-cm) by 1.451-in (3.69-cm) with exterior walls of thickness 0.372-in (0.94-cm), interior walls of thickness 0.245-in (0.62-cm) and flanges of thickness 0.266-in (0.68-cm). These specimens are most likely to have been extruded, but the specific conditions of the process and formulation to produce these specimens have not been disclosed to the experimenter. Static bending tests were performed upon 15 samples and mean flexural mechanical properties were found to be:

- Ultimate strain ($\varepsilon_{failure}$) = 0.016-in/in
- Modulus of elasticity (MOE) = 686,894-psi (4736.0-Mpa)
- Modulus of rupture (MOR) = 4,395-psi (30.3-Mpa).

B.3.3 Mechanical Test Methods

For both materials an identical procedure for creep testing was followed as proposed by Kobbe in 2005. Twenty-four test frames, operated within a controlled environment, were used for flexure creep tests. Weak-axis flexural creep was the loading mode of interest for both sets of material. Each frame has a support span of 24 inches (0.61-m), and two equal point loads were applied at the third points (8-in or 20.3-cm) from the support. Weights, used to supply the specified constant stress, were hung from a pulley providing an approximate 8:1 mechanical advantage. Each control specimen was subjected to a constant stress for 26 days while the experimental material was tested for a 30-day period. Center span displacement was measured with a linear position transducer.

Data acquisition software recorded displacement and time values throughout the test. Loads were determined by calculating percentages of MOR from static bending test data. The focus of determining loads this way was to determine if the material behaves linearly viscoelastic at stresses near design level. Thus, stress levels were targeted to be near 10, 15, 25, 35, and 45-percent of the mean ultimate bending stress.

For the control material, the percentages of MOR corresponded with maximum constant stresses of 649, 974, 1624, 2273, and 2922-psi (4.5, 6.7, 11.2, 15.7, and 20.1-Mpa) and were applied to eight specimens in each of the five groups. For the University of Maine material, the same percentages of MOR were used, and corresponded to maximum constant stresses of 440, 659, 1099, 1538, and 1978-psi (3.0, 4.5, 7.6, 10.6 and 13.6-Mpa). These loads were applied to seven specimens in each of the five groups. These percentages of MOR approximately correspond to 30, 40, 70, 100, and 130-percent of the design bending stress, assuming that design level stresses are typically around 35% ultimate strength.

B.4 Analytical Methods

B.4.1 Beam Theory

Deflection data was obtained for each specimen at each load level. This data was then averaged over the specimens for each reading. This average deflection value, δ, was then used in Equation (1) to arrive at a maximum strain in the outer fibers:

$$\varepsilon_{\max} = \frac{108\delta h}{23L^2} \qquad (1)$$

where: δ = averaged maximum mid-span deflection; h = thickness of the specimen; and L = span length (24-in for all load frames), to calculate the maximum strain, ε_{max}, in the

outer fiber at the mid-span. The corresponding maximum fiber stress, σ_{max}, was calculated using the relation:

$$\sigma_{\max} = \frac{PLh}{12I} \quad (2)$$

where P = applied load and I = moment of inertia about the weak axis. Equation (2) is a special form of the flexural formula:

$$\sigma = \frac{My}{I} \quad (3)$$

where M = bending moment ($PL/6$ for third point bending) and y = distance to the neutral axis (assumed to be $h/2$). Equation (A5) is obtained by combining equations (A1), (A2) and the constitutive equation (A4):

$$\sigma = E\varepsilon \quad (4)$$

Thus, one arrives at a form relating displacement to only one unknown, E:

$$\delta = \frac{23L^3P}{1296EI} \quad (A5)$$

B.4.2 Findley's Power Law

The general form of the Findley Power Law is dependent upon stress-dependent parameters. Therefore, the general form of Findley's Power Law looks like:

$$\varepsilon_t = \varepsilon_0 + m\left(\frac{t}{t_0}\right)^n \quad (A6)$$

Where ε_t is the strain at time t, ε_0 is the initial strain at load application, m is an empirical creep coefficient, t is the time of interest, t_0 is the time increment (most often taken as unity), and n is an exponential empirical constant. Of these parameters, the initial strain and coefficient, m, depend substantially upon stress level. The exponential variable, n, is effectively constant over all stress levels.

The general form of the power law, Equation (A6) above, can then be made stress independent by substituting the hyperbolic-sine function and dimensionless ratios of stress in place of the initial strain and coefficient parameters. These stress independent

parameters are shown as ε_0' and m' below and are related to the corresponding stress dependent values via the expressions below:

$$\varepsilon_0 = \varepsilon_0' \sinh\left(\frac{\sigma}{\sigma_\varepsilon}\right) \tag{A7}$$

$$m = m' \sinh\left(\frac{\sigma}{\sigma_m}\right) \tag{A8}$$

Values for the remaining undefined terms in the expressions above, σ_ε and σ_m, are empirical values determined by maximizing the linearity of the relationships between ε_0 and $\sinh(\sigma/\sigma_\varepsilon)$ and m and $\sinh(\sigma/\sigma_m)$. To better illustrate where these values of reference stresses come from, they are represented as the slopes of the fit lines in Figure C.3 and Figure C.4. Also, because the parameter, n, is nearly stress independent, the value used in the stress independent form is considered to be the average of all the n-values for the data from the stress dependent form.

Strain at any time, t, may then be calculated for this loading pattern with reasonable accuracy according to the stress independent formula shown below:

$$\varepsilon_t = \varepsilon_0' \sinh\left(\frac{\sigma}{\sigma_\varepsilon}\right) + m' \sinh\left(\frac{\sigma}{\sigma_m}\right)\left(\frac{t}{t_0}\right)^n \tag{A9}$$

Furthermore, inputting the calculated constants from Table C.3, the equation for the University of Maine experimental specimens becomes:

$$\varepsilon_t = 5.68e^{-3} \sinh\left(\frac{\sigma}{3814\,psi}\right) + 1.16e^{-4} \sinh\left(\frac{\sigma}{1094\,psi}\right)\left(\frac{t}{1.0\,\min}\right)^{0.240} \tag{A10}$$

As stated earlier, the preceding constants are only valid for the University of Maine material under moderate stress ranges (less than 50% of MOR). Furthermore, keep in mind that the strains determined by this equation may differ from experimental

strains by up to 8%. These results indicate that Findley's power law modeling is an acceptably accurate model to evaluate the time-dependent creep behavior of both materials, at least with respect to most Civil Engineering applications.

B.5 Results and Discussion

Experimental and theoretical creep-strain curves for the control material are shown in Figure C.1. Figure C.2 illustrates the same parameters for the undisclosed University of Maine, or experimental, formulation. Mathematical predictions are formulated using both the general form of the Findley Power Law as well as the stress independent model of the same power law. The general model requires fitting the creep parameters *m* and *n* to experimental data at each specific stress level. The initial elastic strain, ε_0, was taken as the strain recorded immediately following load application.

Table C.1 summarizes the strains arrived at through testing at specific points in time for the five percentages of MOR for both the control and the experimental materials. These experimentally obtained values were then compared with values calculated using the Findley Power Law in both stress dependent and stress independent forms. Calculated strain values predicted by the Findley Power Law and the parameters used to determine these predicted strains are presented in Table C.2 for the general power law (stress dependent) and Table C.3 for the stress independent power law. Note that the results for both power law calculations are in general agreement with the experimental results with the general power law deviating from the experimental by no more than 1.81% and the stress-independent by no more than 7.59%.

Figures C.7 and C.8 compare creep compliance values for the five percentages of MOR for both the control and University of Maine materials. Evaluation of the compliance data indicates that both materials exhibit non-linear mechanical behavior even at low levels of stress. The rate of change of the compliance also varies throughout the time span of the test – in that the compliance increases rapidly at the start of testing but increases at a decreasing rate. A constant compliance would indicate entering a secondary creep stage for materials such as these.

Serviceability is often a major concern for wood-plastic composite materials. These tests clearly indicate that creep behavior will contribute substantially to deflection concerns. For the control material, deflections ranged from L/268 to L/53 at the onset of loading while the University of Maine material ranged from L/445 to L/93. However, at the end of testing, the deflections had increased to range from L/142 to L/19 for the control material and L/270 to L/35 for the University of Maine material. L in this case is the span length and corresponds to 24 inches.

B.6 Conclusions

Findley's power law is a reasonably accurate method for predicting creep behavior of both a control wood-plastic material and an undisclosed wood-plastic formulation from the University of Maine. Using Findley's stress-independent model, maximum strains were calculated within tolerances generally accepted by the civil engineering community. This predictive procedure is only valid, however, for primary viscoelastic creep of these materials. Changes in creep mechanism or transitioning from primary to secondary creep are not phenomena able to be explained by Findley's power

law. Both wood-plastic materials exhibited non-linear viscoelastic mechanical behavior, even at low stress levels. Similar to previous findings, serviceability may end up being a limiting factor for the uses of both these formulations. Serviceability remains a major consideration when using these materials.

Comparing these two materials, there are a number of performance parameters that warrant consideration. Compliance is of primary concern for comparison of these two types of specimens. Similar percentages of MOR for each material determined that the experimental material produces higher values for compliance than the control material. This is the case not only for initial compliance, J(0), but also values throughout the duration of testing. Furthermore, even at similar stress levels, compliance was greater for the experimental material throughout the duration of testing.

Another aspect to consider when comparing these two materials would be to examine the data at common percentages of MOR. This is because code-based design often is based upon utilization of its strength up to a percentage of its ultimate capacity. Assuming that code-based percentage to only allow 35% of ultimate will allow comparisons between these two materials in similar service conditions (remembering that load magnitudes would then be different). At this common percentage of MOR, the control material deflected approximately double the amount that the material from University of Maine did. Also, as stated previously, the compliance for the material from Maine was of larger magnitude throughout testing than the values for the control material. For the control material, the extreme fiber strains were 0.0066 in/in (55% of $\varepsilon_{ultimate}$ for the material) whereas the strain in the University of Maine material was only 0.0058 in/in (37% of $\varepsilon_{ultimate}$ for the material).

The last perspective to compare these two materials is their performance under a loading condition that causes similar stresses throughout their cross-sections. In this light, it would be best to compare the performance of the control material at a maximum stress of 1624 psi with the experimental material at a stress of 1566 psi. These are the loading scenarios that are closest in magnitude and will not exhibit uncharacteristic behavior from low levels of stress. The trend with compliance magnitudes continues with the experimental material having substantially higher values throughout testing. However, with respect to long-term deflection and maximum strains at the end of testing, both materials are very similar, with the control material deflecting 0.42 inches and having maximum strains of 35% of $\varepsilon_{ultimate}$ whereas the University of Maine material deflected 0.50 inches and encompassed 37% of $\varepsilon_{ultimate}$ for the material.

These two materials seem to have very different applications. The control material exhibits lower compliance and has a higher modulus of rupture. The differences in deflection demonstrated by these two sets of boards is influenced greatly by the complex cross section of the University of Maine samples as compared to the solid cross section of the control material, and not solely to differences in mechanical properties themselves. But, keeping this difference in geometry in mind, the in-service design level stresses appear to cause greater deflections in the control material and would make serviceability more of a concern. If serviceability concerns can be addressed, one major obstacle blocking the full utilization of either of these materials will be overcome.

B.7 References

Findley, W.N., "Mechanisms and Mechanics of Creep of Plastics." SPEJ, Vol. 16, pp. 57-65, January 1960.

Findley, W.N., Lai, J.S., and Onaran, K., "Creep and Relaxation of Nonlinear Viscoelastic Materials." North-Holland Publishing Company, New York, NY, 1976.

Findley, W.N., "26-year Creep and Recovery of Polyvinylchloride and Polyethylene." Polymer Engineering and Science, Vol. 27, No. 8, pp. 582-585, 1987.

Flugge, W., "Viscoelasticity." Blaisdell, Waltham, MA, 1967.

Fung, Y.C., "Foundations of Solid Mechanics." Prentice Hall, Englewood Cliffs, NJ, 1965.

Jazouli, S., Luo, W., Bremand, F., and Vu-Khanh, T., " Application of Time-stress Equivalence to Nonlinear Creep of Polycarbonate." Polymer Testing, Vol. 24, pp. 463-467, 2005.

Kobbe, R.G., "Creep Behavior of Wood-Polypropylene Composites." Chapter 3, Master Thesis, Washington State University, June 2005.

Lou, Y.C. and Schapery, R.A., "Viscoelastic Characterization of a Nonlinear Fiber-Reinforced Plastic," Journal of Composite Materials, Vol. 5, pp. 208-234, 1971.

Rand, J.L., "A Nonlinear Viscoelastic Creep Model." Tappi Journal, Vol. 78, No. 7, pp. 178-182, July 1995.

Schapery, R.A., "On the Characterization of Nonlinear Viscoelastic Materials." Polymer Engineering and Science, Vol. 9, No. 4, pp. 295-310, 1969.

Slaughter, A.E., "Design and Fatigue of a Structural Wood-Plastic Composite." Master Thesis, Washington State University, August 2004.

B.8 Tables

Table B.1. Experimental strain values at specific points in time at the five different percentages of MOR for both the control material and the Univ. of Maine specimens.

			Average Experimental Strain (%)			
Specimens	% of MOR	Stress (psi)	t = 1	t = 12,000	t = 24,000	t = 36,000
Control Specimens	45.0	2922	0.396	0.876	0.961	0.991
	35.0	2273	0.297	0.588	0.961	0.657
	25.0	1624	0.202	0.370	0.402	0.412
	15.0	974	0.119	0.200	0.209	0.215
	10.0	649	0.076	0.118	0.128	0.136
U of Maine Specimens	45.3	1993	0.326	0.519	0.556	0.574
	35.6	1566	0.255	0.385	0.409	0.422
	25.6	1123	0.182	0.255	0.271	0.280
	15.0	661	0.108	0.150	0.160	0.165
	10.0	438	0.066	0.081	0.087	0.089

Table B.2. Calculated Findley's general power law parameters and the predicted strains at specific points in time and their difference from the experimental results reported in Table C.1.

Specimens Loaded	% of MOR	Stress (psi)	Creep Parameters				General Power Law Predicted Strain (%)				Ave. Error From Experimental Values
			εo (%)	m(ε)	n	r^2	t = 1	t = 12,000	t = 24,000	t = 36,000	
Control Specimens	45.0%	2922	0.370	0.039	0.263	0.985	0.41	0.835	0.928	0.991	-1.26%
	35.0%	2273	0.281	0.025	0.259	0.984	0.306	0.566	0.622	0.659	-0.92%
	25.0%	1624	0.194	0.014	0.260	0.985	0.208	0.358	0.39	0.412	-0.89%
	15.0%	974	0.113	0.009	0.229	0.990	0.122	0.192	0.206	0.215	-0.79%
	10.0%	649	0.072	0.006	0.222	0.985	0.078	0.119	0.127	0.132	-0.10%
U of Maine Specimens	45.3%	1993	0.304	0.035	0.253	0.985	0.339	0.514	0.554	0.586	1.19%
	35.6%	1566	0.243	0.023	0.256	0.984	0.265	0.382	0.409	0.430	1.27%
	25.6%	1123	0.175	0.014	0.252	0.976	0.189	0.257	0.273	0.285	1.81%
	15.0%	661	0.104	0.009	0.223	0.968	0.113	0.149	0.156	0.162	0.43%
	10.0%	438	0.064	0.004	0.215	0.977	0.068	0.083	0.086	0.088	0.21%

Table B.3. Calculated Findley's stress-independent power law parameters and the predicted strains at specific points in time and their difference from the experimental results reported in Table C.1.

Specimens Loaded	% of MOR	Stress (psi)	Creep Parameters (Stress Independent)				Stress-Independant Power Law Predicted Strain (%)				Ave. Error From Experimental Values
			εo (%)	εo' (%)	m' (ε)	n	t = 1	t = 12,000	t = 24,000	t = 36,000	
Control Specimens	45.0%	2922	0.370	0.332	0.012	0.246	0.417	0.777	0.852	0.902	-7.59%
	35.0%	2273	0.281	0.332	0.012	0.246	0.301	0.529	0.576	0.607	-7.34%
	25.0%	1624	0.194	0.332	0.012	0.246	0.204	0.341	0.369	0.388	-5.66%
	15.0%	974	0.113	0.332	0.012	0.246	0.118	0.191	0.206	0.216	-1.64%
	10.0%	649	0.072	0.332	0.012	0.246	0.078	0.124	0.134	0.141	3.86%
U of Maine Specimens	45.3%	1993	0.304	0.568	0.012	0.240	0.345	0.509	0.540	0.566	-0.11%
	35.6%	1566	0.243	0.568	0.012	0.240	0.270	0.370	0.390	0.407	-1.65%
	25.6%	1123	0.175	0.568	0.012	0.240	0.189	0.250	0.263	0.273	-1.08%
	15.0%	661	0.104	0.568	0.012	0.240	0.109	0.141	0.148	0.153	-5.44%
	10.0%	438	0.064	0.568	0.012	0.240	0.072	0.093	0.097	0.088	7.19%

B.9 Figures

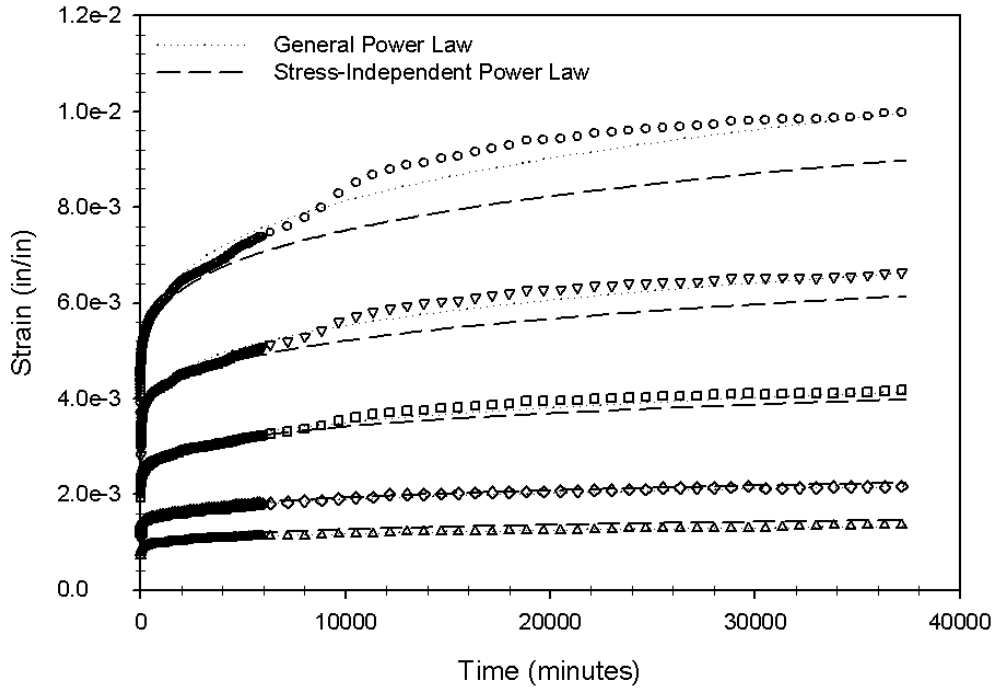

Figure B.1. Measurements and predictions for the control material wrt creep strain in flexure.

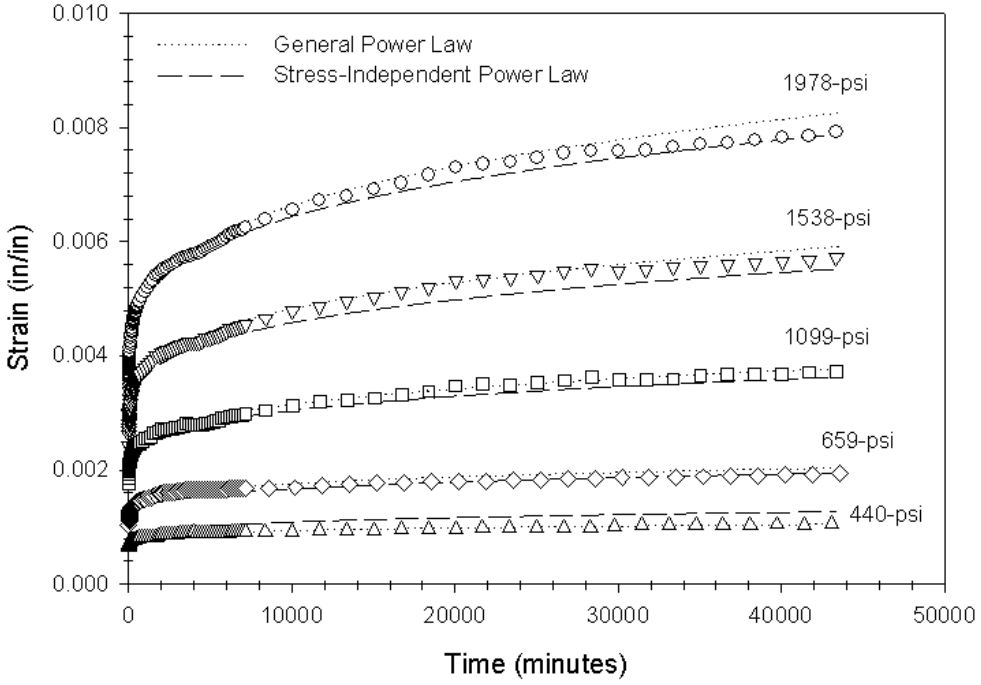

Figure B.2. Measurements and predictions for the Univ. of Maine material wrt creep strain in flexure.

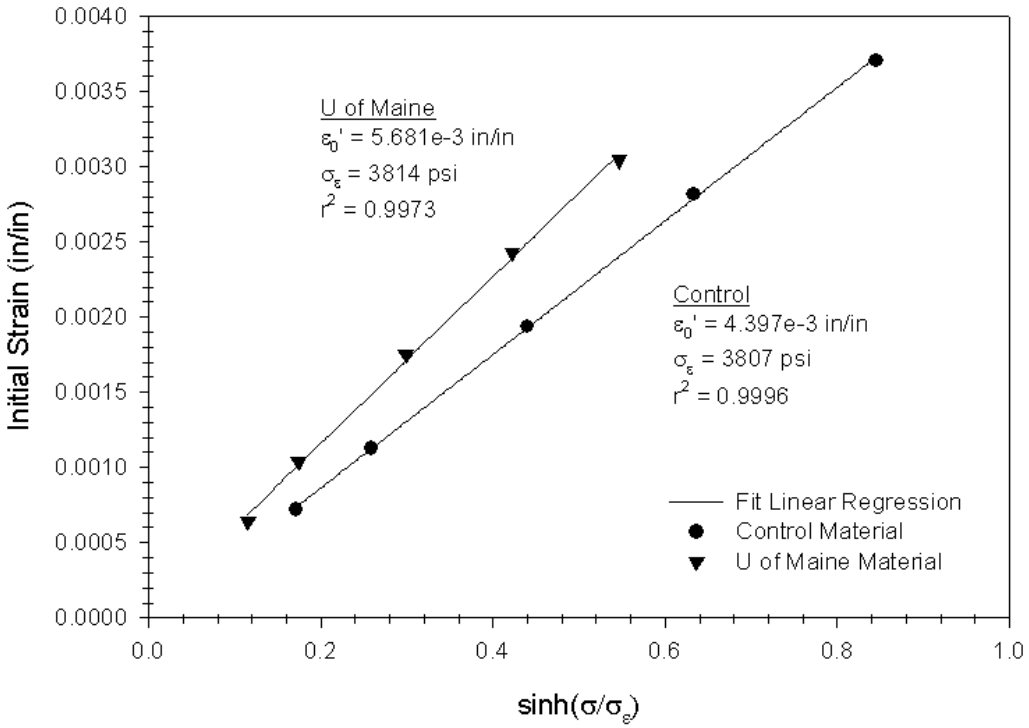

Figure B.3. Evaluation of creep parameters ε_0' and σ_ε for both materials.

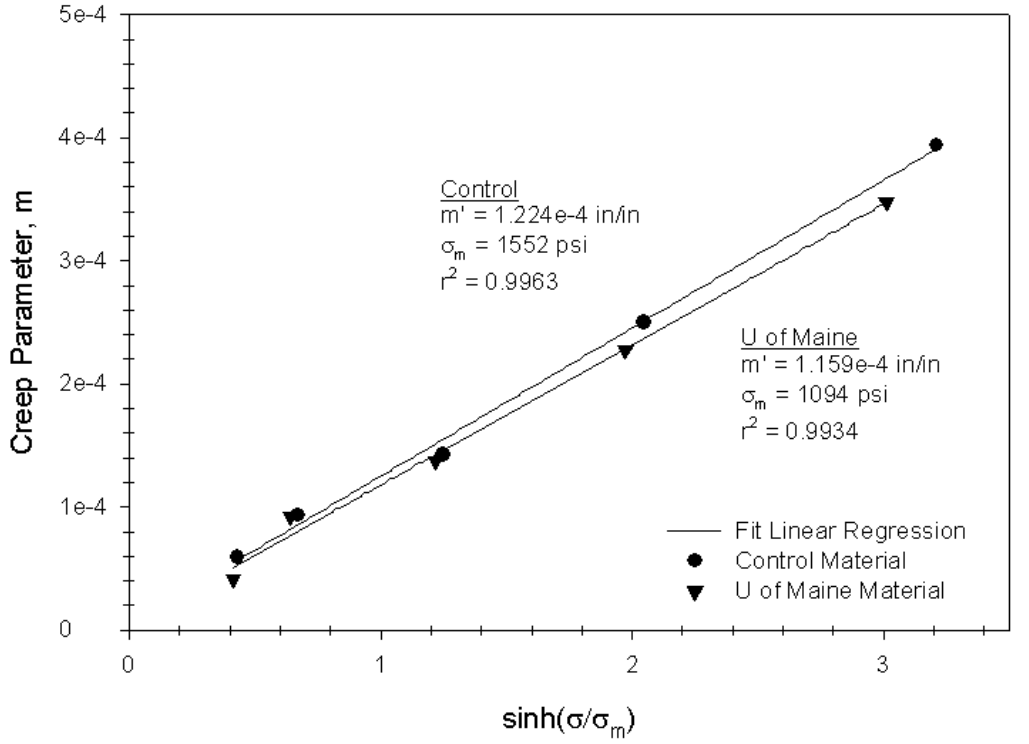

Figure B.4. Evaluation of creep parameters m and σ_m for both materials.

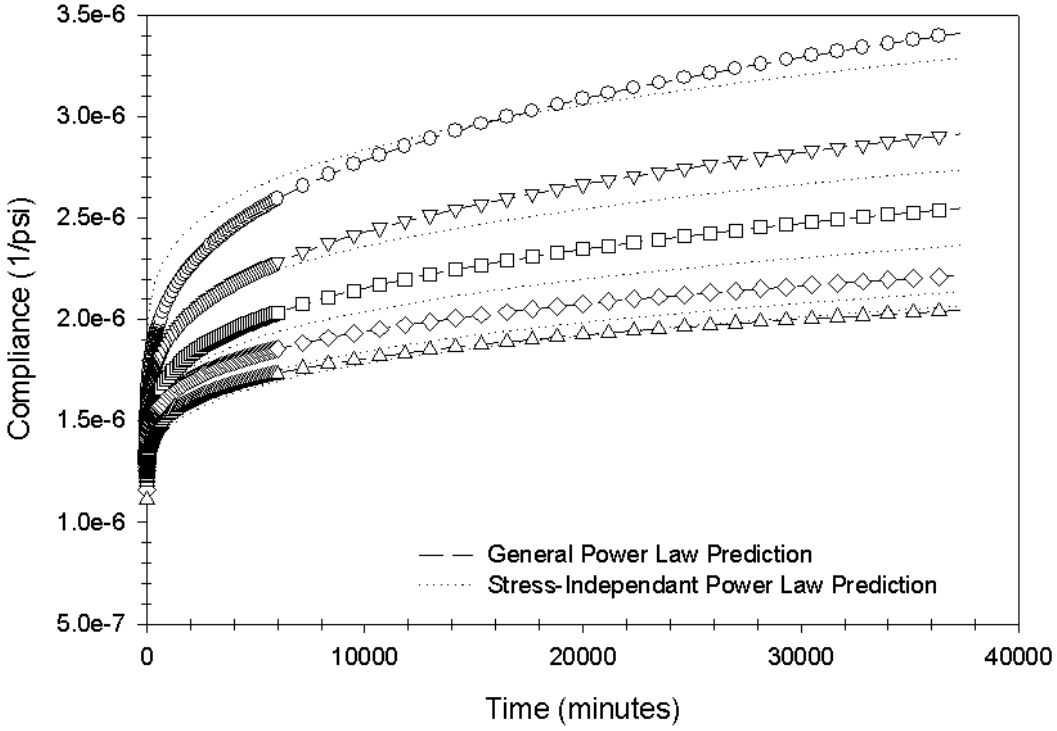

Figure B.5. Creep compliance measurements for the control material in flexure.

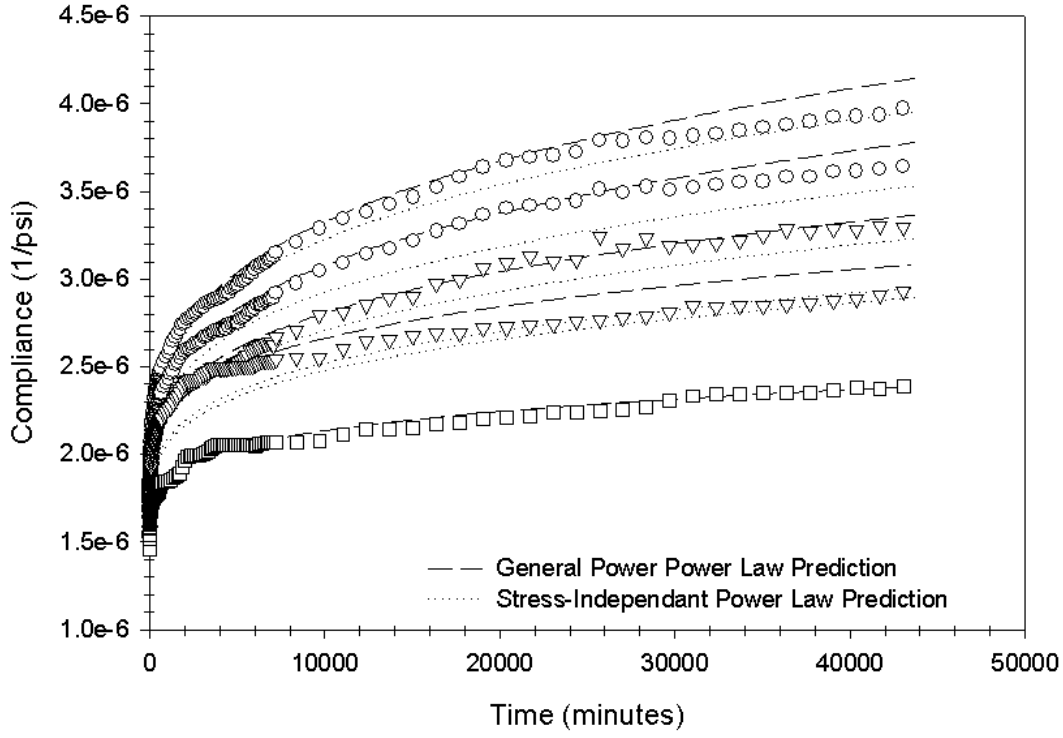

Figure B.6. Creep compliance measurements for the U of Maine material in flexure.

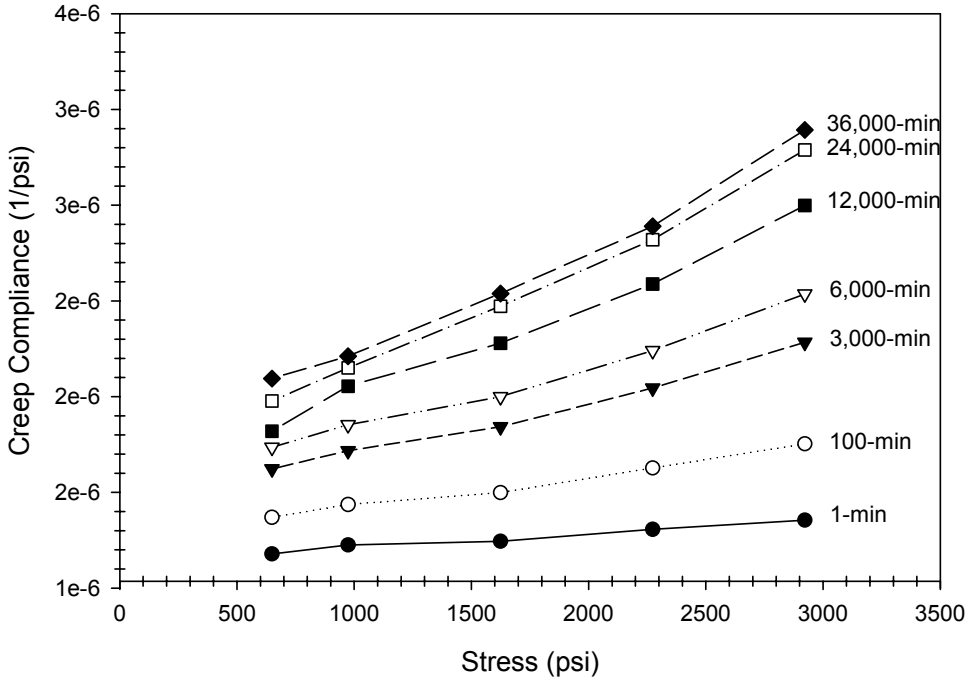

Figure B.7. Creep compliance measurements for the control material at various times throughout the test.

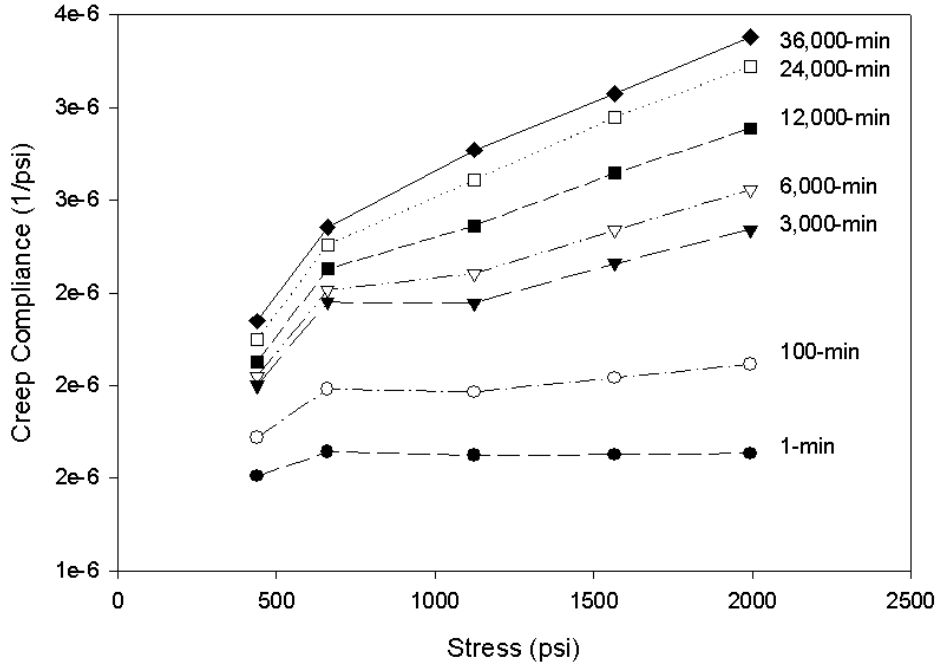

Figure B.8. Creep compliance measurements for the Univ. of Maine material at various times throughout the test.

APPENDIX C

TABULATED EXPERIMENTAL TEST RESULTS

Table C.1. Summary table of static test results from tension tests conducted at 21.1°C (70°F).

					Used to Calculate E				
Specimen Number	Max Load	Max Strain (%)	Average Area	Average Stress (psi)	Low Stress (psi)	Low Strain (in/in)	High Stress (psi)	High Strain (in/in)	Elastic Modulus (psi)
A1-26	796.19	1.0810	0.2727	2919.38	246.96	0.00048	497.48	0.00105	439504.67
A1-33	815.72	1.0460	0.2491	3274.58	261.52	0.00052	486.40	0.00104	432464.73
A2-31	661.23	0.7010	0.2870	2303.81	207.85	0.00031	384.83	0.0007	453793.58
A2-32	791.41	0.8050	0.2995	2642.85	260.91	0.0004	436.62	0.00079	450552.86
A2-33	719.29	0.8320	0.2717	2647.62	217.08	0.00038	468.23	0.00078	627889.33
A2-34	799.51	0.8530	0.2997	2667.89	238.49	0.00041	475.48	0.00083	564280.12
A2-23	805.42	0.9410	0.2656	3032.11	237.86	0.00045	441.85	0.00089	463615.75
A2-24	735.45	0.9800	0.2901	2535.33	290.51	0.00049	514.38	0.00097	466394.01
A2-25	774.02	0.9090	0.2950	2623.55	255.92	0.00045	488.98	0.00089	529662.88
A2-26	642.87	0.7300	0.2895	2220.60	166.23	0.00036	347.03	0.00067	583208.08
A2-27	721.39	0.9790	0.2933	2459.25	252.23	0.00047	488.35	0.00097	472243.76
A2-39	627.05	0.8730	0.2838	2209.56	208.91	0.00042	388.75	0.00083	438615.79
A1-29	577.25	0.7560	0.2555	2259.52	176.04	0.00036	343.81	0.00071	479337.05
A1-20	812.31	1.0280	0.2565	3166.48	247.44	0.00046	468.39	0.00101	401718.80
A2-35	720.07	0.9050	0.2893	2488.62	196.91	0.00042	423.30	0.00086	514524.29
A2-36	757.76	0.9960	0.2765	2740.12	251.00	0.00049	471.32	0.00098	449648.70
A2-37	715.04	0.9850	0.2799	2554.39	270.49	0.00048	481.86	0.00098	422728.37
A2-38	690.48	0.7490	0.2609	2646.88	223.70	0.00037	435.50	0.00074	572429.98
A2-22	609.77	0.6840	0.2767	2203.45	196.80	0.00034	442.97	0.00068	724033.75
A2-21	814.36	1.0370	0.2653	3069.48	250.15	0.00049	499.74	0.00103	462208.31
A2-20	775.78	0.8530	0.3077	2520.83	203.84	0.00042	402.60	0.00083	484777.20
A2-10	755.03	1.0930	0.2838	2660.35	262.49	0.00052	510.57	0.00109	435236.92
A2-11	733.98	0.8170	0.2917	2516.30	217.36	0.00037	446.25	0.0008	532306.60
A2-30	623.15	0.6400	0.2564	2430.02	138.84	0.00032	252.70	0.00064	355834.41
A2-29	688.23	0.7990	0.2892	2380.03	225.11	0.00037	528.74	0.00077	759080.78
A2-28	721.48	1.1220	0.2815	2562.88	239.13	0.00055	515.82	0.0011	503063.32
A1-34	776.47	1.0380	0.2649	2930.66	298.86	0.00049	571.01	0.00101	523355.99
A1-35	695.90	0.9980	0.2329	2987.99	321.56	0.00047	643.76	0.00099	619605.36
Mean	727.02	0.9011	0.2774	2630.52	234.43	0.00043	459.16	0.00088	505789.83
Std. Dev.	67.89	0.1357	0.0176	294.48	40.00	6.5E-05	75.10	0.00014	92506.28
COV	9.33%	15.06%	6.35%	11.19%	17.06%	15.10	16.36	15.76	18.29%

Table C.2. Summary table of static test results from tension tests conducted at 30°C (86°F).

Specimen Number	Max Load	Max Strain (%)	Average Area	Average Stress (psi)	Used to Calculate E: Low Stress (psi)	Low Strain (in/in)	High Stress (psi)	High Strain (in/in)	Elastic Modulus (psi)
AJ 49 T2	744.82	1.2240	0.2827	2634.51	302.48	0.00056	623.83	0.00122	486897.62
A2-09	657.91	1.3010	0.2873	2289.70	260.79	0.00062	497.59	0.00124	381932.53
A1-18	671.19	1.2870	0.2562	2619.75	310.54	0.00064	600.56	0.00128	453155.37
AJ 47 B1	598.93	0.9020	0.2751	2177.10	193.37	0.00038	386.55	0.00081	449262.36
AJ 36 B2	628.17	1.1460	0.2776	2262.98	214.02	0.00055	411.41	0.0011	358891.71
A1-05	674.27	1.0060	0.2583	2610.34	179.79	0.00045	361.29	0.00096	355873.37
AJ 47 B2	695.51	1.1720	0.2758	2522.06	334.42	0.00057	559.51	0.00116	381500.81
AJ 36 B4	657.13	1.0360	0.2764	2377.15	245.64	0.00047	482.64	0.00102	430909.46
A1-06	695.31	1.2300	0.2603	2671.38	317.18	0.00059	570.67	0.00122	402354.60
AJ 43 B2	627.34	0.8980	0.2693	2329.85	301.00	0.00044	547.67	0.00089	548151.83
AJ 43 T2	705.66	1.2060	0.2734	2581.13	254.69	0.00059	443.13	0.0012	308912.81
AJ 47 B3	656.89	1.1130	0.2746	2392.14	301.55	0.00055	517.35	0.00103	449586.42
A1-09	746.34	1.0780	0.2572	2902.05	320.62	0.00051	600.04	0.00106	508045.27
AJ 43 T3	702.73	1.1730	0.2735	2569.00	260.47	0.00055	456.62	0.00115	326929.39
AJ 36 B3	616.02	1.0870	0.2799	2200.58	276.94	0.00054	495.25	0.00104	436624.95
AJ 43 T1	702.15	1.1540	0.2738	2564.37	181.14	0.00056	376.67	0.00114	337111.07
AJ 43 B4	616.02	0.7850	0.2702	2279.68	393.17	0.00033	675.37	0.00077	641375.30
AJ 43 B3	656.74	0.9730	0.2700	2432.43	380.61	0.00047	643.22	0.00096	535928.48
A1-32	648.05	1.1390	0.2561	2530.03	339.37	0.00054	650.15	0.00112	535836.43
A1-31	734.47	1.2640	0.2576	2850.88	270.51	0.00063	567.61	0.0012	521230.91
A1-25	785.79	1.5220	0.2618	3002.04	385.39	0.00074	721.53	0.0015	442284.06
AJ 49 T1	681.45	1.1230	0.2832	2405.86	212.16	0.00056	505.23	0.0011	542719.55
A1-37	663.28	1.2690	0.2547	2603.86	195.01	0.00061	439.11	0.00119	420858.42
A1-44	703.22	1.1080	0.2610	2694.47	207.83	0.00052	416.04	0.00103	408246.02
A1-36	758.15	1.5940	0.2560	2961.24	270.88	0.00076	615.45	0.00159	415151.97
AJ 43 T4	700.10	1.2450	0.2750	2545.46	179.88	0.00062	404.32	0.0012	386973.26
A1-30	849.22	1.3740	0.2943	2885.92	247.23	0.00067	527.68	0.00134	418578.27
AJ 36 B1	589.60	0.8790	0.2748	2145.46	221.42	0.00042	431.82	0.00085	489305.64
Mean	684.52	1.1531	0.2702	2537.19	269.93	0.00055	518.87	0.00112	441950.99
Std. Dev.	58.34	0.1815	0.0107	238.74	63.55	0.00010	98.76	0.00019	78191.20
COV	8.52%	15.74%	3.96%	9.41%	23.54%	17.73%	19.03%	16.59%	17.69%

Table C.3. Summary table of static test results from tension tests conducted at 40°C (104°F).

					Used to Calculate E				
Specimen Number	Max Load	Max Strain (%)	Average Area	Average Stress (psi)	Low Stress (psi)	Low Strain (in/in)	High Stress (psi)	High Strain (in/in)	Elastic Modulus (psi)
AJ 49 B4	631.35	1.2490	0.2750	2295.53	261.88	0.0006	553.15	0.00121	477499.35
AJ 38 T2	633.01	1.2780	0.2725	2322.57	185.76	0.00063	385.79	0.00124	327910.15
AJ 39 B3	654.49	1.4460	0.2805	2333.02	264.94	0.00072	500.91	0.00144	327729.86
AJ 42 B2	687.99	1.7110	0.2737	2513.42	253.60	0.00083	527.43	0.00169	318411.62
AJ 42 B1	649.12	1.2870	0.2767	2346.32	231.18	0.00063	427.03	0.00128	301312.01
AJ 36 T4	609.08	1.0730	0.2781	2189.81	235.24	0.00049	499.17	0.00104	479877.63
AJ 36 T3	585.79	1.4730	0.2771	2113.89	290.71	0.00072	505.03	0.00145	293596.77
AJ 49 B3	593.56	1.1440	0.2746	2161.73	232.39	0.00052	422.22	0.00113	311209.78
AJ 46 B1	574.85	1.0020	0.2698	2130.96	176.66	0.00048	331.78	0.00098	310231.61
AJ 38 T3	626.17	1.5480	0.2686	2331.04	221.67	0.00076	434.26	0.00153	276094.02
AJ 42 B3	664.45	1.6670	0.2723	2440.37	213.53	0.00079	446.60	0.00165	271002.57
AJ 42 B4	627.44	1.3640	0.2683	2338.21	172.21	0.00067	361.40	0.00131	295595.01
AJ 38 B1	589.89	1.2040	0.2742	2150.96	365.41	0.00058	588.51	0.0012	359835.45
AJ 38 B2	594.87	1.0210	0.2743	2168.61	392.59	0.00051	605.36	0.00102	417201.93
AJ 38 B3	575.54	1.0700	0.2747	2094.98	256.97	0.00052	494.65	0.00107	432144.46
AJ 38 B4	581.64	1.1750	0.2780	2092.19	242.97	0.00056	485.25	0.00117	397177.92
AJ 38 T1	643.16	1.5560	0.2766	2325.09	207.86	0.00073	441.06	0.00154	287902.16
AJ 39 B1	609.28	1.3640	0.2801	2175.34	231.71	0.00067	450.25	0.00135	321378.33
AJ 39 B2	652.88	1.6180	0.2831	2305.79	269.46	0.00075	526.53	0.00161	298928.37
AJ 47 B4	627.49	1.3290	0.2745	2285.63	301.95	0.00066	510.93	0.00125	354211.41
A1-02	619.04	1.1980	0.2568	2410.49	321.43	0.00056	559.51	0.00117	390283.62
AJ 37 B1	616.90	1.3360	0.2747	2245.80	181.94	0.00064	412.47	0.00133	334095.52
AJ 37 B2	584.67	1.3380	0.2725	2145.66	196.12	0.00066	415.51	0.00133	327459.19
AJ 36 T1	567.97	1.0330	0.2815	2017.55	270.36	0.0005	454.21	0.00103	346887.46
AJ 48 T3	585.84	1.1190	0.2729	2146.83	299.29	0.0005	484.66	0.00105	337025.24
AJ 40 T2	514.01	0.9350	0.2647	1942.08	259.37	0.00043	430.86	0.00093	342977.34
AJ 40 T1	551.61	1.0140	0.2662	2072.04	259.54	0.00049	442.50	0.00101	351842.63
AJ 48 T4	556.01	1.2570	0.2713	2049.43	262.67	0.00061	466.18	0.00124	323038.22
Mean	607.43	1.2789	0.2737	2219.48	252.12	0.00061	470.11	0.00126	343316.42
Std. Dev.	38.75	0.2141	0.0055	137.51	52.79	0.00011	64.85	0.00021	54902.30
COV	6.38%	16.74%	2.01%	6.20%	20.94%	17.41%	13.79%	16.95%	15.99%

Table C.4. Summary table of static test results from tension tests conducted at 50°C (122°F).

					Used to Calculate E				
Specimen Number	Max Load	Max Strain (%)	Average Area	Average Stress (psi)	Low Stress (psi)	Low Strain (in/in)	High Stress (psi)	High Strain (in/in)	Elastic Modulus (psi)
A1-07	582.57	1.5020	0.2535	2297.99	325.94	0.00075	584.90	0.00150	345275.75
A1-08	480.57	1.2520	0.2563	1874.89	259.02	0.00060	470.16	0.00122	340556.61
A1-13	576.37	1.4530	0.2623	2197.33	302.07	0.00071	524.16	0.00144	304234.84
A1-12	488.57	1.3110	0.2681	1822.21	228.16	0.00064	394.57	0.00131	248366.25
A1-15	646.58	1.5990	0.2618	2469.40	312.54	0.00078	581.10	0.00155	348780.35
A1-16	579.98	1.4340	0.2568	2258.33	248.45	0.00070	459.35	0.00141	297029.77
A1-21	609.03	1.5690	0.2598	2343.83	286.90	0.00077	543.24	0.00156	324482.55
A1-22	599.27	1.6450	0.2640	2270.34	264.70	0.00081	533.47	0.00164	323818.67
A1-23	510.60	1.3310	0.2631	1940.46	234.69	0.00066	400.44	0.00133	247379.76
A1-24	584.67	1.5510	0.2593	2254.92	294.35	0.00076	537.76	0.00152	320268.71
AJ 38 T4	529.40	1.5220	0.2634	2009.50	251.55	0.00074	440.16	0.00151	244952.40
AJ 41 T4	576.56	1.7270	0.2668	2161.22	289.62	0.00084	542.86	0.00171	291073.97
AJ 48 B2	507.76	1.3750	0.2662	1907.20	199.84	0.00067	367.25	0.00137	239167.18
AJ 48 B3	531.40	1.6630	0.2666	1993.47	202.74	0.00083	351.26	0.00165	181121.42
AJ 48 T1	531.79	1.2180	0.2765	1923.31	234.63	0.00058	426.21	0.00120	309001.37
AJ 40 B4	564.06	1.2780	0.2793	2019.38	263.79	0.00060	476.11	0.00122	342448.99
AJ 48 T2	542.68	1.2470	0.2732	1986.08	291.27	0.00060	524.72	0.00120	389077.10
AJ 37 T2	577.25	1.6960	0.2799	2062.69	293.84	0.00080	529.65	0.00168	267960.12
AJ 39 T3	567.97	1.5280	0.2741	2072.37	321.05	0.00075	539.13	0.00148	298747.63
AJ 39 T4	569.63	1.5880	0.2743	2076.32	372.63	0.00078	595.00	0.00154	292596.14
AJ 47 T1	550.88	1.4880	0.2761	1995.56	313.22	0.00071	541.35	0.00147	300159.45
AJ 47 T2	544.48	1.1130	0.2753	1977.75	289.44	0.00054	457.01	0.00107	316183.95
AJ 47 T3	571.09	1.3970	0.2754	2073.82	202.42	0.00067	399.34	0.00137	281316.94
AJ 47 T4	585.06	1.3830	0.2759	2120.37	217.08	0.00069	413.48	0.00138	284629.65
AJ 41 T1	508.45	1.6500	0.2702	1881.78	203.85	0.00081	387.61	0.00155	248330.02
AJ 41 T2	537.60	1.6200	0.2698	1992.36	209.80	0.00081	403.11	0.00162	238655.46
AJ 41 T3	559.42	1.6320	0.2659	2103.92	195.00	0.00081	385.57	0.00160	241229.35
AJ 42 T4	615.04	1.5750	0.2773	2217.68	186.79	0.00068	376.75	0.00155	218342.53
Mean	558.17	1.4767	0.2683	2082.30	260.55	0.00072	470.92	0.00145	288756.68
Std. Dev.	38.77	0.1637	0.0075	158.82	48.59	0.00008	75.37	0.00017	46674.34
COV	6.95%	11.08%	2.81%	7.63%	18.65%	11.75%	16.01%	11.40%	16.16%

Table C.5. Summary table of static test results from tension tests conducted at 65.6°C (150°F).

					Used to Calculate E				
Specimen Number	Max Load	Max Strain (%)	Average Area	Average Stress (psi)	Low Stress (psi)	Low Strain (in/in)	High Stress (psi)	High Strain (in/in)	Elastic Modulus (psi)
A2-08	533.15	1.7730	0.2611	2041.73	289.09	0.00085	472.31	0.00176	201339.16
A1-43	464.84	1.4000	0.2453	1894.67	214.90	0.00069	438.67	0.00139	319671.12
A1-42	531.54	2.1620	0.2556	2079.54	324.28	0.00108	558.46	0.00207	236546.55
A1-41	505.18	1.3060	0.2574	1962.70	227.57	0.00060	407.97	0.00129	261435.47
A1-40	464.50	1.5680	0.2561	1813.82	244.79	0.00076	441.54	0.00156	245931.77
A1-39	472.12	1.8490	0.2590	1823.10	287.51	0.00092	516.77	0.00180	260518.63
A1-38	573.15	2.1080	0.2556	2242.38	366.31	0.00104	640.85	0.00206	269156.73
AJ 37 B3	492.87	1.8690	0.2719	1812.70	261.76	0.00092	510.77	0.00185	267747.01
AJ 37 B4	489.55	1.8210	0.2646	1850.25	247.29	0.00090	467.13	0.00181	241578.34
AJ 43 B1	462.55	1.5960	0.2697	1714.74	256.98	0.00078	486.03	0.00156	293647.84
A2-12	476.56	1.6390	0.2755	1730.01	285.85	0.00079	481.72	0.00159	244840.66
A2-13	525.44	1.3750	0.2935	1790.12	213.92	0.00067	425.83	0.00136	307116.94
A2-14	535.94	1.8850	0.2926	1831.76	289.33	0.00093	546.30	0.00186	276305.52
A2-15	487.40	1.6660	0.2801	1739.96	245.62	0.00082	466.68	0.00165	266334.94
A2-16	562.94	1.8120	0.2960	1901.57	310.34	0.00088	540.70	0.00178	255957.06
A2-17	533.84	1.7980	0.2980	1791.13	294.15	0.00088	546.03	0.00177	283006.84
A2-18	528.03	1.4600	0.2793	1890.86	213.71	0.00072	403.53	0.00145	260035.30
A2-19	458.45	1.9830	0.2782	1648.02	331.08	0.00094	556.95	0.00194	225863.10
A1-03	439.99	1.8690	0.2663	1652.14	266.94	0.00093	483.46	0.00186	232823.19
A1-04	521.19	1.6380	0.2579	2020.54	285.77	0.00078	497.51	0.00159	261398.02
A1-45	543.99	1.8860	0.2568	2117.97	332.99	0.00092	622.48	0.00188	301544.94
A2-01	525.54	1.8680	0.2949	1782.30	268.26	0.00089	524.37	0.00186	264031.82
A2-02	487.45	1.7740	0.2965	1644.07	232.54	0.00088	460.29	0.00176	258808.91
A2-03	516.65	1.9130	0.3124	1653.55	276.49	0.00092	509.80	0.00186	248197.54
A2-04	522.17	1.3200	0.2686	1943.95	171.90	0.00066	329.59	0.00132	238915.74
A2-05	549.32	1.9120	0.2669	2058.01	364.89	0.00094	610.12	0.00189	258133.27
A2-06	496.63	1.5750	0.2912	1705.51	274.25	0.00076	470.60	0.00154	251733.89
A2-07	507.28	1.5050	0.2924	1734.84	285.47	0.00075	475.16	0.00150	252928.68
Mean	507.44	1.7261	0.2748	1852.57	273.71	0.00084	496.13	0.00170	260198.18
Std. Dev.	33.93	0.2276	0.0174	157.59	45.85	0.00011	68.46	0.00022	25109.39
COV	6.69%	13.19%	6.34%	8.51%	16.75%	13.64%	13.80%	12.79%	9.65%

Table C.6. Summary table of static test results from tension tests conducted at 80°C (176°F).

					Used to Calculate E				
Specimen Number	Max Load	Max Strain (%)	Average Area	Average Stress (psi)	Low Stress (psi)	Low Strain (in/in)	High Stress (psi)	High Strain (in/in)	Elastic Modulus (psi)
A3-05	407.62	1.8560	0.2298	1773.51	233.91	0.00092	439.83	0.00182	228791.71
A3-47	435.06	2.0310	0.2308	1884.62	325.34	0.00101	586.53	0.00202	258611.10
A3-63	380.52	1.8120	0.2224	1710.64	216.19	0.00090	392.55	0.00180	195955.36
A3-43	411.08	1.6890	0.2290	1794.99	226.54	0.00083	436.19	0.00166	252591.50
A3-12	435.45	2.0120	0.2296	1896.73	278.89	0.00099	527.70	0.00198	251321.81
A3-06	397.90	1.9350	0.2326	1710.79	264.73	0.00094	499.24	0.00192	239298.94
A3-46	423.68	1.9660	0.2269	1867.65	274.71	0.00095	524.68	0.00190	263127.15
A3-48	362.50	2.0410	0.2238	1619.53	180.87	0.00100	391.70	0.00201	208746.61
A3-64	395.41	2.2320	0.2247	1759.82	242.84	0.00110	508.28	0.00222	236995.87
A3-57	338.57	1.7830	0.2305	1468.79	191.21	0.00089	360.88	0.00175	197295.94
A3-41	398.73	2.0750	0.2283	1746.45	240.80	0.00100	493.82	0.00207	236469.55
A3-51	399.71	2.4680	0.2200	1816.69	286.41	0.00119	566.37	0.00240	231366.51
A3-24	434.62	1.5490	0.2269	1915.62	250.55	0.00076	483.44	0.00154	298583.35
A3-67	387.94	2.0090	0.2277	1703.76	211.78	0.00099	419.69	0.00194	218846.56
A3-31	344.43	1.9240	0.2268	1518.90	271.41	0.00094	457.69	0.00189	196080.73
A3-32	388.53	1.7980	0.2282	1702.89	268.58	0.00085	462.54	0.00176	213146.23
A3-58	448.15	1.8900	0.2304	1945.13	266.20	0.00090	512.09	0.00186	256130.37
A3-55	408.64	1.8900	0.2218	1841.98	327.16	0.00094	536.81	0.00189	220685.40
A3-11	338.33	1.7060	0.2278	1485.46	187.36	0.00082	367.01	0.00165	216439.23
A3-62	353.27	1.7590	0.2233	1581.75	208.30	0.00081	407.57	0.00166	234432.67
A3-44	352.44	1.6870	0.2297	1534.39	185.00	0.00084	363.63	0.00161	231988.33
A3-34	421.39	2.0090	0.2269	1856.78	293.07	0.00100	519.57	0.00198	231121.32
A3-38	427.25	1.9780	0.2254	1895.28	298.95	0.00097	506.25	0.00196	209392.73
A3-10	391.55	2.0990	0.2298	1704.16	230.02	0.00100	457.91	0.00206	214995.02
A3-61	357.37	1.5970	0.2240	1595.49	270.63	0.00078	425.39	0.00154	203643.69
A3-23	403.42	1.7320	0.2274	1773.67	286.88	0.00086	485.71	0.00172	231203.31
A3-18	427.78	2.1460	0.2281	1875.16	338.86	0.00103	610.76	0.00212	249448.14
A3-25	428.27	2.2190	0.2258	1896.78	345.40	0.00108	611.49	0.00216	246382.14
Mean	396.41	1.9247	0.2271	1745.62	257.24	0.00094	476.98	0.00189	231181.83
Std. Dev.	32.39	0.2071	0.0030	140.38	46.87	0.00010	71.43	0.00021	23520.09
COV	8.17%	10.76%	1.33%	8.04%	18.22%	10.71%	14.98%	11.06%	10.17%

Table C.7. Summary table of static test results from compression tests conducted at 21.1°C (70°F).

					Used to Calculate E				
Specimen Number	Max Load	Max Strain (%)	Average Area	Average Stress (psi)	Low Stress (psi)	Low Strain (in/in)	High Stress (psi)	High Strain (in/in)	Elastic Modulus (psi)
AJ 49 L4	20418.94	0.0281	2.7880	7323.78	939.95	0.00138	1680.42	0.00275	540488.48
AJ 48 R5	20667.48	0.0290	2.7841	7423.42	936.09	0.00137	1888.30	0.00282	656694.48
AJ 36 L6	17997.07	0.0319	2.7591	6522.70	813.85	0.00154	1494.95	0.00312	431075.13
AJ 40 R2	18573.73	0.0339	2.7750	6693.27	642.57	0.00169	1340.13	0.00337	415215.00
AJ 40 R3	18307.62	0.0336	2.7783	6589.54	293.18	0.00157	923.66	0.00332	360276.88
AJ 44 R5	20936.53	0.0392	2.7577	7592.02	987.23	0.00194	1865.88	0.00391	446015.66
AJ 48 R4	19320.80	0.0289	2.7988	6903.19	603.16	0.00139	1325.24	0.00285	494575.29
AJ 30 R4	19608.89	0.0269	2.7979	7008.52	734.16	0.00131	1519.47	0.00269	569060.65
AJ 47 L4	18866.70	0.0281	2.7589	6838.51	911.93	0.00133	1597.58	0.00277	476147.29
AJ 45 R1	18424.32	0.0194	2.7841	6617.80	918.58	0.00094	1518.07	0.00190	624464.56
AJ 40 R1	19272.95	0.0347	2.7836	6923.71	704.04	0.00169	1552.04	0.00344	484572.37
AJ 36 L3	19189.45	0.0295	2.7678	6933.13	907.37	0.00143	1690.22	0.00294	518444.89
AJ 46 R6	20116.21	0.0271	2.8137	7149.42	816.83	0.00130	1584.62	0.00270	548421.62
AJ 31 R6	20345.22	0.0395	2.8029	7258.51	1025.41	0.00195	1909.84	0.00392	448949.15
AJ 29 L6	19124.02	0.0326	2.7580	6933.93	833.29	0.00161	1594.78	0.00323	470052.76
AJ 38 R3	20442.38	0.0364	2.7762	7363.34	942.75	0.00174	1778.84	0.00362	444730.07
AJ 37 L4	18539.06	0.0334	2.7886	6648.24	613.67	0.00161	1320.34	0.00332	413256.34
AJ 45 R5	20980.96	0.0363	2.7727	7567.05	1178.48	0.00181	2026.48	0.00347	510844.58
AJ 46 R5	21727.05	0.0356	2.8063	7742.25	952.56	0.00171	1893.73	0.00348	531736.39
AJ 41 R1	19449.22	0.0289	2.7720	7016.22	918.23	0.00142	1674.99	0.00284	532927.25
AJ 36 R3	19945.31	0.0329	2.7800	7174.60	1174.10	0.00159	1987.60	0.00328	481361.11
AJ 41 L5	19096.68	0.0315	2.7932	6836.79	656.58	0.00151	1391.97	0.00312	456764.21
AJ 40 R5	20233.40	0.0255	2.7702	7304.05	1192.84	0.00125	1903.71	0.00255	546824.08
AJ 48 L4	18540.04	0.0271	2.7741	6683.21	943.28	0.00132	1640.49	0.00266	520306.82
AJ 49 L5	20349.61	0.0308	2.7883	7298.12	1033.64	0.00144	1860.28	0.00305	513438.32
AJ 46 R3	22511.72	0.0434	2.8009	8037.23	1364.65	0.00216	2421.94	0.00430	494059.92
AJ 29 R3	19681.15	0.0252	2.7839	7069.74	1051.33	0.00122	1745.92	0.00250	542643.90
AJ 37 L6	19921.39	0.0328	2.7736	7182.57	800.89	0.00163	1557.47	0.00322	475837.52
Mean	19735.28	0.0315	2.7817	7094.10	888.95	0.00153	1667.46	0.00311	498185.17
Std. Dev.	1072.13	0.0050	0.0151	372.37	218.04	0.00026	285.58	0.00050	63242.44
COV	5.43%	16.01%	0.54%	5.25%	24.53%	16.79%	17.13%	16.08%	12.69%

Table C.8. Summary table of static test results from compression tests conducted at 30°C (86°F).

					Used to Calculate E				
Specimen Number	Max Load	Max Strain (%)	Average Area	Average Stress (psi)	Low Stress (psi)	Low Strain (in/in)	High Stress (psi)	High Strain (in/in)	Elastic Modulus (psi)
AJ 49 R5	19604.98	0.0408	2.7959	7011.94	1050.80	0.00200	1929.07	0.00403	432641.00
AJ 44 L2	18435.55	0.0359	2.8233	6529.71	1093.42	0.00172	1938.85	0.00357	456988.45
AJ 49 R1	18415.04	0.0372	2.7923	6594.95	934.32	0.00177	1794.42	0.00370	445646.87
AJ 44 L1	19083.01	0.0387	2.7847	6852.72	976.76	0.00193	1909.33	0.00387	480708.18
AJ 42 R6	19943.85	0.0351	2.8193	7074.08	951.61	0.00173	1802.63	0.00344	497671.02
AJ 47 R1	17515.14	0.0344	2.7899	6278.03	987.76	0.00171	1741.33	0.00341	443275.50
AJ 39 L1	16935.55	0.0303	2.7360	6189.85	1106.17	0.00151	1845.76	0.00301	493065.16
AJ 46 L3	17481.93	0.0289	2.7845	6278.30	898.17	0.00142	1593.06	0.00282	496350.05
AJ 43 R4	17516.60	0.0281	2.8170	6218.14	948.82	0.00137	1638.47	0.00276	496151.58
AJ 44 R1	17724.12	0.0319	2.7624	6416.19	1096.39	0.00159	1868.29	0.00318	485475.24
AJ 29 R6	17081.54	0.0376	2.7630	6182.24	866.21	0.00188	1624.15	0.00376	403156.74
AJ 31 L1	17070.31	0.0372	2.7715	6159.15	769.98	0.00185	1481.12	0.00366	392890.12
AJ 30 L1	17242.19	0.0376	2.7553	6257.94	934.15	0.00186	1774.68	0.00376	442388.97
AJ 49 R4	19330.08	0.0380	2.8079	6884.23	1067.40	0.00180	1893.44	0.00374	425795.75
AJ 48 L2	17335.45	0.0331	2.7593	6282.60	959.47	0.00164	1652.79	0.00325	430632.39
AJ 36 R6	17694.34	0.0272	2.7790	6367.05	1194.71	0.00131	1912.13	0.00268	523663.10
AJ 46 R2	18486.33	0.0296	2.7667	6681.82	1277.31	0.00144	2047.12	0.00293	516651.07
AJ 36 L2	16560.55	0.0294	2.7384	6047.56	790.24	0.00141	1463.83	0.00286	464540.33
AJ 37 L1	16627.44	0.0301	2.7691	6004.55	1015.70	0.00150	1720.55	0.00293	492898.00
AJ 48 L1	17104.98	0.0347	2.7634	6189.92	934.15	0.00173	1691.56	0.00345	440355.06
AJ 37 L5	16610.35	0.0315	2.7759	5983.68	553.26	0.00155	1222.30	0.00315	418152.08
AJ 29 R1	14402.83	0.0365	2.7530	5231.70	562.69	0.00182	1182.31	0.00364	340450.69
AJ 36 L4	16102.05	0.0349	2.7777	5796.87	567.93	0.00168	1183.18	0.00349	339919.30
AJ 47 L5	18257.81	0.0345	2.7541	6629.37	790.42	0.00170	1549.57	0.00343	438818.96
AJ 31 R2	17494.63	0.0365	2.7778	6298.06	857.83	0.00176	1674.97	0.00357	451456.86
AJ 31 R3	17702.64	0.0368	2.7896	6346.01	991.60	0.00184	1758.97	0.00357	443563.66
AJ 45 R2	17461.43	0.0416	2.7947	6248.06	706.59	0.00202	1488.45	0.00409	377710.18
AJ 41 L2	16153.32	0.0319	2.7870	5795.97	638.66	0.00152	1309.97	0.00314	414390.99
Mean	17549.07	0.0343	2.7782	6315.38	911.52	0.00168	1667.58	0.00339	445907.40
Std. Dev.	1159.59	0.0039	0.0226	391.12	186.20	0.00019	237.07	0.00039	47467.64
COV	6.61%	11.31%	0.81%	6.19%	20.43%	11.50%	14.22%	11.54%	10.65%

Table C.9. Summary table of static test results from compression tests conducted at 40°C (104°F).

					Used to Calculate E				
Specimen Number	Max Load	Max Strain (%)	Average Area	Average Stress (psi)	Low Stress (psi)	Low Strain (in/in)	High Stress (psi)	High Strain (in/in)	Elastic Modulus (psi)
AJ 45 R4	15725.59	3.6790	2.7688	5679.53	850.18	0.00183	1576.04	0.00367	394487.73
AJ 47 L2	15657.23	2.7120	2.7441	5705.84	860.41	0.00135	1428.26	0.00270	420627.90
AJ 36 R5	14481.93	2.5690	2.7926	5185.83	739.79	0.00126	1247.32	0.00252	402806.05
AJ 47 R4	16204.59	3.2350	2.7914	5805.14	862.71	0.00156	1578.16	0.00315	449970.20
AJ 31 L6	16341.80	3.8420	2.7879	5861.63	983.33	0.00191	1691.37	0.00380	374627.43
AJ 38 L2	15705.57	3.4330	2.7710	5667.79	773.47	0.00169	1458.95	0.00340	400861.62
AJ 44 L4	14420.90	3.2560	2.8090	5133.74	650.20	0.00162	1259.49	0.00323	378440.95
AJ 30 L4	17449.22	4.1640	2.7853	6264.71	915.26	0.00208	1760.15	0.00416	406198.79
AJ 48 L3	16592.29	3.3210	2.7713	5987.26	1157.21	0.00166	1874.78	0.00326	448480.42
AJ 29 L3	18188.48	4.5170	2.7660	6575.63	1328.45	0.00225	2190.62	0.00447	388367.38
AJ 38 R4	17791.99	4.3710	2.7844	6389.93	1181.37	0.00217	2054.48	0.00437	396868.12
AJ 48 L5	15716.31	3.5000	2.7764	5660.66	772.59	0.00164	1546.94	0.00350	416319.14
AJ 49 L6	17069.34	4.9810	2.7858	6127.34	922.31	0.00249	1770.38	0.00488	354840.22
AJ 47 L3	16281.74	3.1390	2.7445	5932.50	667.66	0.00156	1347.84	0.00306	453455.11
AJ 41 L6	15809.08	4.2210	2.7851	5676.24	767.65	0.00209	1532.48	0.00419	364205.12
AJ 37 R4	15430.66	3.0220	2.7786	5553.36	869.05	0.00147	1526.49	0.00301	426904.94
AJ 47 R6	16699.22	3.9900	2.7787	6009.64	1075.91	0.00192	1852.03	0.00395	382323.55
AJ 46 L5	16617.19	4.2190	2.7900	5956.06	916.14	0.00205	1693.14	0.00413	373557.10
AJ 46 L6	16925.78	4.6890	2.7884	6070.03	909.97	0.00233	1732.29	0.00464	355983.12
AJ 42 L5	17210.94	4.1790	2.8079	6129.54	1082.26	0.00207	1879.72	0.00416	381557.66
AJ 30 L3	16496.09	3.9200	2.7826	5928.21	852.83	0.00195	1626.12	0.00390	396561.73
AJ 44 L6	16843.26	3.7030	2.8364	5938.23	960.23	0.00182	1721.53	0.00368	409303.21
AJ 39 L6	16034.67	3.6850	2.7992	5728.22	831.31	0.00184	1537.95	0.00364	392575.07
AJ 46 L1	13586.43	2.3980	3.0100	4513.71	762.01	0.00117	1341.67	0.00236	487111.92
AJ 44 L3	16507.32	3.6560	2.7994	5896.69	1009.25	0.00171	1766.15	0.00355	411355.91
AJ 37 R2	15177.25	2.8470	2.7750	5469.19	690.94	0.00138	1319.80	0.00284	430729.26
AJ 36 R1	16007.32	3.9070	2.7579	5804.20	881.40	0.00195	1600.91	0.00380	388923.51
AJ 41 R6	17151.86	3.5470	2.7979	6130.32	854.24	0.00173	1637.59	0.00354	432788.78
Mean	16218.72	3.6679	2.7916	5813.61	897.43	0.00181	1626.88	0.00363	404294.00
Std. Dev.	1022.90	0.6393	0.0468	406.18	159.49	0.00033	227.90	0.00063	31363.08
COV	6.31%	17.43%	1.68%	6.99%	17.77%	18.03%	14.01%	17.48%	7.76%

Table C.10. Summary table of static test results from compression tests conducted at 50°C (122°F).

					Used to Calculate E				
Specimen Number	Max Load	Max Strain (%)	Average Area	Average Stress (psi)	Low Stress (psi)	Low Strain (in/in)	High Stress (psi)	High Strain (in/in)	Elastic Modulus (psi)
AJ 30 R3	14555.18	4.3050	2.7849	5226.49	896.13	0.00214	1554.68	0.00423	315095.75
AJ 45 L4	15551.76	4.1960	2.7659	5622.76	966.96	0.00206	1697.75	0.00418	344710.80
AJ 38 L1	14553.22	3.5090	2.7754	5243.59	1158.95	0.00170	1824.51	0.00350	369757.40
AJ 42 L3	15338.87	3.8140	2.8410	5399.09	970.12	0.00188	1709.32	0.00378	389054.24
AJ 43 L6	15575.68	3.7850	2.7717	5619.50	781.63	0.00187	1494.71	0.00372	385447.80
AJ 38 L6	14846.68	3.6450	2.7767	5346.92	826.34	0.00182	1525.22	0.00363	386119.76
AJ 42 R1	15392.58	3.2960	2.8125	5472.96	988.70	0.00164	1664.43	0.00323	424989.00
AJ 39 R6	14625.98	3.3700	2.7856	5250.54	853.17	0.00164	1505.93	0.00327	400468.63
AJ 38 L3	14547.85	4.1240	2.7812	5230.71	818.10	0.00203	1531.18	0.00411	342826.17
AJ 39 R2	14525.88	3.8490	2.7671	5249.53	977.48	0.00189	1611.83	0.00376	339226.61
AJ 39 L3	14085.45	3.7920	2.7856	5056.59	891.74	0.00187	1533.46	0.00370	350665.66
AJ 49 L3	14927.25	3.9230	2.7897	5350.87	823.89	0.00188	1504.53	0.00390	336951.43
AJ 30 R1	13893.56	4.4940	2.7547	5043.57	911.03	0.00221	1587.81	0.00437	313326.22
AJ 38 L4	14162.11	3.3700	2.7901	5075.89	952.06	0.00166	1620.95	0.00337	391166.39
AJ 46 L4	14825.20	3.5270	2.7832	5326.64	997.99	0.00173	1697.40	0.00350	395142.63
AJ 45 L6	14448.73	3.8200	2.7646	5226.40	948.37	0.00189	1597.98	0.00382	336584.40
AJ 44 R4	14400.39	2.9290	2.7781	5183.56	1067.95	0.00141	1605.87	0.00283	378817.59
AJ 44 R2	13716.31	4.1460	2.7751	4942.57	573.51	0.00203	1203.83	0.00411	303039.07
AJ 45 R3	14430.18	3.4750	2.7831	5184.93	869.65	0.00172	1495.06	0.00346	359432.13
AJ 30 R6	13346.68	3.2530	2.7531	4847.95	728.16	0.00161	1297.46	0.00325	347137.45
AJ 46 R4	15017.58	3.4300	2.8110	5342.47	1046.21	0.00169	1692.84	0.00343	371624.81
AJ 38 R6	14170.90	3.2590	2.7849	5088.51	833.01	0.00161	1439.31	0.00324	371963.73
AJ 43 L2	13952.15	3.5340	2.7541	5065.98	993.61	0.00173	1606.40	0.00353	340437.80
AJ 38 R5	14216.31	3.7840	2.7909	5093.79	872.63	0.00187	1505.93	0.00376	335080.24
AJ 42 L1	13915.53	3.7190	2.7849	4996.85	923.65	0.00176	1567.47	0.00370	331866.84
AJ 41 L1	13137.70	3.1470	2.7578	4763.76	922.60	0.00154	1492.43	0.00308	370020.44
AJ 29 L5	15105.96	3.7720	2.7700	5453.37	922.43	0.00187	1585.36	0.00376	350758.23
AJ 30 R5	13618.16	3.1460	2.7844	4890.86	786.89	0.00154	1362.86	0.00311	366858.71
Mean	14460.14	3.6576	2.7806	5199.88	903.68	0.00180	1554.16	0.00362	358877.50
Std. Dev.	634.42	0.3801	0.0188	214.56	114.49	0.00019	128.41	0.00038	28991.67
COV	4.39%	10.39%	0.68%	4.13%	12.67%	10.58%	8.26%	10.43%	8.08%

Table C.11. Summary table of static test results from compression tests conducted at 65.6°C (150°F).

					Used to Calculate E				
Specimen Number	Max Load	Max Strain (%)	Average Area	Average Stress (psi)	Low Stress (psi)	Low Strain (in/in)	High Stress (psi)	High Strain (in/in)	Elastic Modulus (psi)
AJ 43 R2	11933.59	3.9720	2.8000	4262.01	836.18	0.00195	1356.73	0.00397	257694.79
AJ 45 L1	12892.58	5.1550	2.7658	4661.45	854.84	0.00257	1483.85	0.00513	245707.77
AJ 39 R1	11738.28	3.4790	2.7618	4250.29	795.03	0.00169	1322.02	0.00347	296065.16
AJ 31 L5	12001.95	3.7780	2.7798	4317.52	848.22	0.00178	1401.37	0.00376	279370.65
AJ 30 R2	11892.58	3.3400	2.7803	4277.45	910.82	0.00166	1452.64	0.00333	324442.44
AJ 47 R5	12042.48	3.5810	2.7868	4321.29	841.59	0.00177	1376.96	0.00357	297425.95
AJ 48 L6	11517.58	3.7200	2.7710	4156.49	814.73	0.00184	1333.53	0.00371	277433.10
AJ 30 L2	12194.82	4.1070	2.7944	4363.96	885.19	0.00203	1433.11	0.00403	273961.23
AJ 39 R4	11988.77	2.7200	2.7850	4304.81	920.59	0.00136	1435.55	0.00268	390123.57
AJ 42 L2	11786.13	3.7810	2.8291	4166.02	714.46	0.00188	1260.99	0.00372	297025.79
AJ 31 R5	11710.94	3.2320	2.8139	4161.81	790.67	0.00158	1290.11	0.00323	302692.78
AJ 37 R6	11860.84	3.1480	2.7737	4276.15	845.77	0.00157	1346.44	0.00310	327231.01
AJ 41 L3	11767.09	3.6490	2.7927	4213.45	926.86	0.00182	1470.43	0.00363	300310.94
AJ 41 L4	12902.34	4.0130	2.7847	4633.28	1022.60	0.00193	1619.35	0.00401	286899.40
AJ 41 R2	11435.55	3.6260	2.7945	4092.18	862.52	0.00178	1367.02	0.00359	278729.41
AJ 48 R1	12248.05	3.4310	2.7735	4416.08	785.79	0.00165	1299.88	0.00338	297162.82
AJ 47 R3	11866.70	3.6040	2.7791	4269.92	847.17	0.00176	1388.99	0.00353	306112.36
AJ 40 R4	12030.27	3.4390	2.7837	4321.62	791.02	0.00166	1290.29	0.00335	295425.11
AJ 44 R3	12101.07	3.5940	2.7717	4365.89	739.05	0.00175	1274.59	0.00348	309561.07
AJ 45 L5	12821.78	4.3980	2.7724	4624.85	915.53	0.00212	1543.32	0.00438	277783.71
AJ 30 L6	11876.47	3.3140	2.7508	4317.52	823.63	0.00162	1324.64	0.00326	305495.56
AJ 49 R2	11703.13	2.9950	2.7813	4207.76	769.57	0.00149	1249.48	0.00297	324264.60
AJ 38 L5	11300.29	2.8650	2.7912	4048.48	803.75	0.00137	1325.69	0.00284	355060.43
AJ 43 R5	11666.99	3.5990	2.7992	4168.04	829.73	0.00171	1340.33	0.00354	279018.48
AJ 48 R2	11570.80	2.5850	2.7770	4166.62	796.77	0.00120	1236.92	0.00258	318950.39
AJ 36 R4	11056.15	3.2730	2.7830	3972.69	834.96	0.00163	1305.28	0.00322	295798.85
AJ 46 L2	11651.37	3.7400	2.7680	4209.29	765.03	0.00180	1323.07	0.00372	290644.15
AJ 39 L4	11561.04	3.9940	2.7987	4130.80	613.49	0.00190	1171.53	0.00395	272212.88
Mean	11897.13	3.5761	2.7837	4274.20	828.06	0.00175	1358.00	0.00354	298664.44
Std. Dev.	432.57	0.5178	0.0161	162.99	76.71	0.00026	96.93	0.00052	28804.87
COV	3.64%	14.48%	0.58%	3.81%	9.26%	14.82%	7.14%	14.65%	9.64%

Table C.12. Summary table of static test results from compression tests conducted at 80°C (176°F).

					Used to Calculate E				
Specimen Number	Max Load	Max Strain (%)	Average Area	Average Stress (psi)	Low Stress (psi)	Low Strain (in/in)	High Stress (psi)	High Strain (in/in)	Elastic Modulus (psi)
AJ 31 R4	9885.25	3.8790	2.8234	3501.22	691.77	0.00187	1145.40	0.00385	229105.14
AJ 39 L5	9882.81	3.2820	2.7789	3556.40	726.19	0.00162	1155.26	0.00322	268168.95
AJ 37 R1	9782.72	2.9560	2.7708	3530.64	720.31	0.00141	1131.74	0.00292	272470.25
AJ 49 R3	10687.50	3.4950	2.8033	3812.41	814.04	0.00169	1290.84	0.00349	264890.12
AJ 43 R6	9907.23	2.9790	2.7896	3551.54	681.39	0.00145	1112.54	0.00295	287430.57
AJ 42 R2	10255.37	3.2310	2.8199	3636.79	728.95	0.00159	1166.67	0.00323	266900.87
AJ 31 L3	10173.83	3.2660	2.7843	3654.00	730.34	0.00158	1162.17	0.00321	264930.81
AJ 40 R6	10308.11	3.5570	2.7646	3728.64	654.41	0.00169	1134.85	0.00347	269906.97
AJ 40 L5	10049.32	3.1030	2.7497	3654.71	734.49	0.00155	1172.38	0.00305	291926.85
AJ 45 L3	10105.96	3.6730	2.7526	3671.42	761.98	0.00183	1206.62	0.00367	241649.48
AJ 37 R5	9786.13	2.7100	2.7796	3520.67	692.98	0.00132	1098.36	0.00268	298071.35
AJ 36 R2	9866.21	3.8460	2.7749	3555.47	745.21	0.00191	1198.15	0.00383	235904.40
AJ 41 R4	9909.18	3.4760	2.8072	3529.94	610.66	0.00173	1049.93	0.00346	253915.65
AJ 41 L4	10125.00	3.5340	2.7847	3635.93	693.85	0.00176	1160.27	0.00351	266529.13
AJ 29 L2	10416.50	3.7870	2.7770	3751.04	763.37	0.00185	1226.68	0.00377	241308.69
AJ 36 L1	10074.71	3.2720	2.7481	3666.00	827.36	0.00162	1277.18	0.00324	277668.61
AJ 44 R6	10634.77	3.0280	2.7651	3846.13	888.58	0.00146	1333.91	0.00297	294918.39
AJ 47 R2	10161.13	3.8030	2.7911	3640.54	718.40	0.00186	1187.94	0.00372	252440.28
AJ 43 R1	10195.31	3.8190	2.8086	3630.06	694.54	0.00189	1133.81	0.00376	234905.73
AJ 30 L5	9936.52	3.6610	2.7593	3601.08	597.17	0.00183	1057.37	0.00361	258539.38
AJ 36 L5	9633.79	3.8340	2.7527	3499.70	654.76	0.00189	1114.61	0.00381	239507.32
AJ 39 R5	10224.61	3.7440	2.7972	3655.29	754.55	0.00186	1207.31	0.00374	240831.71
AJ 31 L2	10161.62	3.7650	2.7830	3651.32	773.74	0.00188	1219.59	0.00375	238420.13
AJ 43 L4	9746.09	3.6430	2.7876	3496.27	751.78	0.00180	1176.70	0.00356	241431.40
AJ 43 L5	9659.67	3.4730	2.7723	3484.37	683.47	0.00171	1076.57	0.00339	233986.97
AJ 41 R3	9818.36	4.5390	2.7910	3517.82	651.13	0.00222	1134.16	0.00452	210012.37
AJ 43 L1	9882.81	3.9570	2.7700	3567.83	744.69	0.00193	1203.16	0.00393	229235.30
AJ 29 R4	9901.37	4.5090	2.7788	3563.14	555.15	0.00225	1045.61	0.00443	224983.76
Mean	10041.85	3.5650	2.7809	3611.08	715.90	0.00175	1163.56	0.00353	254642.52
Std. Dev.	264.95	0.4238	0.0201	94.91	69.90	0.00022	69.80	0.00042	23014.47
COV	2.64%	11.89%	0.72%	2.63%	9.76%	12.34%	6.00%	12.04%	9.04%

Table C.13. Summary table of 100-minute tension creep test results

Temperature	Test	Initial Strain	Applied Stress	Strain at 100-min
21.1	Test 1	0.00220	1046.49	0.00324
	Test 2	0.00205	1061.83	0.00304
	Test 3	0.00229	1049.63	0.00344
	Test 4	0.00260	1024.23	0.00364
	Test 5	0.00231	1080.21	0.00339
	Test 6	0.00255	1052.42	0.00368
	Test 7	0.00251	1060.89	0.00381
	Test 8	0.00207	1021.44	0.00300
30	Test 1	0.00289	1016.61	0.00421
	Test 2	0.00240	1040.91	0.00397
	Test 3	0.00271	1060.17	0.00462
	Test 4	0.00251	1070.68	0.00438
	Test 5	0.00298	1057.16	0.00466
	Test 6	0.00330	1016.62	0.00497
	Test 7	0.00245	1057.17	0.00415
	Test 8	0.00363	1017.48	0.00555
40	Test 1	0.00349	1044.15	0.00558
	Test 2	0.00391	1053.36	0.00655
	Test 3	0.00373	1002.70	0.00687
	Test 4	0.00374	1162.96	0.00710
	Test 5	0.00360	1067.67	0.00658
	Test 6	0.00371	1030.68	0.00673
	Test 7	0.00375	1137.45	0.00724
	Test 8	0.00310	1022.95	0.00555
50	Test 1	0.00349	1078.04	0.00656
	Test 2	0.00383	1077.96	0.00799
	Test 3	0.00327	1019.85	0.00624
	Test 4	0.00395	1126.42	0.00879
	Test 5	0.00372	1013.77	0.00646
	Test 6	0.00486	1130.57	0.01063
	Test 7	0.00389	1033.59	0.00734
	Test 8	0.00371	1068.37	0.00697
65.6	Test 1	0.00451	1054.89	0.00940
	Test 2	0.00440	1104.60	0.01222
	Test 3	0.00507	1066.19	0.01130
	Test 4	0.00515	1101.58	0.01487
	Test 5	0.00511	1028.27	0.01179
	Test 6	0.00590	1093.27	0.02134
	Test 7	0.00484	988.99	0.01266
	Test 8	0.00499	1056.25	0.01699

Table C.14. Summary table of 100-minute compression creep test results

Temperature	Test	Initial Strain	Applied Stress	Strain at 100-min
21.1	Test 1	0.00364	2834.37	0.00675
	Test 2	0.00528	2837.73	0.00899
	Test 3	0.00279	2826.39	0.00573
	Test 4	0.00298	2827.74	0.00528
	Test 5	0.00461	2828.57	0.00900
	Test 6	0.00351	2826.90	0.00653
	Test 7	0.00382	2833.28	0.00704
	Test 8	0.00387	2833.93	0.00620
30	Test 1	0.00454	2848.63	0.00949
	Test 2	0.00478	2832.16	0.01006
	Test 3	0.00378	2802.89	0.00791
	Test 4	0.00345	2871.75	0.00757
	Test 5	0.00454	2838.07	0.00984
	Test 6	0.00323	2845.46	0.00711
	Test 7	0.00238	2863.66	0.00574
	Test 8	0.00431	2795.47	0.00877
40	Test 1	0.00438	2843.07	0.01131
	Test 2	0.00489	2869.63	0.01172
	Test 3	0.00492	2833.33	0.01173
	Test 4	0.00482	2843.81	0.01153
	Test 5	0.00461	2828.66	0.01362
	Test 6	0.00359	2816.51	0.00967
	Test 7	0.00462	2810.11	0.01108
	Test 8	0.00506	2757.65	0.01031
50	Test 1	0.00780	2851.86	0.01929
	Test 2	0.00686	2869.56	0.01696
	Test 3	0.00528	2814.02	0.01561
	Test 4	0.00569	2837.48	0.01513
	Test 5	0.00598	2846.86	0.01465
	Test 6	0.00646	2815.27	0.01666
	Test 7	0.00526	2795.36	0.01541
	Test 8	0.00788	2766.75	0.01981
65.6	Test 1	0.01033	2892.72	0.03529
	Test 2	0.00611	2911.65	0.02324
	Test 3	0.01008	2791.98	0.03735
	Test 4	0.00786	2850.73	0.02733
	Test 5	0.00972	2838.05	0.03053
	Test 6	0.01012	2823.33	0.03414
	Test 7	0.00915	2780.10	0.03041
	Test 8	0.00833	2779.14	0.02657